

Dark Matter Indirect Signatures

Signatures indirectes des Particules de Matière Noire

Julien Lavalley^a, Pierre Salati^b

^a*Laboratoire Univers & Particules de Montpellier (LUPM)
CNRS-IN2P3 & Université Montpellier II (UMR-5299), Place Eugène Bataillon
F-34095 Montpellier Cedex 05 — France*

^b*LAPTh, CNRS & Université de Savoie
9, Chemin de Bellevue B.P.110, 74941 Annecy-le-Vieux Cedex, France
Tel. +33 (0)4 50 09 16 90 and Fax +33 (0)4 50 09 89 13*

Abstract

The astronomical dark matter could be made of weakly interacting and massive particles. If so, these species would be abundant inside the Milky Way, where they would continuously annihilate and produce cosmic rays. Those annihilation products are potentially detectable at the Earth, and could provide indirect clues for the presence of dark matter species within the Galaxy. We will review here the various cosmic radiations which the dark matter can produce. We will examine how they propagate throughout the Milky Way and compare the dark matter yields with what pure astrophysical processes are expected to generate. The presence of dark matter substructures might enhance the signals and will be briefly discussed.

Résumé

La matière noire astronomique pourrait être constituée de particules massives aux interactions évanescentes. Si tel était le cas, ces particules se retrouveraient en abondance au sein de la Voie Lactée où elles s'annihileraient en permanence, produisant de multiples radiations cosmiques. Celles-ci sont éventuellement visibles de la Terre et constituent dès lors des sortes d'empreintes spectrales, véritables signatures indirectes des candidats potentiels à la matière noire galactique. Dans cet article, nous passons en revue les différentes espèces cosmiques susceptibles d'être produites, et comparons leur flux avec celui des radiations engendrées par les processus astrophysiques conventionnels. L'existence de condensations de matière noire est brièvement discutée. Le taux d'annihilation pourrait être amplifié au sein de telles structures, conduisant à des signatures indirectes plus intenses que dans le cas d'un halo galactique lisse.

Email addresses: lavalle@in2p3.fr (Julien Lavalley), salati@lapp.in2p3.fr (Pierre Salati)

Keywords: Astronomical dark matter; Cosmic rays; Galactic antimatter; Gamma-rays; Neutrinos

Mots-clés : Matière noire astronomique; Rayons cosmiques; Anti-matière galactique; Rayons gamma; Neutrinos

preprint: LAPTH-020/12 and LUPM:12-024

1. The messengers of dark matter annihilation

The nature of the astronomical dark matter (DM) is still unknown. This component, which contributes a quarter to the energy balance of the universe, cannot be made of atoms and nuclei like ordinary matter. An exciting, and quite plausible possibility, lies in the existence of a population of weakly interacting and massive particles, dubbed the acronym WIMP. Should DM species pervade the halo of the Milky Way, their mutual annihilations would yield several indirect signatures. These are potentially detectable at the Earth under the form of spectral distortions appearing in various cosmic radiations

$$\chi + \chi \rightarrow q\bar{q}, W^+W^-, \dots \rightarrow \bar{p}, \bar{D}, e^+ \gamma \& \nu's \quad . \quad (1)$$

Detection of the DM annihilation products has motivated the spectacular development of several new experimental techniques. Searches for antiprotons and positrons are performed by balloon and satellite-borne devices. Because the flux depends on the square of the WIMP density n_χ , the limit which may be set on the annihilation cross section scales very roughly as m_χ^2 . That type of search is a priori mostly sensitive to small WIMP masses. Actually, the recent discovery of a positron excess above 10 GeV by the PAMELA collaboration has triggered a lot of excitement in the field, and many new possibilities have been explored, which may lead to a strong signal even in the TeV window. Alas, the DM interpretation of the positron excess raises more problems than it solves, and the current explanation of that anomaly lies in the existence of nearby pulsars. High-energy photons are detected both by air Cherenkov telescopes (ACT) and by satellite-borne instruments. The WIMP annihilation rate and hence the gamma-ray signal both scale as m_χ^{-2} . Because of the background in which that signal is swamped, the experimental reach on the annihilation cross section approximately scales as the mass m_χ . A smoking gun signature of the presence of DM particles would be the detection of a hot spot in the gamma-ray sky. The neutrino channel is mostly sensitive to large values of m_χ . The limit which may be set on the annihilation cross section does not depend too much on the WIMP mass and this channel is complementary to the other searches. Large areas under the ice cap of the South Pole are equipped for the detection of high-energy up-going muons, and the theoretical predictions start to be within reach and will soon be checked.

Various species can be produced by WIMP annihilations among which are antimatter cosmic rays, high-energy photons and neutrinos. The corresponding

rate $q_{\text{DM}}(\mathbf{x}, E)$ for the production of these particles depends on their energy E and is related to the WIMP annihilation cross section σ_{ann} through

$$q_{\text{DM}}(\mathbf{x}, E) = \eta \langle \sigma_{\text{ann}} v \rangle \left\{ \frac{\rho(\mathbf{x})}{m_\chi} \right\}^2 f(E) . \quad (2)$$

The coefficient η is a quantum factor equal to 1/2 for a self-conjugate particle like a Majorana fermion or to 1/4 otherwise. The annihilation cross section is averaged over the momenta of the incoming DM particles to yield $\langle \sigma_{\text{ann}} v \rangle$, whose value depends on the specific microscopic interactions involved in the annihilation process. The DM density at location \mathbf{x} is denoted by $\rho(\mathbf{x})$, while $f(E)$ stands generically for the energy distribution dN/dE of the species generated in a single annihilation event.

Once produced, the cosmic radiations propagate within the Milky Way and eventually reach the Earth. A key issue is the transport of charged cosmic rays throughout the magnetic fields of the Galaxy. An overview of the subject is given in section 2. This allows us to focus on antimatter particles. Although produced by conventional astrophysical processes, these species are not abundant. They are promising targets insofar as their spectra could be distorted should additional (and exotic) sources, of DM origin in our case, operate. Sections 3, 4 and 5 are respectively devoted to antiprotons, positrons and antideuterons. Attention is paid to the astrophysical backgrounds inside which the DM signals are buried. The PAMELA positron excess is also discussed, and its interpretation in terms of WIMPs is shown to have difficulties. The gamma-ray and neutrino skies are the subjects of sections 6 and 7. Finally, the possibility that DM is clumpy is rapidly examined in section 4.3. The existence of substructures has been extensively used in the literature as a pretext for arbitrarily enhancing the fluxes from DM origin. These are generally depressingly weaker than the backgrounds inside which they are hidden. However, a recent analysis has established that the boost factor from DM clumpiness cannot exceed on average a generous factor of ~ 20 . Alternatively, nothing precludes a DM clump to lie close to the Earth and produce locally an intense flux of cosmic radiations. But the odds for this to happen are not large.

For a more extensive view of the dark matter enigma, we refer the reader to the complementary contributions of Silk [1], Hooper & Tait [2], and Armengaud [3] in the present issue.

2. An overview of cosmic ray transport

We will focus this section on the transport of charged cosmic rays. Photons and neutrinos propagate along straight lines, and their fluxes at a distance r from a point source decrease as r^{-2} . Some extinction can take place along the line of sight though, but this is negligible for gamma-rays in the GeV to TeV energy range. The situation for neutrinos is more complicated as oscillations among the various families is known to occur in empty space, and is even resonantly

enhanced inside the Sun and the Earth. Neutrino transport is broached in section 7.1.

Once charged cosmic rays have been accelerated, or created by spallations of other nuclear species or through DM annihilation, they propagate through the Galactic magnetic field and are deflected by its irregularities : the Alfvén waves. In the regime where the magnetic turbulence is strong, which is actually the case for the Milky Way, cosmic ray (CR) transport needs to be investigated numerically. Monte Carlo simulations [4] indicate that it is similar to space diffusion with a coefficient

$$K(E) = K_0 \beta (\mathcal{R}/1 \text{ GV})^\delta , \quad (3)$$

which increases as a power law with the rigidity $\mathcal{R} = p/q$ of the particle. In addition, because the scattering centers drift inside the Milky Way with a velocity $V_a \sim 20$ to 100 km s^{-1} , a second order Fermi mechanism is responsible for some mild diffusive reacceleration. Its coefficient K_{EE} depends on the particle velocity β and total energy E , and is related to the space diffusion coefficient $K(E)$ through

$$K_{EE} = \frac{2}{9} V_a^2 \frac{E^2 \beta^4}{K(E)} . \quad (4)$$

In the case of positrons, diffusive reacceleration is completely dominated by energy losses. Finally, Galactic convection wipes cosmic rays away from the disk with a velocity $V_C \sim 5$ to 15 km s^{-1} .

Radio observations indicate that the magnetic fields of galaxies are not confined to the visible matter which they host, but extend far away in space. An illustration is provided by the maps of the radio continuum halo of NGC 4631, taken at 610 and 1412 MHz [6]. The synchrotron emission from electrons spiraling inside the magnetic field of NGC 4631 probes the structure of its magnetic halo. This halo, inside which charged particles are trapped and diffuse, extends well above and beneath the luminous disk. Inspired by this example, we can model the magnetic halo of our Galaxy (the so-called diffusive halo or DH) as a thick disk which matches the circular structure of the Milk Way, as shown in Fig. 1. The Galactic disk of stars and gas, where primary cosmic rays are accelerated, lies in the middle. Primary species, such as CR protons, helium nuclei and electrons, are believed to be accelerated by the shock waves driven by supernova explosions. These take place mostly in the Galactic disk which extends radially 20 kpc from its center, and has a half-thickness h of 100 pc. Confinement layers, where cosmic rays are trapped by diffusion, lie above and beneath this thin disk of gas. The intergalactic medium starts at the vertical boundaries $z = \pm L$, as well as beyond a radius of $r = R \equiv 20 \text{ kpc}$. Notice that the half-thickness L of the diffusive halo is not known and reasonable values range from 1 to 15 kpc. The diffusion coefficient K is assumed to be the same everywhere inside the DH, whereas the convective velocity is exclusively vertical with component $V_C(z) = V_C \text{ sign}(z)$. This Galactic wind, which is produced by the bulk of the disk stars like the Sun, drifts away from its progenitors along the vertical directions, hence the particular form assumed here for V_C .

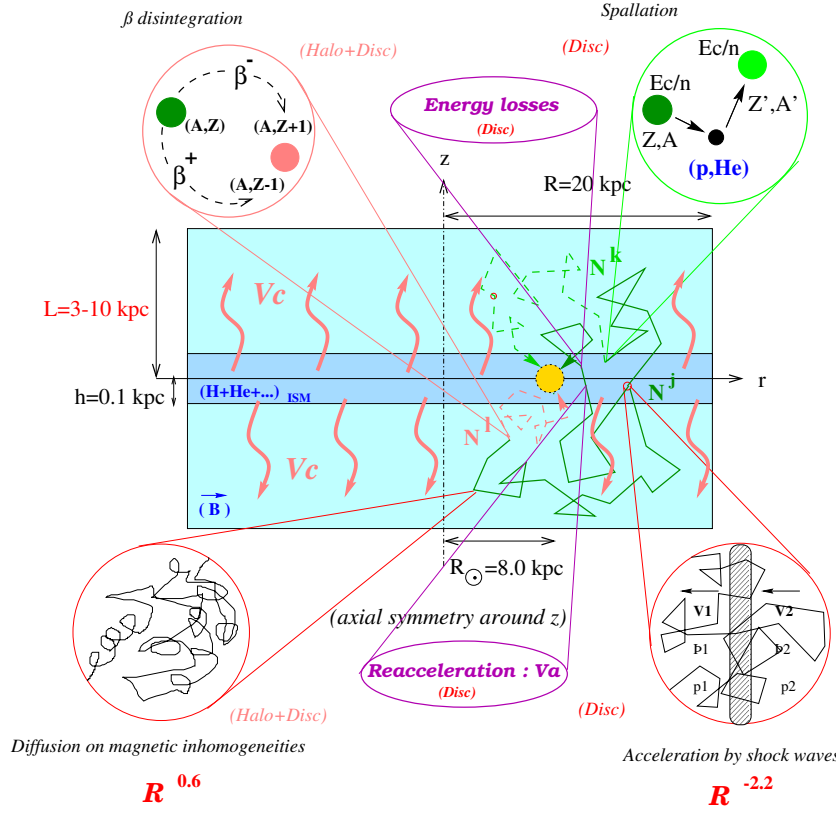


Figure 1: Schematic edge-on view of the Milky Way diffusive halo (DH) as seen by a cosmic ray physicist. The stellar and gaseous disk is sandwiched between two thick layers which contain turbulent magnetic fields. After having been accelerated by supernova driven shock waves or produced by DM species annihilating in the Galactic halo, cosmic rays diffuse on magnetic inhomogeneities and are wiped away by a Galactic wind with velocity V_C . They can lose energy and are also mildly subject to diffusive reacceleration. The former process is by far the dominant one in the case of electrons and positrons. This diagram has been borrowed from the review [5].

The master equation for CR transport may be expressed as

$$\frac{\partial \psi}{\partial t} + \partial_z (V_C \psi) - K \Delta \psi + \partial_E \{ b^{\text{loss}}(E) \psi - K_{EE}(E) \partial_E \psi \} = q(\mathbf{x}, E) , \quad (5)$$

where $\psi = dn/dE$ denotes the CR space and energy distribution function. This relation applies to any species (protons, antiprotons or positrons) as long as the rates for production q and energy loss $b^{\text{loss}}(E)$ are properly accounted for. Most of the analyses devoted to Galactic cosmic rays are based on the assumption that the acceleration and propagation of charged particles have reached a steady state. The diffusion time of a 10 GeV proton throughout the magnetic inhomogeneities of the Milky Way disk is of order 7 million years whereas

the rate of supernova explosions is 1 to 3 every century. The case for steady state is made even stronger when the escape time $\sim L^2/K$ from the DH as a whole is considered instead of the Galactic disk residence time. A 10 GeV proton spends on average 2.9×10^8 years before it escapes into intergalactic space. During that period, approximately 3 to 9 million supernova explosions have taken place. It is then reasonable to describe these sources as if they were continuously spread along the Galactic disk and were steadily accelerating charged particles. Different methods have been proposed to solve the CR diffusion equation (5). The purely numerical approach followed in the GALPROP public code [7]¹ is based on the well-known Crank-Nicholson semi-implicit scheme, where the time-dependent equation is evolved on a space and energy grid until convergence is reached. This method allows to treat inhomogeneous cases where, for instance, K or V_C depend on the location \mathbf{x} within the DH. It is time consuming though, and particular attention needs to be paid to the boundary conditions. More recently, the DRAGON package [8]² has been made publicly available. Most of the building blocks of DRAGON come from GALPROP, but this code relies on a faster solver.

Another route has been taken by the USINE collaboration, based on two semi-analytic methods.

(i) The Bessel expansion technique takes advantage of the axial symmetry of the DH and enforces a vanishing cosmic ray flux at a distance $R = 20$ kpc from the rotation axis of the Galaxy. This condition is actually implemented naturally by the following series expansion for ψ

$$\psi(\mathbf{x}, E) \equiv \psi(r, z, E) = \sum_{i=1}^{+\infty} P_i(z, E) J_0(\alpha_i r/R) . \quad (6)$$

The Bessel function of zeroth order J_0 vanishes at the points α_i . The radial dependence of ψ is now taken into account by the set of its Bessel transforms $P_i(z, E)$. The source term $q(\mathbf{x}, E) \equiv q(r, z, E)$ may also be Bessel expanded into the corresponding functions $Q_i(z, E)$ so that the master equation (5) becomes

$$\partial_z(V_C P_i) - K \partial_z^2 P_i + K \left\{ \frac{\alpha_i}{R} \right\}^2 P_i + \partial_E \{ b^{\text{loss}}(E) P_i - K_{EE}(E) \partial_E P_i \} = Q_i(z, E) . \quad (7)$$

In the case of CR nuclei and antinuclei, energy losses and diffusive reacceleration are confined inside the Galactic disk, considered here as infinitely thin, and an effective term $2h\delta(z)$ should be in factor of the energy derivative.

(ii) The solution of the master equation (5) may also be generically expressed as the integral

$$\psi(\mathbf{x}_\odot, E) = \int dE_S \int_{\text{DH}} d^3\mathbf{x}_S G(\mathbf{x}_\odot, E \leftarrow \mathbf{x}_S, E_S) q(\mathbf{x}_S, E_S) . \quad (8)$$

1. See the web site <http://galprop.stanford.edu/> and references therein.

2. See the web site <http://www.desy.de/~maccione/DRAGON/> and references therein.

The energy E_S at the source runs over a range which depends on the CR species and on the production mechanism. The space integral is performed over the DH. The convolution (8) involves the Green function G which describes the probability for a cosmic ray produced at location \mathbf{x}_S with energy E_S to reach, for instance, the Earth located at \mathbf{x}_\odot , where it is detected with energy E . The cosmic ray space and energy density ψ can be translated into the differential flux $\Phi \equiv (\beta/4\pi)\psi$ where β stands for the particle velocity. This flux is expressed in units of $\text{m}^{-2} \text{s}^{-1} \text{sr}^{-1} \text{GeV}^{-1}$. The flux of antinuclei or positrons produced by WIMP annihilations may be written as the product

$$\Phi(\odot, E) = \mathcal{F} \int dE_S f(E_S) I(E, E_S) , \quad (9)$$

where the information related to particle physics has been factored out in

$$\mathcal{F} = \eta \frac{\beta}{4\pi} \langle \sigma_{\text{ann}} v \rangle \left\{ \frac{\rho_\odot}{m_\chi} \right\}^2 . \quad (10)$$

The energy distribution $f(E_S)$ describes the spectrum at the source and depends on the details of the WIMP annihilation mechanism. The information on the Galactic DM density profile ρ , as well as on the propagation of cosmic rays within the Milky Way DH, is summarized in the halo integral

$$I(E, E_S) = \int_{\text{DH}} d^3\mathbf{x}_S G(\mathbf{x}_\odot, E \leftarrow \mathbf{x}_S, E_S) \left\{ \frac{\rho(\mathbf{x}_S)}{\rho_\odot} \right\}^2 , \quad (11)$$

where the solar neighborhood DM density is denoted by ρ_\odot . The halo integral $I(E, E_S)$ is a key ingredient for the derivation of the flux at the Earth of an antimatter species produced inside the Galactic DH by WIMP annihilations. The spatial reach of the Green function G depends on the nature of the CR particle (antinuclei or positrons) and on the energies E and E_S . This range delineates the region of the Milky Way from which most of the signal detected at the Earth originates. It corresponds to the extension of the so-called horizon beyond which the Green function vanishes. The antiproton horizon reaches the Galactic center at high energy, and the antiproton flux at the Earth starts to be sensitive to the DM distribution there. On the contrary, the positron horizon shrinks at high energy. Above tens of GeV, positrons detected at the Earth originate from its vicinity.

The normalization coefficient K_0 , the spectral index δ , the Galactic drift velocity V_C and the Alfvén velocity V_a are all unknown. We have already mentioned that such is the case for the DH half-thickness L . This situation can be remedied with the help of the boron to carbon ratio B/C which is quite sensitive to CR transport and which may be used as a constraint. The three propagation models featured in table 1 have been drawn from [10]. The MED configuration provides the best fit to the B/C measurements whereas the MIN and MAX models lead respectively to the minimal and maximal allowed antiproton fluxes which can be produced by WIMP annihilations. The three sets of parameters

Case	δ	K_0 [kpc ² /Myr]	L [kpc]	V_C [km/s]	V_a [km/s]
MIN	0.85	0.0016	1	13.5	22.4
MED	0.70	0.0112	4	12	52.9
MAX	0.46	0.0765	15	5	117.6

Table 1: Typical combinations of diffusion parameters that are compatible with the B/C analysis [9]. As shown in [10], these propagation models correspond respectively to minimal, medium and maximal primary antiproton fluxes.

of table 1 belong to an ensemble of more than 1,600 other models which have been shown in [9] to be also compatible with the B/C ratio. That analysis has been recently improved by several groups. In particular, the USINE collaboration has constrained the CR propagation parameters with the help of a Markov chain Monte Carlo technique [11] which allows to explore rapidly the parameter space. The resulting best fit is somewhat different from what has been derived ten years ago, but one of the important messages is the difficulty to get a precise value for L which still lies between 1 and 16 kpc.

3. Antiprotons as a robust probe for DM species

3.1. Calculation of the antiproton flux at the Earth

Antiprotons are produced during the collisions undergone by primary CR nuclei on the interstellar gas, *i.e.*, within the Galactic disk. Because they are not directly injected in the interstellar medium (ISM) but are sourced by primary species, these astrophysical antiprotons are dubbed secondaries. The rate with which they are produced may be expressed as

$$q_{\bar{p}}^{\text{sec}}(r, E_{\bar{p}}) = \int_{E_{\bar{p}}^0}^{+\infty} n_{\text{H}} \times \beta_{\text{p}} \psi_{\text{p}}(r, E_{\text{p}}) \times dE_{\text{p}} \times \frac{d\sigma}{dE_{\bar{p}}}(E_{\text{p}} \rightarrow E_{\bar{p}}) , \quad (12)$$

in the case of interactions between CR protons and hydrogen atoms. The various contributions from the spallations of interstellar H and He by CR protons and alpha particles need to be taken into account. Details on how the cross sections of these processes are parameterized are given in [12] and [13]. In addition to this conventional mechanism, antiprotons may be directly produced as primary CR species by DM annihilation. The corresponding source term $q_{\bar{p}}^{\text{prim}}(r, z, E)$ has already been discussed and is generically given by expression (2), where $f(E)$ stands here for the antiproton spectrum $dN_{\bar{p}}/dE_{\bar{p}}$. Notice that WIMP annihilations take place all over the diffusive halo and are not restricted to the $z = 0$ region. We therefore anticipate a different sensitivity of that component to the CR propagation parameters than in the case of secondary antiprotons.

Once produced, antiprotons propagate inside the DH. They can collide elastically on interstellar H and He atoms. However, they are preferentially scattered

forward, so that these interactions are innocuous and will be disregarded. Antiprotons can also annihilate on interstellar H and He. This leads to a negative source term $-\Gamma_{\bar{p}}^{\text{ann}} \psi_{\bar{p}}$, where the annihilation rate $\Gamma_{\bar{p}}^{\text{ann}}$ is defined as

$$\Gamma_{\bar{p}}^{\text{ann}} = \sigma_{\bar{p}\text{H}}^{\text{ann}} \beta_{\bar{p}} n_{\text{H}} + \sigma_{\bar{p}\text{He}}^{\text{ann}} \beta_{\bar{p}} n_{\text{He}} . \quad (13)$$

The annihilation cross section $\sigma_{\bar{p}\text{H}}^{\text{ann}}$ can be borrowed from [14, 15] and multiplied by a factor of $4^{2/3} \sim 2.5$, taking into account the higher geometric cross section, to get $\sigma_{\bar{p}\text{He}}^{\text{ann}}$. The average hydrogen n_{H} and helium n_{He} densities in the Galactic disk can be respectively averaged to 0.9 and 0.1 cm^{-3} . Last but not least, a tertiary component arises from the inelastic and non-annihilating interactions which antiprotons undergo with the ISM. Antiprotons can actually collide on a nucleon at rest and transfer enough energy to excite it as a Δ resonance. This mechanism redistributes antiprotons toward lower energies and flattens their spectrum as shown in [16]. It yields the source term

$$\begin{aligned} q_{\bar{p}}^{\text{ter}}(r, E_{\bar{p}}) &= \int_{E_{\bar{p}}}^{+\infty} \frac{d\sigma_{\bar{p}\text{H}\rightarrow\bar{p}\text{X}}}{dE_{\bar{p}}}(E'_{\bar{p}} \rightarrow E_{\bar{p}}) n_{\text{H}} \beta'_{\bar{p}} \psi_{\bar{p}}(r, E'_{\bar{p}}) dE'_{\bar{p}} \\ &- \sigma_{\bar{p}\text{H}\rightarrow\bar{p}\text{X}}(E_{\bar{p}}) n_{\text{H}} \beta_{\bar{p}} \psi_{\bar{p}}(r, E_{\bar{p}}) , \end{aligned} \quad (14)$$

where the inelastic and non-annihilating differential cross section in this expression can be approximated by $d\sigma_{\bar{p}\text{H}\rightarrow\bar{p}\text{X}}/dE_{\bar{p}} \simeq \sigma_{\bar{p}\text{H}\rightarrow\bar{p}\text{X}}/T'_{\bar{p}}$. This parameterization can be improved by using the Anderson prescription [17] as described in [18, 19]. In relation (14), the initial antiproton kinetic energy is denoted by $T'_{\bar{p}}$. In order to take into account elastic scatterings on helium, one simply has to replace the hydrogen density by $n_{\text{H}} + 4^{2/3} n_{\text{He}}$.

The antiproton background and DM signal are reliably computed with the Bessel expansion approach. This method encodes directly the presence of radial boundaries for the magnetic halo. The full expression for the master equation describing the Bessel transformed antiproton distribution function $\bar{P}_i(z, E)$ may be expressed as

$$\begin{aligned} \partial_z(V_C \bar{P}_i) - K \partial_z^2 \bar{P}_i + K \left\{ \frac{\alpha_i^2}{R^2} \right\} \bar{P}_i \\ + 2h \delta(z) \partial_E \{ b^{\text{loss}}(E) \bar{P}_i - K_{EE}(E) \partial_E \bar{P}_i \} = \\ - 2h \delta(z) \Gamma_{\bar{p}}^{\text{ann}} \bar{P}_i + Q_{\bar{p},i}^{\text{prim}}(z, E) + 2h \delta(z) \{ Q_{\bar{p},i}^{\text{sec}} + Q_{\bar{p},i}^{\text{ter}} \} . \end{aligned} \quad (15)$$

The various source terms have been specified above. Annihilations of antiprotons take place inside the Galactic disk. This is also true for the production of secondary and tertiary antiprotons. All those processes involve the ISM. We have already mentioned, as a side remark on equation (7), that energy losses and diffusive reacceleration are also confined inside the Galactic disk. The approximation of infinitely thinness for the disk leads to the effective term $2h\delta(z)$ in the above expression. Integrating it through the infinitely thin disk, along the vertical axis z , leads finally to a diffusion equation in energy which the Bessel

transforms $\bar{P}_i(0, E)$ fulfill

$$\begin{aligned} \bar{\mathcal{A}}_i \bar{P}_i(0, E) + 2h \partial_E \{ b^{\text{loss}}(E) \bar{P}_i(0, E) - K_{EE}(E) \partial_E \bar{P}_i(0, E) \} = \\ 2h \{ Q_{\bar{p},i}^{\text{sec}} + Q_{\bar{p},i}^{\text{ter}} \} + 2 \int_0^L dz Q_{\bar{p},i}^{\text{prim}}(z, E) e^{-\frac{V_C z}{2K}} \mathcal{F}_i(z) . \end{aligned} \quad (16)$$

The coefficients $\bar{\mathcal{A}}_i$ which appear in the above expression are given by

$$\begin{aligned} \bar{\mathcal{A}}_i(E) = V_C + 2h \Gamma_{\bar{p}}^{\text{ann}}(E) + K(E) S_i \coth \left\{ \frac{S_i L}{2} \right\} \\ \text{where } S_i^2 = (V_C/K)^2 + (2\alpha_i/R)^2 , \end{aligned} \quad (17)$$

while the vertical functions $\mathcal{F}_i(z)$ are defined as

$$\mathcal{F}_i(z) = \sinh \left\{ \frac{S_i}{2} (L - z) \right\} / \sinh \left\{ \frac{S_i}{2} L \right\} . \quad (18)$$

For each Bessel order i , the integro-differential equation (16) is solved following the procedure explained in the appendix B of [20]. Evolving in time an initial burst with the help of a semi-implicit Crank-Nicholson scheme allows to check the convergence of that procedure. The tertiary component is computed by re-injecting several times the total antiproton yield $\psi_{\bar{p}}$ in the integral over energy of relation (14). Convergence is reached very rapidly.

3.2. Antiproton background and signal

The spallations of interstellar H and He by cosmic ray primaries, essentially protons and alpha particles, produce an irreducible background of secondary antiprotons inside which the signal from DM species is hidden. The precise determination of this background is crucial in order to disentangle a possible WIMP signature. The semi-analytic treatment of CR propagation which has been discussed in section 2, and which is based on the Bessel expansion (6), is a convenient framework to derive the theoretical uncertainties associated to the various parameters at stake, namely K_0 , δ , V_a , V_C and the DH half-thickness L . The space of these propagation parameters has been extensively scanned [9] in order to select the allowed regions where the predictions on B/C, a typical CR secondary to primary ratio, match the observations. Several hundreds of different propagation models have survived that test. The propagation parameters are thus only loosely constrained by the CR nuclei abundances so far observed. The yellow band presented in each of the figures of this section is actually the envelope of the secondary antiproton spectra computed with the set of those $\sim 1,600$ different propagation models found in [9] to pass the B/C test. This band comprises the theoretical uncertainty in the determination of the secondary antiproton flux. It is confined by the MIN and MAX configurations of table 1. As a first observation, notice how narrow the uncertainty strip is between ~ 10 and 100 GeV. In spite of this, the theoretical predictions are in remarkable agreement with the recent antiproton measurements [24] of

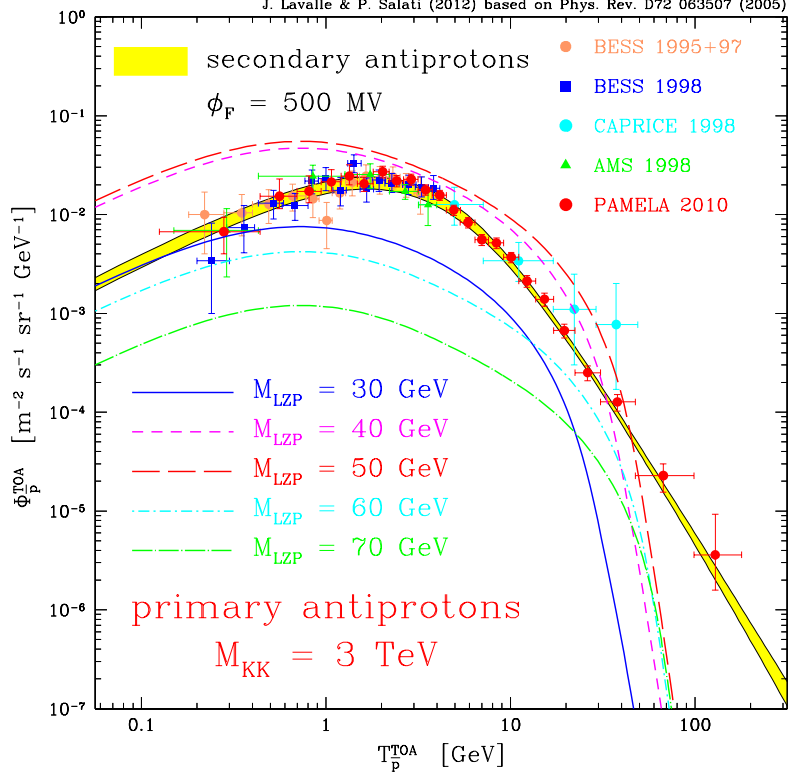


Figure 2: The astrophysical antiproton background lies within the yellow band whose thickness indicates the theoretical uncertainty arising from CR propagation. This band actually encompasses the secondary antiproton yields computed for more than 1,600 different sets of CR propagation parameters, all compatible with the B/C ratio. The primary antiproton fluxes are produced by the annihilation of a Kaluza-Klein WIMP that appears in the higher dimensional warped Grand Unified Theories of [21, 22]. The mass of that DM species (dubbed LKP) has been varied from 30 to 70 GeV with a Kaluza-Klein scale M_{KK} of 3 TeV. When the LKP mass is close to $M_{Z^0}/2$, the annihilation becomes resonant and the primary signal may even exceed the background. The MAX diffusion parameters of table 1 have been used for the LKP antiproton spectra, with a canonical isothermal DM distribution. This figure has been borrowed from [23].

the PAMELA collaboration. These span 4 orders of magnitude between 1 and 100 GeV. At higher energies, the yellow band widens as a result of the energy dependence of the diffusion coefficient K . We expect antiproton propagation to be dominated by pure diffusion in that energy range. A very crude approximation for the antiproton Green function is obtained in the limit where the DH is

infinite and may be expressed as

$$G_{\bar{p}}(\mathbf{x}_{\odot} \leftarrow \mathbf{x}_S) \equiv \frac{1}{4\pi K(E)} \frac{1}{r_{\oplus}} , \quad (19)$$

where r_{\oplus} denotes the distance between the Earth and the source. The antiproton flux is expected to scale as $\Phi_{\bar{p}}/K(E) \propto E^{-\alpha-\delta}$, where α is the spectral index of the proton flux at high energies. From the B/C analysis, the spectral index δ of the diffusion coefficient K may take any value between 0.46 and 0.85. Its spread $\Delta\delta = 0.4$ translates for the antiproton flux into a factor of 3 of uncertainty at 1 TeV. Notice that PAMELA and AMS-02 will considerably improve the measurements of the CR nuclei abundances, with a determination of the B/C ratio to a better accuracy and over a wider energy range than available so far. This will translate into improved constraints on the propagation parameters and eventually into a thinner uncertainty yellow strip for the antiproton astrophysical background.

The antiproton signal from annihilating DM species leads to a primary component directly produced throughout the DH. It depends on many unknown ingredients as is clear from relation (2). The annihilation cross section $\langle\sigma_{\text{ann}}v\rangle$ at freeze-out is related to the WIMP cosmological relic abundance through

$$\Omega_{\chi} h^2 \simeq \frac{3 \times 10^{-27} \text{ cm}^3 \text{ s}^{-1}}{\langle\sigma_{\text{ann}}v\rangle} . \quad (20)$$

A value of $\Omega_{\text{DM}} \sim 0.21$ translates into a typical WIMP annihilation cross section of order $3 \times 10^{-26} \text{ cm}^3 \text{ s}^{-1}$. Although this is strictly true only at decoupling, we can keep in mind that value as a benchmark (see below though). The antiproton spectrum $f(E)$ at the source is also model dependent. Antiprotons are generated through quark or gauge boson jets. Since the WIMPs are at rest in the Galactic frame, the antiproton spectrum tends to flatten at low energy. The production of tertiary antiprotons leading to the same effect, we do expect a flat spectrum below a few GeV, whatever the production mechanism. The primary and secondary fluxes displayed in Fig. 2 and 3 have actually fairly similar spectra at low energy. The WIMP mass is a key ingredient. The production rate q_{DM} scales as m_{χ}^{-2} . The largest DM antiproton signals are generally expected in the case of light DM candidates. For illustration, we have selected among the realm of possible DM candidates a particular Kaluza-Klein WIMP which appears in the context of higher dimensional warped Grand Unified Theories [21, 22]. In these models, a stable KK fermion can arise as a consequence of imposing proton stability in a way very reminiscent of R-parity stabilizing the lightest supersymmetric particle in supersymmetric models. The symmetry is called Z_3 and the Lightest Z_3 Particle (LZP) is stable since it cannot decay into standard model particles. It is actually identified with a KK Dirac right-handed (RH) neutrino with a mass in the 1 GeV to 1 TeV range. This RH neutrino has gauge interactions in particular with additional KK Z' gauge bosons. Nevertheless, its interactions with ordinary matter are feeble because they involve heavy gauge bosons with a mass $M_{\text{KK}} \gtrsim 3 \text{ TeV}$. The primary antiproton flux at

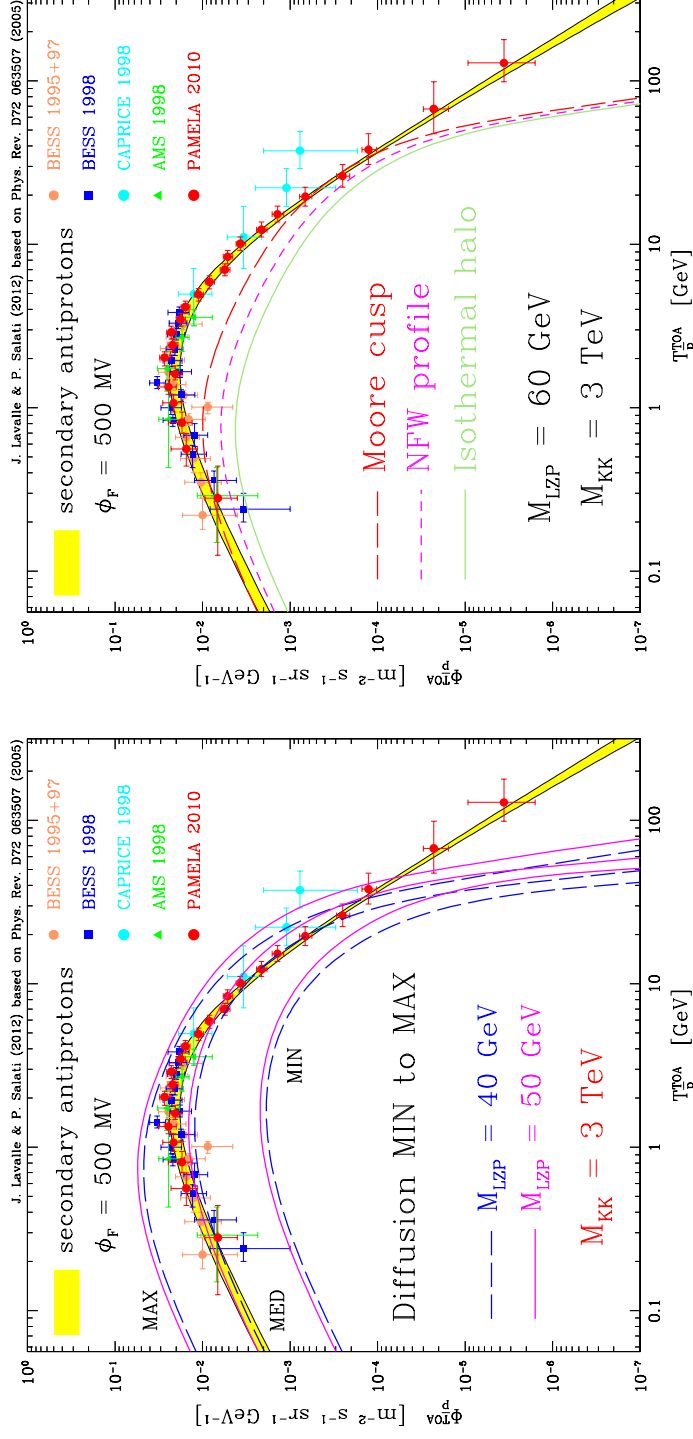


Figure 3: **Left panel** – When the diffusion parameters are varied over the entire domain found to be compatible with the B/C ratio, antiproton primary fluxes span two orders of magnitude while the secondary component lies within the much narrower yellow band. The case of a resonant LZP has been featured here with $M_{\text{LZP}} = 40$ (blue dashed) and 50 GeV (solid magenta). A canonical isothermal DM distribution has been assumed. The LZP signal is well below the background in the case of the MIN model of table 1. **Right panel** – The effect of the Galactic DM halo profile is investigated. The mass of the LZP has been set equal to $M_{\text{LZP}} = 60$ GeV with a Kaluza-Klein scale M_{KK} of 3 TeV. The more divergent and concentrated the LZP distribution at the center of the Milky Way, the larger the antiproton yield. That effect is particularly acute in this plot where the MAX propagation parameters have been assumed. These figures have been borrowed from [23].

the top of the atmosphere (TOA) is plotted in Fig. 2 as a function of antiproton kinetic energy for five different values of the LZP mass. The most optimistic Galactic diffusion scheme MAX as well as a canonical isothermal Galactic DM halo have been assumed for the primary signal. The curves corresponding to $M_{\text{LZP}} = 40$ (short dashed magenta) and 50 GeV (long dashed red) exceed the background and should have already led to a detection would our assumptions on Galactic diffusion and halo profile be correct. For $M_{\text{LZP}} = M_{Z^0}/2$, the LZP annihilation is actually driven by the Z -resonance and is significantly enhanced.

The antiproton DM signal is more sensitive to Galactic CR propagation than the secondary component. The latter is generated through the interactions of CR protons and helium nuclei with the ISM, a process quite similar to the production of boron through the spallation of carbon or nitrogen nuclei impinging on interstellar gas. Although the subnuclear processes at stake are different, secondary antiprotons share a few similarities with boron nuclei. In particular, the production site is the Galactic disk in both cases. It is no surprise then if the yellow band of uncertainty is so narrow once the B/C constraint has been taken into account. Such is not the case for the antiproton DM signal which is produced all over the magnetic halo, in regions far away from the disk. We do expect then a larger variance for that signal than for the background as the CR propagation parameters are varied over the range allowed by the B/C measurements. In the left panel of Fig. 3, the primary antiproton flux produced by a 40 or 50 GeV LZP species decreases by two orders of magnitude between the most optimistic (MAX) and the most pessimistic (MIN) diffusion cases of table 1. In the last configuration, the antiproton signal is now well below the background.

The distribution of DM inside galaxies is still an open question. From one side, results from cosmological N-body simulations in Λ -CDM models [25, 26] indicate a universal and coreless DM density profile. At small radii, the DM density diverges with the distance r from the Galactic center as $r^{-\gamma}$, with $\gamma \sim 1$ to 1.5. Other results, also obtained from simulations of halo formation, strongly disfavour a singularity as steep as 1.5 and seem to point toward slopes logarithmically dependent on the distance from the Galactic center and no steeper than ~ 1.2 [27, 28]. On the other side, several analyses of rotational curves observed for galaxies of different morphological types [29, 30] put serious doubts on the existence of DM cusps in the central regions of the considered objects. Instead of a central singularity, these studies rather suggest a cored DM distribution, flattened toward the central regions. The DM profile inside the Milky Way can be parameterized by the generic distribution

$$\rho(r) = \rho_{\odot} \left\{ \frac{r_{\odot}}{r} \right\}^{\gamma} \left\{ \frac{1 + (r_{\odot}/a)^{\alpha}}{1 + (r/a)^{\alpha}} \right\}^{(\beta-\gamma)/\alpha}, \quad (21)$$

where $r_{\odot} = 8.5$ kpc is the distance of the solar system from the Galactic center. The local DM density has been set equal to $\rho_{\odot} = 0.3 \text{ GeV cm}^{-3}$ — note that this canonical value is slightly lower than more recent estimates made in *e.g.* Refs. [31, 32, 33, 34], which agree on a central value around 0.4 GeV/cm^{-3} . In the case of the pseudo-isothermal profile [35], the typical length scale a is

the radius of the central core. The profile indices α , β and γ for the DM distributions considered in Fig. 2 and 3 are indicated in table 2. As is clear in

Halo model	α	β	γ	a [kpc]
Cored isothermal [35]	2	2	0	4
Navarro, Frenk & White [25]	1	3	1	25
Moore [26]	1.5	3	1.3	30

Table 2: Dark matter distribution profiles in the Milky Way.

the right panel of Fig. 3, where the case of a 60 GeV LZP is considered, the Galactic DM distribution $\rho(\mathbf{x})$ is also a source of uncertainty in the calculation of the antiproton DM signal. The MAX set of CR propagation parameters, which has been assumed in that example, makes it possible for primary antiprotons produced at the central Galactic cusp to reach the solar circle. The degeneracy among the various DM distributions is not lifted if the MIN propagation model replaces the MAX configuration. In that case, the three colored curves are one and the same.

Because the astrophysical background of secondary antiprotons is well under control once the B/C constraint is taken into account, antiprotons offer a unique probe of the presence of annihilating DM species within the Galactic halo. This is especially true for light candidates. The DM signal is expected to be the strongest in that case. As a matter of fact, recent observations collected by the direct detection experiments CDMS-II [36] and CoGENT [37] are compatible with a light WIMP with mass around 10 GeV. Should such a particle couple preferentially to quarks, it would generate a sizable amount of antiprotons at low energy, and would be excluded by observations as shown in [38]. A light neutralino arises in supersymmetric extensions of the standard model with an extra gauge singlet superfield. Generic models embedding an additional Majorana fermion associated to two new scalar fields are constrained by antiprotons, although some regions of the parameter space still pass the test [39].

The annihilation rate of a heavy WIMP is suppressed by a factor of m_χ^{-2} . The antiproton DM signal is hidden in the background, unless the annihilation cross section $\langle\sigma_{\text{ann}}v\rangle$ is abnormally large. This situation may happen in supersymmetric models where the neutralino is almost a pure Wino, as expected for example in anomaly mediated supersymmetry breaking (AMSB) scenarios [40]. For Winos, the preferred mass from relic density requirements is peaked at about 1.7 TeV [41]. Non-perturbative binding energy effects then result in greatly enhanced annihilation cross sections today, when the neutralinos have very small Galactic velocities [42, 43]. In this limit, heavy Winos annihilate almost exclusively into gauge bosons. The case of a heavy Wino particle is featured in Fig. 4. The annihilation cross section today $\langle\sigma_{\text{ann}}v\rangle$ is equal to $1.02 \times 10^{-24} \text{ cm}^3 \text{ s}^{-1}$ [13], well above the decoupling value. That species anni-

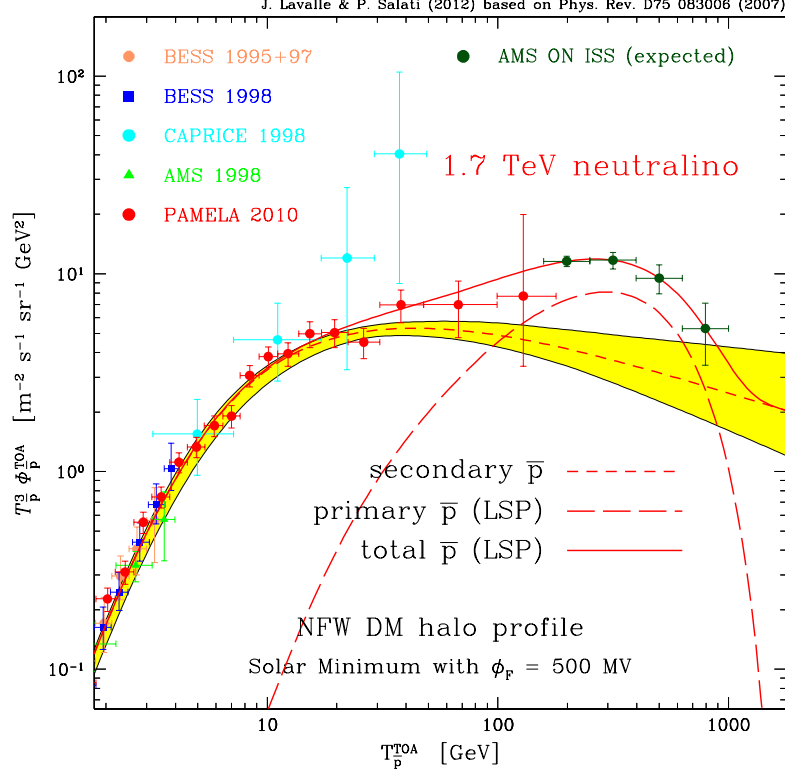


Figure 4: The yellow band features the expected antiproton background for the full range of diffusion parameters allowed by the B/C ratio. A heavy WIMP is also considered. This DM species is almost a pure Wino and its annihilation cross section is significantly enhanced today by non-perturbative, binding energy effects. The corresponding primary (long dashed) and total (solid) fluxes have been derived for a NFW halo profile and for the MED set of diffusion parameters. For illustration, a global boost factor of 2 has also been included in the signal. The antiproton flux is compared to several measurements, whereas the expected statistical error after 3 years of data sampling by AMS-02 is indicated. This plot has been borrowed from [13].

hilate predominantly into W^+W^- (79.9%) and ZZ (20.1%) gauge boson pairs. For illustration, a global boost factor of 2 has also been included in the DM signal. The three last PAMELA data (red) points lie just between the astrophysical background (yellow band) and the predicted signal (red solid). The error bars are sufficiently large to still allow the presence of a 1.7 TeV Wino-like species in the Galactic halo, although the pure astrophysical explanation is perfectly compatible with the measurements. The AMS-02 experiment is now on board the ISS, and its large acceptance and impressive statistics should allow to disentangle both possibilities, as indicated by the theoretical dark-green data

points.

4. The PAMELA positron excess

The confirmation by the PAMELA collaboration [44] of a positron excess above 10 GeV has been triggering a lot of excitement in the field of particle astrophysics since its announcement three years ago. This excess has been readily considered as the first long waited hint of the presence of WIMPs in our Galaxy. However, the DM candidates which can potentially lead to this positron anomaly must have quite special properties. They are also severely constrained by radio and gamma-ray observations, unless they are tightly packed inside improbable or bizarre clumps. These species could also be unstable with abnormally long lifetimes. In order to reach any conclusion, we need to investigate how positrons (and electrons) propagate throughout the DH and we must calculate the astrophysical background to the PAMELA signal. Although this positron excess could be generated by annihilating or decaying DM particles, William of Ockham would warn us that a more natural explanation is to be found in pulsars for instance, and that *entia non sunt multiplicanda praeter necessitatem*.

4.1. Positron propagation and associated Green function

The propagation of CR positrons in the magnetic halo of the Galaxy differs from that of nuclei in several respects. Although space diffusion is still an essential ingredient common to all CR species, positrons undergo mostly inverse Compton and synchrotron energy losses, as discussed in [45] for instance, whereas nuclei and antinuclei are mostly sensitive to the Galactic wind and to nuclear interactions as they cross the Milky Way disk. As a result, a positron line injected by a source leads to an extended positron spectrum once propagated. This is at variance with most of nuclear species for which energy losses can be neglected in a first approximation. Consequently, the diffusion equation that relates the positron space and energy density ψ to the source term $q(\mathbf{x}, E)$ takes the form

$$- K_0 \left(\frac{E}{E_0} \right)^\delta \Delta \psi + \frac{\partial}{\partial E} \{ b^{\text{loss}}(E) \psi \} = q(\mathbf{x}, E) . \quad (22)$$

The first term is simply the diffusion coefficient written as $K(E) \approx K_0(E/E_0)^\delta$, where $E_0 \equiv 1$ GeV will be used hereafter to keep track of the correct units. The synchrotron and inverse Compton processes lead to energy losses with the rate

$$b^{\text{loss}}(E) \equiv \frac{dE}{dt} = - \frac{E_0}{\tau_E} \epsilon^2 , \quad (23)$$

where $\epsilon = E/E_0$ is the reduced positron energy. The energy loss timescale τ_E is set equal to 0.6×10^{16} s. The master equation (22) can be solved with Baltz & Edsjö [46] clever trick which consists in translating the energy E into the pseudo-time

$$\tilde{t}(E) = \tau_E \times \left\{ v(E) = \frac{\epsilon^{\delta-1}}{1-\delta} \right\} . \quad (24)$$

In this formalism, the energy losses which positrons experience boil down to a mere evolution in the pseudo-time \tilde{t} and the diffusion equation (22) simplifies into the well-known heat equation

$$\frac{\partial \tilde{\psi}}{\partial \tilde{t}} - K_0 \Delta \tilde{\psi} = \tilde{q}(\mathbf{x}, \tilde{t}) . \quad (25)$$

The positron density is now $\tilde{\psi} = \epsilon^2 \psi$ whereas the positron production rate has become $\tilde{q}_{e^+} = \epsilon^{2-\delta} q_{e^+}$. Both $\tilde{\psi}$ and \tilde{q} have the same dimensions as before, because ϵ is a dimensionless variable. The Green function \tilde{G} of the heat equation (25) leads to the positron propagator through

$$G_{e^+}(\mathbf{x}, E \leftarrow \mathbf{x}_S, E_S) = \frac{\tau_E}{E_0 \epsilon^2} \tilde{G}(\mathbf{x}, \tilde{t} \leftarrow \mathbf{x}_S, \tilde{t}_S) , \quad (26)$$

where the connection between the energy E and pseudo-time \tilde{t} is given by relation (24). We are led to express the density of positrons resulting from their transport within the Milky Way as the convolution

$$\psi_{e^+}(\mathbf{x}, E) = \int_{E_S=E}^{E_S=+\infty} dE_S \int_{\text{DH}} d^3 \mathbf{x}_S G_{e^+}(\mathbf{x}, E \leftarrow \mathbf{x}_S, E_S) q_{e^+}(\mathbf{x}_S, E_S) , \quad (27)$$

recovering thus the generic expression (8). The positron propagator $G_{e^+}(\mathbf{x}, E \leftarrow \mathbf{x}_S, E_S)$ measures the probability for a positron injected at \mathbf{x}_S with energy E_S to reach the location \mathbf{x} with the degraded energy $E \leq E_S$. In the 3D limiting case of an infinite magnetic halo, the heat Green function connecting the source \mathbf{x}_S to the Earth is the Gaussian distribution

$$\tilde{G}(\mathbf{x}_\odot, \tilde{t} \leftarrow \mathbf{x}_S, \tilde{t}_S) = \Theta(\tilde{\tau}) \left\{ \frac{1}{4\pi K_0 \tilde{\tau}} \right\}^{3/2} \exp \left\{ -\frac{r_\oplus^2}{4 K_0 \tilde{\tau}} \right\} , \quad (28)$$

where $\tilde{\tau} = \tilde{t} - \tilde{t}_S$ is the typical duration, including the diffusion process, over which the positron energy decreases from E_S to E . The distance between the Earth and the source is denoted by

$$r_\oplus = \{(x_\odot - x_S)^2 + (y_\odot - y_S)^2 + (z_\odot - z_S)^2\}^{1/2} . \quad (29)$$

The radial behavior of the heat propagator (28) suggests to define the characteristic diffusion length $\lambda_D = \sqrt{4K_0 \tilde{\tau}}$ which sets the scale of the positron sphere, *i.e.*, the region where most of the positrons detected at the Earth are produced. It depends on the injected E_S and detected E positron energies through the pseudo-time difference $\tilde{\tau}$. Above GeV energies, λ_D is typically smaller than 5 kpc. Most of the positrons detected by high-energy experiments like PAMELA have a local origin.

The magnetic halo is nevertheless finite, with radial and vertical boundaries. Taking into account the former requires to use an expansion over Bessel functions as explained in [47]. However, in most situations, it is safe to ignore the radial boundaries and to picture the DH as an infinite slab with half-thickness

L . Sources located beyond $R = 20$ kpc should be disregarded though, since the convolution (27) is only performed over the DH. The infinite slab hypothesis allows the radial and vertical directions to be disentangled and the reduced propagator \tilde{G} may be expressed as

$$\tilde{G}(\mathbf{x}, \tilde{t} \leftarrow \mathbf{x}_S, \tilde{t}_S) = \frac{\Theta(\tilde{\tau})}{4\pi K_0 \tilde{\tau}} \exp\left\{-\frac{r^2}{4K_0 \tilde{\tau}}\right\} \tilde{V}(z, \tilde{t} \leftarrow z_S, \tilde{t}_S) \quad , \quad (30)$$

where $\tilde{\tau} = \tilde{t} - \tilde{t}_S$ as before. The radial distance between the source \mathbf{x}_S and the point \mathbf{x} of observation is now defined as $r = \{(x_\odot - x_S)^2 + (y_\odot - y_S)^2\}^{1/2}$. The vertical boundary conditions need to be implemented. Wherever the source inside the slab, the positron density vanishes at $z = \pm L$.

(i) A first approach relies on the method of the so-called electrical images and has been discussed in [46]. Any point-like source inside the slab is associated to the infinite series of its multiple images through the boundaries, at $z = \pm L$, which act as mirrors. The n -th image is located at $z_n = 2nL + (-1)^n z_S$, and has a positive or negative contribution depending on whether n is even or odd. When the diffusion time $\tilde{\tau}$ is small, the vertical function \tilde{V} is well approximated by its infinite 1D limit

$$\tilde{V}(z, \tilde{t} \leftarrow z_S, \tilde{t}_S) \simeq \mathcal{V}_{1D}(z, \tilde{t} \leftarrow z_S, \tilde{t}_S) = \frac{\Theta(\tilde{\tau})}{\sqrt{4\pi K_0 \tilde{\tau}}} \exp\left\{-\frac{(z - z_S)^2}{4K_0 \tilde{\tau}}\right\} \quad . \quad (31)$$

A relevant parameter is the ratio $\zeta = L^2/(4K_0\tilde{\tau}) \equiv L^2/\lambda_D^2$. In the regime where it is much larger than 1, the propagation is insensitive to the vertical boundaries. On the contrary, when ζ is much smaller than 1, a large number of images needs to be taken into account in the sum

$$\tilde{V}(z, \tilde{t} \leftarrow z_S, \tilde{t}_S) = \sum_{n=-\infty}^{+\infty} (-1)^n \mathcal{V}_{1D}(z, \tilde{t} \leftarrow z_n, \tilde{t}_S) \quad , \quad (32)$$

and convergence may be a problem.

(ii) It is fortunate that a quite different approach is possible in that case. The 1D version of equation (25) actually looks like the Schrödinger equation (though in imaginary time) that accounts for the behavior of a particle inside an infinitely deep 1D potential well extending from $z = -L$ to $z = +L$. The eigenfunctions of the associated Hamiltonian are given by

$$\varphi_n(z) = \sin\{k_n(L - |z|)\} \text{ (even)} \quad \text{and} \quad \varphi'_n(z) = \sin\{k'_n(L - z)\} \text{ (odd)} \quad . \quad (33)$$

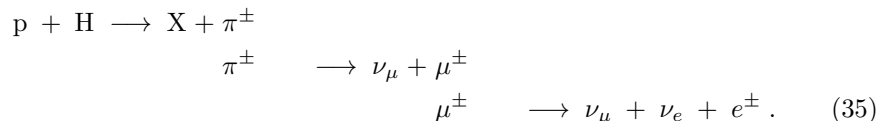
They depend on the vertical coordinate z through the wave-vectors $k_n = (n - 1/2)\pi/L$ (even) and $k'_n = n\pi/L$ (odd). The vertical propagator may be expanded as the series

$$\tilde{V}(z, \tilde{t} \leftarrow z_S, \tilde{t}_S) = \sum_{n=1}^{+\infty} \frac{1}{L} \left\{ e^{-\lambda_n \tilde{\tau}} \varphi_n(z_S) \varphi_n(z) + e^{-\lambda'_n \tilde{\tau}} \varphi'_n(z_S) \varphi'_n(z) \right\} \quad , \quad (34)$$

where the time constants λ_n and λ'_n are respectively equal to $K_0 k_n^2$ and $K_0 k_n'^2$. In the regime where ζ is much smaller than 1, *i.e.*, for very large values of the diffusion time $\tilde{\tau}$, just a few eigenfunctions need to be considered in order for the sum (34) to converge. Notice finally that the energies E and E_S always come into play in the reduced propagator \tilde{G} through the diffusion length λ_D .

4.2. The background of secondary positrons

Like for antiprotons, an irreducible background of secondary positrons is produced by primary CR nuclei colliding on the ISM. The dominant mechanism is the collision of protons with hydrogen atoms at rest, producing charged pions π^\pm which decay into muons μ^\pm . These are also unstable and eventually lead to electrons and positrons through the chain



In proton-proton collisions, pions can be produced in two different ways, depending on the energy E_p of the incoming proton. Below ~ 3 GeV, one of the protons is predominantly excited to a Δ^+ resonance which subsequently decays into a nucleon and a pion. As isospin is conserved, the branching ratios into $\text{p} + \pi^0$ and $\text{n} + \pi^+$ are respectively equal to $2/3$ and $1/3$. Above ~ 7 GeV, the pion production (35) is well described in the framework of the scaling model. Various parameterizations are given in the literature [48, 12] for the Lorentz invariant pion production cross section $E_\pi (d^3\sigma/d^3p_\pi)$. Positrons may also be produced through kaons generated in proton-proton collisions. In a first chain of reactions, the kaon plays the same role as the pion in the set of decays (35). The branching ratio of the $K^\pm \rightarrow \nu_\mu + \mu^\pm$ decay channel is 63.5%. The kaon may also decay into a pair of pions, through the reaction $K^\pm \rightarrow \pi^0 + \pi^\pm$, with a branching ratio of 21%. The charged pion π^+ subsequently follows the chain (35) and yields a positron. These two main kaon decay modes contribute together a few percent to the total positron production differential cross section. Parameterizations of kaon production in proton-proton interactions can also be found in [12, 48] for the scaling regime. Useful parametric expressions for the yield and spectra of stable secondary species produced in proton-proton collisions have been derived from experimental data and summarized in [49]. Primary CR protons induce a production of positrons whose rate, per unit of volume and energy, is given by the integral over proton energy

$$q_{e^+}^{\text{sec}}(\mathbf{x}, E_e) = 4 \pi n_{\text{H}}(\mathbf{x}) \int \Phi_{\text{p}}(\mathbf{x}, E_p) \times dE_p \times \frac{d\sigma}{dE_e}(E_p \rightarrow E_e) . \quad (36)$$

As in the case of antiprotons, this relation can be generalized in order to incorporate CR alpha particles as well as interstellar helium. The positron production rate $q_{e^+}^{\text{sec}}(\mathbf{x}, E_e)$ can be approximated by its solar value since most of the

positrons detected at the Earth originate from the solar neighborhood. Folding that rate in relation (27) yields the flux

$$\Phi_{e^+}^{\text{sec}}(\odot, \epsilon \equiv E_e/E_0) = \frac{\beta_{e^+}}{4\pi} \times \frac{\tau_E}{\epsilon^2} \times \int_{\epsilon}^{+\infty} d\epsilon_S \times \tilde{I}(\lambda_D) \times q_{e^+}^{\text{sec}}(\odot, \epsilon_S) \quad . \quad (37)$$

The integral \tilde{I} is the convolution of the reduced positron Green function over the Galactic disk alone

$$\tilde{I}(\lambda_D) = \int_{\text{disk}} d^3 \mathbf{x}_S \tilde{G}(\mathbf{x}_\odot \leftarrow \mathbf{x}_S; \lambda_D) \quad . \quad (38)$$

As regards observations, the ATIC [56], HESS [57, 58] and Fermi [53] collaborations have reported measurements of the total CR electron and positron flux at high energy. The Fermi-LAT instrument, in particular, has collected high precision data between 20 GeV and 1 TeV, which can be fitted by the simple power-law spectrum [59]

$$\Phi_{e^\pm} = \{175.40 \pm 6.09 \text{ GeV}^{-1} \text{ m}^{-2} \text{ s}^{-1} \text{ sr}^{-1}\} \epsilon^{-(3.045 \pm 0.008)} \quad , \quad (39)$$

where $\epsilon = E/E_0$ is the reduced lepton energy. Primary CR electrons are believed to originate from the interstellar medium, like most of the primary CR nuclei, and are accelerated by supernova driven shock waves which inject them with a spectral index $\alpha \sim 2.2 \pm 0.1$ inside the Milky Way disk. They subsequently propagate within the magnetic halo and lose energy. A detailed investigation [60] leads to a CR electron flux at the Earth of the form

$$\Phi_{e^-} \propto \epsilon^{-\alpha - 0.5 - \delta/2} \quad , \quad (40)$$

with a spectral index of order 3.05 ± 0.15 , in reasonable agreement with the Fermi-LAT measurements should $\delta = 0.7$, as indicated by the MED model of table 1. Some authors [61] find that value too high. It suffices then to increase α in order to match the Fermi-LAT observations. The lepton spectrum contains also a small admixture of secondary electrons and positrons, produced by CR primary nuclei impinging on interstellar gas. These spallation reactions generate many charged pions which eventually decay into positrons and, in a lesser extent, into electrons. The source spectral index is set by the CR proton and helium fluxes. With a gross value of $\alpha = 2.7$, we expect a spectral index of 3.55 ± 0.05 for secondary positrons.

The PAMELA collaboration has measured [44] the positron fraction $e^+/(e^- + e^+)$ over a large energy range. From the above mentioned arguments, we would naively expect that fraction to decrease with energy as $\epsilon^{-1/2}$. A more refined analysis [55] confirms that trend, as featured by the banana shape region of Fig. 5. The thickness of the yellow band gauges the uncertainties arising from CR transport. In spite of these, the positron fraction is expected to decrease above 10 GeV. The PAMELA measurements establish on the contrary that the positron fraction increases at high energy. This very important observation is in contradiction with a pure secondary origin for the positrons. Primary sources, which directly inject these particles in the interstellar medium, are necessary.

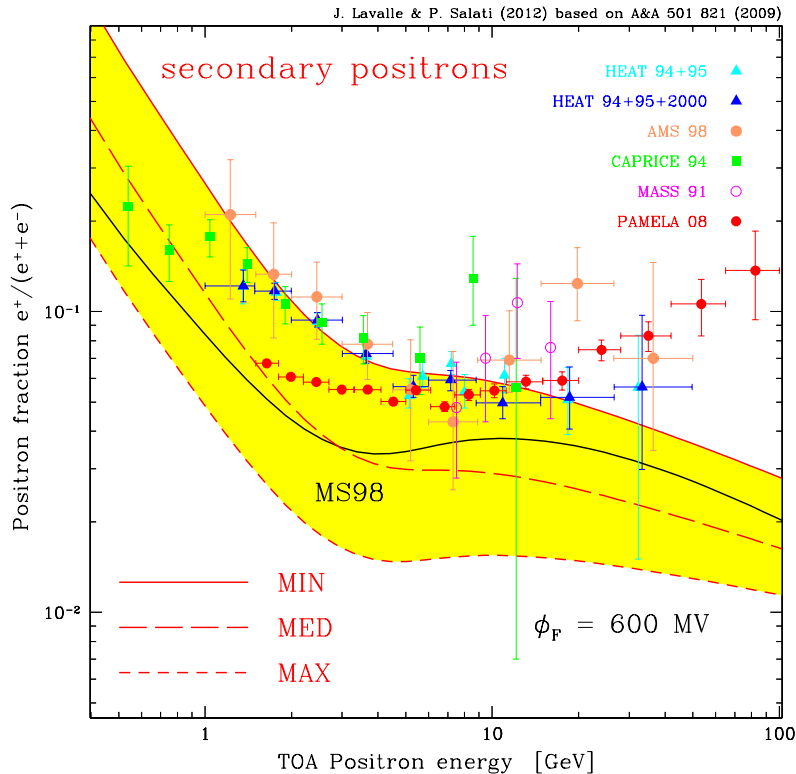


Figure 5: Positron fraction as a function of positron energy. The yellow banana shape region encompasses the astrophysical background of secondary positrons yielded by the 1,600 different configurations of CR propagation parameters, shown in [9] to be compatible with the B/C data. This band is bounded by the MAX (short dashed) and MIN (solid) curves, while the central long-dashed curve stands for the MED model (see table 1). The nuclear cross sections have been parameterized according to [49] whereas the recent PAMELA measurements of the CR proton and helium spectra [50] have been fitted by [51]. In the same figure, the positron fraction obtained with the positron flux calculated by [45] and fitted by [46] is also indicated by the solid black line labeled MS98. The electron and positron flux enters in the denominator of the positron fraction. Measurements from AMS-01 [52] and Fermi-LAT [53] have been parameterized according to [54]. A solar modulation with a Fisk potential of 600 MV has been applied to the positron flux. This corresponds to the level of solar activity during the data taking of AMS-01. This figure has been borrowed from [55].

4.3. The PAMELA excess as a signature for Galactic WIMPs

The announcement of a positron excess by the PAMELA collaboration has triggered a lot of excitement. This excess was actually considered as the first hint of the presence of DM species in the Milky Way halo. Should WIMPs exist, their annihilations would be a source of primary positrons. The production rate

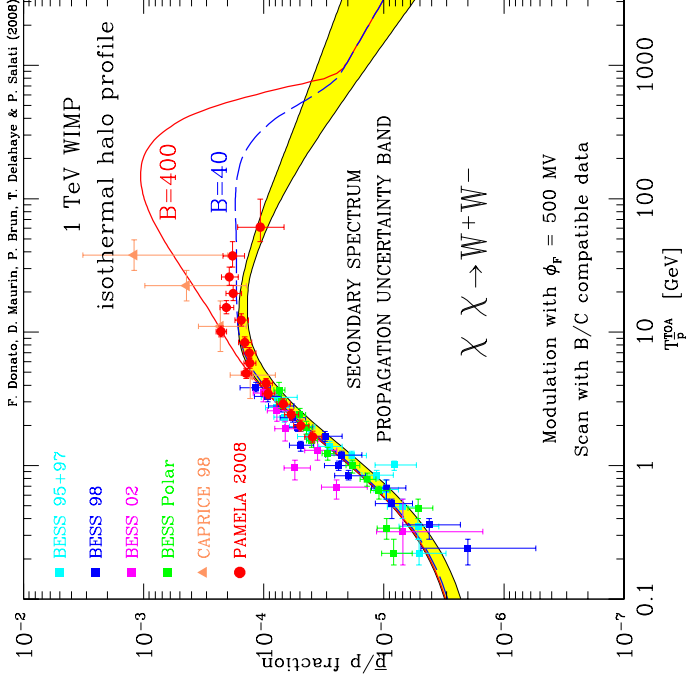


Figure 6: The pedagogical example of a 1 TeV neutralino annihilating into a W^+W^- gauge boson pair is presented. In the left panel, the positron signal which the DM species yield has been increased by a factor of 400, hence the solid curve and a marginal agreement with the PAMELA data. If the so-called Sommerfeld effect [42, 43] is invoked to explain such a large enhancement of the annihilation cross section, the same boost applies to antiprotons, and leads to an unacceptable distortion of their spectrum as indicated by the red solid line in the right panel. The yellow band encompasses the models shown in [9] to be compatible with the B/C data. The antiproton red solid line ($B=400$) lies well above that astrophysical background. Figures and caption are borrowed from [62].

$q_{e^+}^{\text{DM}}$, given by relation (2), yields the positron flux at the Earth

$$\Phi_{e^+}^{\text{DM}}(\odot, \epsilon) = \mathcal{F} \times \frac{\tau_E}{e^2} \times \int_{\epsilon}^{m_\chi/E_0} d\epsilon_S f(\epsilon_S) \tilde{I}_{\text{DM}}(\lambda_D) . \quad (41)$$

The halo integral \tilde{I}_{DM} [47] is the convolution of the reduced positron propagator \tilde{G} with the square of the Galactic DM density

$$\tilde{I}_{\text{DM}}(\lambda_D) = \int_{\text{DH}} d^3\mathbf{x}_S \tilde{G}(\mathbf{x}_\odot \leftarrow \mathbf{x}_S; \lambda_D) \left\{ \frac{\rho(\mathbf{x}_S)}{\rho_\odot} \right\}^2 . \quad (42)$$

The positron excess lies above 10 GeV. It can be generated by a particle with a mass in the range 100 GeV to a few TeV, in good agreement with theoretical expectations for WIMP masses. If the DM species are thermally produced during the big bang, their relic abundance matches the WMAP value [63] of $\Omega_\chi h^2 = 0.1126 \pm 0.0036$ provided that their annihilation cross section, at the time of decoupling, is equal to $\langle \sigma_{\text{ann}} v \rangle \sim 3 \times 10^{-26} \text{ cm}^3 \text{ s}^{-1}$. The energy distribution $f(\epsilon)$ of the positrons produced in a single annihilation event is set by the WIMP type. High energy positrons (and electrons) cannot diffuse on long distances, and those detected at the Earth must have been produced locally, hence a DM density of $\rho_\odot = 0.3 \text{ GeV cm}^{-3}$. Baring in mind these benchmark values, one can estimate $q_{e^+}^{\text{DM}}$ as well as the positron flux $\Phi_{e^+}^{\text{DM}}$. Alas, the signal derived for a large choice of DM candidates, and for various DM Galactic distributions, is way too small to account for the observed excess. For a WIMP mass m_χ of 1 TeV, $q_{e^+}^{\text{DM}}$ needs to be enhanced by a factor of $\sim 10^3$ in order to match the PAMELA measurements, as illustrated in the left panel of Fig. 6.

To save the WIMP explanation of the PAMELA positron anomaly, a first remedy is the possibility that $\langle \sigma_{\text{ann}} v \rangle$ is much larger than what is currently assumed. Three directions at least have been explored so far. To commence, WIMP decoupling in the early universe takes place conventionally during a period of radiation domination. If the universe at that time is dominated by another component, like a scalar field rolling down its potential [64, 65], the expansion rate is significantly increased and the same WIMP relic abundance Ω_χ requires now a much larger annihilation cross section. Another possibility is that WIMPs do not decouple from the primordial plasma. In this class of less natural scenarios, a non-thermal production takes place through the decay of heavier species, like gravitinos or moduli fields [66]. The WIMP relic abundance is no longer determined solely by $\langle \sigma_{\text{ann}} v \rangle$. It also depends on the production rate and lifetime of the unstable heavier states. A final solution relies on the so-called Sommerfeld effect [42, 43]. If the DM species are massive enough and interact through the exchange of a light particle ϕ , they are attracted toward each other at sufficiently low velocities. Their wave functions get focalized at the interaction point so that the annihilation cross section can be significantly enhanced. Scenarios based on that effect have been proposed [67, 68, 69], reviving the idea of secluded dark matter [70]. WIMPs are still thermally produced

in the early universe. Their annihilation cross section at that time is equal to the canonical value of $3 \times 10^{-26} \text{ cm}^3 \text{ s}^{-1}$. As the universe expands, the average WIMP velocity β decreases. The Sommerfeld enhancement sets in as soon as the WIMP kinetic energy is dominated by the interaction energy, *i.e.*, when β no longer exceeds the effective WIMP coupling constant α' . The cross section increases and may be today large enough to account for the PAMELA positron excess. The enhancement saturates when the WIMP de Broglie wavelength $\sim 1/(\beta m_\chi)$ exceeds the range $\sim 1/m_\phi$ of the interaction. This occurs for $\beta \leq m_\phi/m_\chi$. The annihilation cross section is also resonantly increased whenever $\alpha' m_\phi \sim \alpha'^2 m_\chi/n^2$, where n is an integer [71].

Irrespective of the mechanism enhancing $\langle \sigma_{\text{ann}} v \rangle$, WIMPs should not overproduce antiprotons [72, 62]. The annihilation channels leading to antiprotons must be significantly suppressed. The antiproton to proton ratio measured by the PAMELA collaboration [73] does not show actually any excess and is consistent with a pure secondary origin, as featured in the right panel of Fig. 6. Therefore, besides an abnormally large annihilation cross section, DM species preferentially annihilate into charged leptons, a feature which is unusual in supersymmetry, but more typical of Kaluza-Klein theories. From a phenomenological point of view, WIMP annihilations must proceed either directly to lepton pairs or, in some models, through the production of the above mentioned light mediator bosons ϕ which subsequently decay into leptons via

$$\chi + \chi \longrightarrow \phi + \phi \longrightarrow l^+ l^- l^+ l^- . \quad (43)$$

The possibility to explain the PAMELA positron excess by leptophilic DM particles with enhanced annihilation cross section has been extensively investigated. Depending on its magnitude, the injection of high-energy positrons and electrons is associated to clear astrophysical signatures [74]. As they spiral along the Galactic magnetic field lines, these particles produce a radio emission through synchrotron radiation. They also inverse Compton scatter (ICS) photons from the CMB and stellar light. Finally, the charged leptons released by the WIMP annihilations can produce final state radiation photons. After an extensive scan [75, 76, 77] of the various possibilities, the region of the $(m_\chi, \langle \sigma_{\text{ann}} v \rangle)$ plane compatible with the PAMELA and Fermi-LAT measurements is found to be excluded for most of the leptophilic DM candidates. The most stringent limit arises from the synchrotron radio emission produced at the Galactic center, a region where the DM distribution may be cuspy, and where magnetic fields should be strong. That limit weakens considerably, though, as soon as a cored isothermal DM distribution is preferred to the usual Einasto or NFW profile. In that case, leptophilic WIMPs are not excluded by radio observations. A more reliable tool is provided by the ICS of the positrons and electrons produced by WIMP annihilation at high Galactic latitude, a region which is less subject to uncertainties than the center of the Milky Way. A careful investigation [78], performed only in the case where WIMPs annihilate directly into lepton pairs, excludes values of m_χ larger than 1 TeV. Finally, another model independent analysis implies the injection of WIMP annihilation products in the intergalactic medium at redshift ~ 1000 . The recombination process is affected and an

imprint is left on the CMB, which may be searched for in the high precision WMAP data [79]. Most of the PAMELA compatible leptophilic DM candidates still survive that test [80], but will be probed by the Planck mission.

Another way to increase the production rate of DM positrons relies on the existence of substructures inside the smooth DM Galactic distribution. Because $\langle \rho^2(\mathbf{x}) \rangle$ is always larger than $\langle \rho(\mathbf{x}) \rangle^2$, inhomogeneities tend to effectively enhance $q_{e^+}^{\text{DM}}$, a quantity proportional to the square of the DM density $\rho(\mathbf{x})$. How significant is that enhancement depends on the position of the clumps with respect to the smooth component of the DM halo. The inner structure of clumps, as well as their mass distribution, are also key factors. Finally, the lower mass cut-off and the concentration-to-mass relation of the substructures need to be considered. A statistical analysis is mandatory since we live inside one particular realization of the clump distribution, to be taken out of an infinite set of similar realizations. Using the tools specifically forged for computing the odds of that Galactic lottery [81], a comprehensive analysis [82] indicates that the boost factor to be applied to $q_{e^+}^{\text{DM}}$ in the case of a Λ CDM universe cannot exceed at most a factor of 20 at high energy. The correct value is presumably much smaller, *i.e.*, of order unity.

Although a clumpy DM halo does not lead, on average, to an increase of the positron flux at the Earth, the statistical variance of the boost factor is large at high energy, hence the existence of configurations where $q_{e^+}^{\text{DM}}$ could be significantly enhanced. The possibility that a DM clump lies, for instance, in the vicinity of the solar system has been suggested [83, 84] as an explanation for the PAMELA positron anomaly. Such a local substructure would actually outshine the rest of the Galactic DM distribution. Alas, the probability that such a situation occurs in the DM halo of the Milky Way is vanishingly small as demonstrated in an analysis [85] based on the results of the cosmological N-body simulation Via Lactea II [86]. In the favorable case of a 100 GeV DM species annihilating into e^\pm pairs, the PAMELA positron excess is best fitted by a subhalo with annihilation volume

$$\xi \equiv \int_{\text{clump}} \left\{ \frac{\rho(\mathbf{x})}{\rho_\odot} \right\}^2 d^3\mathbf{x} \sim 114 \text{ kpc}^3 , \quad (44)$$

located at 1.22 kpc from the Earth. That configuration has a probability of only 0.37% to occur. Other arrangements are even less probable.

Finally, the possibility of unstable DM candidates with very large lifetimes has also been explored (see for instance [87, 88, 89]). Irrespective of the mechanism which produces them in the early universe, unstable species could in principle generate the PAMELA signal. The production rate (2) can now be written as

$$q_{e^+}^{\text{DM}}(\mathbf{x}) = \tau_{\text{dec}}^{-1} \left\{ \frac{\rho(\mathbf{x})}{m_\chi} \right\} f(\epsilon) , \quad (45)$$

where the quantity $\eta \langle \sigma_{\text{ann}} v \rangle$ (ρ/m_χ) has been replaced by the decay rate τ_{dec}^{-1} . For a 1 TeV WIMP, a lifetime of order 2×10^{26} sec is required to reproduce the positron excess. The synchrotron radio emission from the Galactic center is no

longer a problem, even in the case of a NFW or Einasto profile, since the positron production rate from decaying DM is proportional to the DM density ρ , and not to its square. A detailed analysis [78] excludes however unstable DM as it would unacceptably contribute to the isotropic gamma-ray emission inferred from the Fermi data. This limit does not apply to WIMPs predominantly decaying into muon pairs. The lifetime needs to be fine tuned though. Higher dimension operators must be invoked to explain the large value of τ_{dec} required by PAMELA. If a four-fermion point-like coupling is responsible for the WIMP instability, we anticipate [90] a decay rate $\propto m_\chi^5/M^4$, where M denotes the typical scale of the underlying high-energy theory. If factors of 2 and π are neglected, a GUT mass $M \sim 2.3 \times 10^{16}$ GeV could lead to the required lifetime. Notice that the DM species must also be leptophilic to prevent antiprotons from being overproduced.

The CR lepton anomalies reported three years ago, and the PAMELA positron excess in particular, have triggered a boiling activity in the field of particle astrophysics. The possibility that these signals are produced by WIMPs annihilating or decaying in the Milky Way halo is fading away. The DM explanation is fairly contrived and far from the main stream. The positrons which the DM species are supposed to produce generate in turn radiations which are not seen. As William of Ockham would have pointed out, a more plausible explanation has to be found elsewhere. Actually, a simple one lies in pulsars. These objects are known to exist, and they do inject (primary) positrons in the Galactic disk. The lepton anomalies can be nicely explained by local pulsars and supernova remnants, as pointed out by [91] as well as by a recent and very comprehensive [60] study.

5. Antideuterons or the new challenge

Antideuterons are the nuclei of antideuterium, the element that mirrors deuterium. Although they have been seen in nuclear or lepton interactions at terrestrial accelerators, antideuterons have not yet been detected in the cosmic radiation. A small admixture is nevertheless expected to be astrophysically produced by the spallations of CR protons and helium nuclei on the ISM. Any process that generates at the same time an antiproton and an antineutron could lead to the production of antideuterons. The requisite is the fusion of the antiproton and antineutron pair into an antideuteron. This happens whenever the momenta of the antinucleons are so close to each other that the kinetic energy of the pair, as seen in its rest frame, is of the same order of magnitude as the antideuteron binding energy.

To quantify this effect, let us consider the collisions of CR high-energy protons on hydrogen atoms at rest. The number $d\mathcal{N}_X$ of antiprotons, antineutrons or antideuterons generated in a single reaction, with momenta \mathbf{k}_X , is related to the differential production cross section through

$$d\mathcal{N}_X = \frac{1}{\sigma_{\text{tot}}} d^3\sigma_X(\sqrt{s}, \mathbf{k}_X) , \quad (46)$$

where σ_{tot} denotes the total proton-proton cross section. The total available energy is \sqrt{s} . The corresponding differential probability for the production of the species X is defined as

$$d\mathcal{N}_X = \mathcal{F}_X(\sqrt{s}, \mathbf{k}_X) d^3\mathbf{k}_X . \quad (47)$$

For antiprotons, for instance, it can be expressed in terms of the Lorentz invariant cross section through

$$\sigma_{\text{tot}} E_{\bar{p}} \mathcal{F}_{\bar{p}}(\sqrt{s}, \mathbf{k}_{\bar{p}}) = E_{\bar{p}} \left. \frac{d^3\sigma_{\bar{p}}}{d^3\mathbf{k}_{\bar{p}}} \right|_{\text{LI}} . \quad (48)$$

That cross section is experimentally well-known and a parameterization has been given, for instance, in [14]. Isospin symmetry can be assumed, furthermore, to hold. If so, the production of antineutrons is the same as for antiprotons. The calculation of the probability for the formation of an antideuteron can now proceed in two steps. We first need to estimate the probability for the creation of an antiproton-antineutron pair. Then, the antinucleons merge together to yield an antinucleus of deuterium. As explained in [92], the production of two antinucleons is assumed to be proportional to the square of the production of one of them. The hypothesis that factorization of the probabilities holds is fairly well established at high energies. For spallation reactions, however, the bulk of the antiproton production takes place for an energy $\sqrt{s} \sim 10$ GeV which turns out to be of the same order of magnitude as the antideuteron mass. Pure factorization should break in that case as a result of energy conservation. It needs to be slightly adjusted. Following [92, 93], we may assume that the center of mass energy available for the production of the second antinucleon is reduced by twice the energy carried away by the first antinucleon

$$\mathcal{F}_{\bar{p}, \bar{n}}(\sqrt{s}, \mathbf{k}_{\bar{p}}, \mathbf{k}_{\bar{n}}) = \frac{1}{2} \mathcal{F}_{\bar{p}}(\sqrt{s}, \mathbf{k}_{\bar{p}}) \mathcal{F}_{\bar{n}}(\sqrt{s} - 2E_{\bar{p}}, \mathbf{k}_{\bar{n}}) + (\bar{p} \leftrightarrow \bar{n}) . \quad (49)$$

Once the antiproton and the antineutron are formed, they combine together to give an antideuteron with probability

$$\mathcal{F}_{\bar{D}}(\sqrt{s}, \mathbf{k}_{\bar{D}}) d^3\mathbf{k}_{\bar{D}} = \int d^3\mathbf{k}_{\bar{p}} d^3\mathbf{k}_{\bar{n}} \mathcal{C}(\mathbf{k}_{\bar{p}}, \mathbf{k}_{\bar{n}}) \mathcal{F}_{\bar{p}, \bar{n}}(\sqrt{s}, \mathbf{k}_{\bar{p}}, \mathbf{k}_{\bar{n}}) . \quad (50)$$

The summation is performed on the antinucleon configurations for which $\mathbf{k}_{\bar{p}} + \mathbf{k}_{\bar{n}} = \mathbf{k}_{\bar{D}}$. The coalescence function $\mathcal{C}(\mathbf{k}_{\bar{p}}, \mathbf{k}_{\bar{n}})$ describes the probability for a \bar{p} - \bar{n} pair to yield by fusion an antideuteron. That function depends actually on the difference $\mathbf{k}_{\bar{p}} - \mathbf{k}_{\bar{n}} = 2\mathbf{\Delta}$ between the antinucleon momenta so that relation (50) becomes

$$\mathcal{F}_{\bar{D}}(\sqrt{s}, \mathbf{k}_{\bar{D}}) = \int d^3\mathbf{\Delta} \mathcal{C}(\mathbf{\Delta}) \mathcal{F}_{\bar{p}, \bar{n}}(\sqrt{s}, \mathbf{k}_{\bar{p}} = \frac{\mathbf{k}_{\bar{D}}}{2} + \mathbf{\Delta}, \mathbf{k}_{\bar{n}} = \frac{\mathbf{k}_{\bar{D}}}{2} - \mathbf{\Delta}) . \quad (51)$$

In the center of mass frame of the proton-proton collision, an energy of ~ 3.7 GeV is required to form an antideuteron, to be compared to a binding energy

of $B \sim 2.2$ MeV. The coalescence function is therefore strongly peaked around $\mathbf{\Delta} = \mathbf{0}$ and expression (51) simplifies into

$$\mathcal{F}_{\bar{D}}(\sqrt{s}, \mathbf{k}_{\bar{D}}) \simeq \left\{ \int d^3 \mathbf{\Delta} \mathcal{C}(\mathbf{\Delta}) \right\} \times \mathcal{F}_{\bar{p}, \bar{n}}(\sqrt{s}, \mathbf{k}_{\bar{p}} = \frac{\mathbf{k}_{\bar{D}}}{2}, \mathbf{k}_{\bar{n}} = \frac{\mathbf{k}_{\bar{D}}}{2}) , \quad (52)$$

where the probability for the formation of the \bar{p} - \bar{n} pair has been factored out. The term in brackets may be estimated in the rest frame of the antideuteron through the Lorentz invariant term

$$\int \frac{E_{\bar{D}}}{E_{\bar{p}} E_{\bar{n}}} d^3 \mathbf{\Delta} \mathcal{C}(\mathbf{\Delta}) \simeq \left(\frac{m_{\bar{D}}}{m_{\bar{p}} m_{\bar{n}}} \right) \left(\frac{4}{3} \pi P_{\text{coal}}^3 \right) . \quad (53)$$

In that frame, as already mentioned, the antinucleons merge together if the momentum of the corresponding two-body reduced system is less than some critical value P_{coal} . That coalescence momentum is the only free parameter of this simplistic factorization and coalescence scheme. Theoretical values range from $\sqrt{m_{\bar{p}} B} \sim 46$ MeV, naively derived from the antideuteron binding energy, up to 180 MeV as would follow from a Hulthen parameterization of the deuterium wave function [94]. We therefore expect P_{coal} to lie somewhere in the range between 50 and 200 MeV. Direct comparison with accelerator data yields a phenomenological value of 58 MeV as shown in [92, 93]. A recent upgrade [18, 19] points toward 79 MeV. The Lorentz invariant cross section for the production of antideuterons can now be derived under the form

$$\begin{aligned} E_{\bar{D}} \frac{d^3 \sigma_{\bar{D}}}{d^3 \mathbf{k}_{\bar{D}}} &= \left(\frac{m_{\bar{D}}}{m_{\bar{p}} m_{\bar{n}}} \right) \left(\frac{4}{3} \pi P_{\text{coal}}^3 \right) \times \frac{1}{2 \sigma_{\text{tot}}} \times \\ &\times \left\{ E_{\bar{p}} \frac{d^3 \sigma_{\bar{p}}}{d^3 \mathbf{k}_{\bar{p}}}(\sqrt{s}, \mathbf{k}_{\bar{p}}) \times E_{\bar{n}} \frac{d^3 \sigma_{\bar{n}}}{d^3 \mathbf{k}_{\bar{n}}}(\sqrt{s} - 2E_{\bar{p}}, \mathbf{k}_{\bar{n}}) + (\bar{p} \leftrightarrow \bar{n}) \right\} . \end{aligned} \quad (54)$$

A summation over the production angle θ in the Galactic frame leads to the differential cross section

$$\frac{d\sigma_{\bar{D}}}{dE_{\bar{D}}} \{p(E_p) + H \rightarrow \bar{D}(E_{\bar{D}})\} = 2 \pi k_{\bar{D}} \int_0^{\theta_M} E_{\bar{D}} \frac{d^3 \sigma_{\bar{D}}}{d^3 \mathbf{k}_{\bar{D}}} \Big|_{\text{LI}} d(-\cos \theta) . \quad (55)$$

In that frame, θ denotes the angle between the momenta of the incident proton and produced antideuteron. It is integrated up to a maximal value θ_M set by the requirement that, in the center of mass frame of the reaction, the antideuteron energy $E_{\bar{D}}^*$ cannot exceed the bound

$$E_{\bar{D}, M}^* = \frac{s - 16 m_p^2 + m_{\bar{D}}^2}{2\sqrt{s}} . \quad (56)$$

The integral (55) is performed at fixed antideuteron energy $E_{\bar{D}}^2 = m_{\bar{D}}^2 + k_{\bar{D}}^2$.

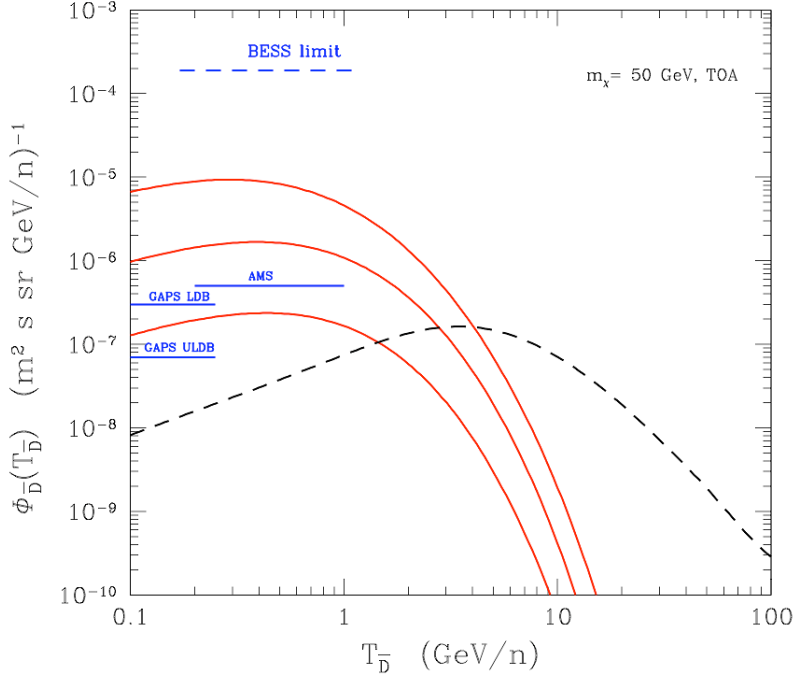


Figure 7: The various contributions to the antideuteron flux at the Earth, modulated at solar minimum, are plotted as a function of kinetic energy per nucleon $T_{\bar{D}}$. The astrophysical background (black dashed line) is generated by the spallations of CR protons and helium nuclei on the ISM. This secondary component is featured for the MED model of table 1. Below a few GeV/n, the interactions of CR antiprotons with the ISM need also to be taken into account. The DM signal (red solid curves) is derived for a $m_\chi = 50$ GeV WIMP and for the three propagation models of table 1. The upper dashed horizontal line features the current BESS upper limit on the search for CR antideuterons. The three horizontal solid (blue) lines are the estimated sensitivities of forthcoming measurements which will be performed by (from top to bottom) AMS-02 [52, 95] and GAPS on a long (LDB) and ultra-long (ULDB) duration balloon flights [96, 97, 98, 99] This figure has been borrowed from [19].

The above factorization and coalescence scheme can also be applied to WIMP annihilation. In that case, the differential multiplicity for antiproton production is expressed as

$$\frac{dN_{\bar{p}}}{dE_{\bar{p}}} = \sum_{F,h} B_{\chi h}^{(F)} \frac{dN_{\bar{p}}^h}{dE_{\bar{p}}} . \quad (57)$$

The annihilation proceeds, through the various final states F, toward the quark or the gluon h with the branching ratio $B_{\chi h}^{(F)}$. Quarks or gluons may be directly produced when DM species self annihilate. They may alternatively result from the intermediate production of a Higgs or gauge boson as well as of a top quark. Each quark or gluon h generates in turn a jet whose subsequent fragmentation

and hadronization yields the antiproton energy spectrum $dN_{\bar{p}}^h/dE_{\bar{p}}$. Because DM particles are at rest with respect to each other, the probability to form, say, an antiproton with momentum $\mathbf{k}_{\bar{p}}$ is essentially isotropic

$$\frac{dN_{\bar{p}}}{dE_{\bar{p}}}(\chi + \chi \rightarrow \bar{p} + \dots) = 4\pi k_{\bar{p}} E_{\bar{p}} \mathcal{F}_{\bar{p}}(\sqrt{s} = 2m_{\chi}, E_{\bar{p}}) . \quad (58)$$

The factorization and coalescence scheme leads to the antideuteron differential multiplicity

$$\frac{dN_{\bar{D}}}{dE_{\bar{D}}} = \left(\frac{4 P_{\text{coal}}^3}{3 k_{\bar{D}}} \right) \left(\frac{m_{\bar{D}}}{m_{\bar{p}} m_{\bar{n}}} \right) \sum_{F,h} B_{\chi^h}^{(F)} \left\{ \frac{dN_{\bar{p}}^h}{dE_{\bar{p}}} \left(E_{\bar{p}} = E_{\bar{D}}/2 \right) \right\}^2 . \quad (59)$$

It may be expressed as a sum, extending over the various quarks and gluons h , as well as over the different annihilation channels F , of the square of the antiproton differential multiplicity. That sum is weighted by the relevant branching ratios. The antineutron and antiproton differential distributions have been assumed to be identical.

The black dashed line of Fig. 7 features the astrophysical contribution to the antideuteron flux at the Earth. It has been derived with the MED model of table 1. Varying the CR propagation parameters does not change much this contribution, with a spread in possible values reaching at most $\pm 40\text{-}50\%$ at energies below 1 GeV/n and decreasing down to $\sim 15\%$ above 10 GeV/n, as shown in [19]. Secondary antideuterons are not much affected by CR propagation uncertainties. We already found a similar trend for secondary antiprotons. Both species are produced by the interactions of primary CR nuclei on the ISM, a process reminiscent of the fragmentation of CR carbon nuclei into boron as they collide on interstellar gas. Constraining CR propagation from the B/C ratio proves to be a powerful mean of predicting the flux of background secondary antiprotons and antideuterons. Such is not the case for the DM signal. The example of a 50 GeV neutralino is presented in Fig. 7 for the three CR propagation configurations of table 1. The spread of the red solid curves reaches now two orders of magnitude. The larger the half-thickness L of the DH, the stronger the signal. The magnetic halo works like a fisher's net inside which the products from DM annihilation are entrapped. As noticed in [93], the DM signal dominates at low energies, below a few GeV/n, over the background. This may potentially help to discriminate it from its astrophysical background, since very few secondary antideuterons are expected in that energy range. Actually, these are produced by energetic CR nuclei impinging upon atoms at rest of the ISM. The center of mass frame of the reaction moves with respect to the Galaxy. Even though a substantial amount of secondary antideuterons are produced with small velocities in this frame, few remain at low energy after the proper boost takes them back to the Galactic frame. On the contrary, DM species annihilate at rest with respect to the Milky Way, hence a dominant contribution of primary antideuterons below a few GeV/n.

A few processes, which were not considered in the exploratory work of [93], have been since then suspected to flatten the spectrum of antideuterons by

replenishing its low energy tail, erasing the above mentioned discriminating difference between the primary and secondary components. Inelastic but non-annihilating (INA) interactions of antideuterons with the ISM may actually lead to such a flattening. In principle, these collisions are expected to essentially break the antideuteron whose binding energy is very small. That is why the INA cross section was disregarded in [93]. But laboratory measurements of the INA cross section of antiprotons colliding on deuterons yield [18] a non-vanishing, albeit small, value of order 4 mb at most. Another source of flattening comes from CR **antiprotons** impinging on the ISM and producing antideuterons. This process cannot be ignored below ~ 1 GeV/n, as featured in Fig. 1 of [19]. Those two mechanisms (INA interactions and production from CR antiprotons) generate tertiary antideuterons and a spectrum at low energy somewhat flatter than previously anticipated [93]. The detailed investigation carried out in [19] confirms nevertheless the possibility of discriminating the DM signal from the astrophysical background, as is clear in Fig. 7. Low energy antideuterons provide then a unique tool to probe the presence of DM particles within the Milky Way halo. The three horizontal solid blue lines of Fig. 7 indicate the potential reach of the forthcoming measurements which will be performed by AMS-02 [52, 95] and by GAPS. The later is a detector with a very high rejection rate against antiprotons. It will be flown on long (LDB) and ultra-long (ULDB) duration balloon flights around Antarctica [96, 97, 98, 99].

The hypothesis that factorization holds is certainly conservative. We have naively assumed that both constituents of the antideuteron are independently and isotropically distributed in the center of mass frame of the reaction. This is certainly true for the first antinucleon and its associated jet. However, once the axis of the pair of jets is determined, the second antinucleon tends also to be aligned along that direction. Assuming that spherical symmetry holds in that case leads to underestimate the probability of fusion. If both antinucleons are back to back, they do not merge actually. But if they belong to the same jet, their angular correlation is stronger than what has been assumed above, hence an enhanced probability of fusion. The naive factorization and coalescence scheme presented in this section has been recently improved by taking into account the collimation of the antinucleons produced inside the same jet. The larger the jet energy, the better the collimation and the easier the fusion. The momenta of antinucleons appear to be more parallel in the Galactic frame than in the jet frame, as a result of the Lorentz transformation that connects both systems of coordinates. Modeling hadronization inside jets with PYTHIA allows to take more accurately into account the angular correlations between the antideuteron constituents than in the naive isotropic scheme. The probability of fusion increases [100] typically like the square of the jet energy. The secondary component is mostly generated at low \sqrt{s} and is not affected by this effect. On the contrary, the collimation of the antinucleons produced by WIMP annihilation leads to a stronger DM signal than previously estimated. The primary component no longer decreases like $1/m_\chi^2$ and may even overcome the background above tens of GeV, should the DM species be very heavy. Notice however that a mass in excess of ~ 10 TeV does not seem very realistic. Be-

sides, such a DM species would still evade [101] the potential reach of the above mentioned forthcoming experiments.

6. Hot spots in the gamma-ray sky

6.1. Production mechanisms and DM line of sight integral

WIMP annihilations also generate high-energy photons whose energy distribution is described by the function $f(E_\gamma) \equiv dN_\gamma/dE_\gamma$. The corresponding flux at the Earth, from the direction toward which the unit vector \mathbf{u} is pointing, is given by the product

$$\Phi_\gamma^{\text{DM}}(E_\gamma, \mathbf{u}) = \frac{\eta}{4\pi} \left\{ \frac{\langle \sigma_{\text{ann}} v \rangle f(E_\gamma)}{m_\chi^2} \right\} \times \int_{\text{los}} \rho^2(\mathbf{x}) ds . \quad (60)$$

This formula is often seen as the emblem of particle astrophysics insofar as it exhibits two distinct pieces. The first part is related to particle physics and encodes information on the WIMP properties such as its mass and annihilation cross section. The second term is clearly astrophysical in nature and deals with the distribution of DM along the line of sight (los) toward which \mathbf{u} is pointing. As regards the particle physics aspect, three different contributions to $f(E_\gamma)$ need to be considered.

(i) The dominant source of high-energy photons is related to the production of quarks and gauge bosons which subsequently fragment and decay into secondary gamma-rays through essentially the two-photon decays of neutral pions

$$\chi + \chi \rightarrow q\bar{q}, W^+W^-, \dots \rightarrow \gamma + X . \quad (61)$$

For each annihilation channel, this leads to a continuum whose spectrum has been parameterized in [102] with the generic form

$$\frac{dN_\gamma^{\text{cont}}}{dx} = x^{-1.5} \exp(a + bx + cx^2 + dx^3) , \quad (62)$$

where $x = E_\gamma/m_\chi$. This distribution exhibits a characteristic $x^{-1.5}$ power law behavior for small values of x and a smooth cut-off when the photon energy is close to the WIMP mass.

(ii) A particularly clear signal of the presence of DM species inside the Milky Way halo is the production of monochromatic gamma-rays [103] through the reaction

$$\chi + \chi \rightarrow \gamma + \gamma \quad \& \quad \gamma + Z^0 . \quad (63)$$

This process gives rise to characteristic line signals which cannot be mistaken for some conventional astrophysical source and which would unequivocally signal the presence of an exotic component inside the Galaxy, should a peak be detected in the high-energy spectrum. The energy of the photons produced in reaction (63) is respectively equal to $E_\gamma = m_\chi$ and $E_\gamma = m_\chi - (m_Z^2/4m_\chi)$.

Because WIMPs are electrically neutral, the production of monochromatic photons is necessarily mediated by loop diagrams. It is generally suppressed and the integrated photon yield amounts to $\sim 10^{-3}$ of the total. This leads to a clear but faint signal which is beyond the reach of current detectors unless the process is efficiently enhanced, as in the case of heavy Wino-like neutralinos discussed in [42, 43, 104].

(iii) Finally, as already pointed out in [105], a single photon may be produced through internal bremsstrahlung as the WIMP pair annihilates. The gamma-ray is radiated by the charged particles that are either exchanged (virtual internal bremsstrahlung or VIB) or produced in the final state (final state radiation or FSR). This process becomes particularly important for a sizable branching ratio into electron-positron pairs, as in the case of MeV DM [106] or Kaluza-Klein inspired models [107]. The FSR spectrum associated to the production of the charged lepton pair l^+l^- is, in leading logarithmic order, well approximated by [107, 108]

$$\frac{dN_\gamma^{\text{FSR}}}{dx} = \frac{d(\sigma_{l+l-\gamma}v)/dx}{\sigma_{l+l^-}v} \simeq \frac{\alpha_{\text{em}}}{\pi} \frac{(x^2 - 2x + 2)}{x} \ln \left\{ \frac{m_\chi^2}{m_l^2} (1-x) \right\} . \quad (64)$$

Final state radiation produces more photons than fragmentation does near the upper edge $E_\gamma = m_\chi$ of the spectrum and is thus responsible for a characteristic sharp cut-off there. For Wino-like heavy neutralinos, photons are radiated by final W^+W^- pairs as discussed in [109].

(iv) Photons can also be produced, albeit indirectly, by the inverse Compton (IC) interactions of CR electrons and positrons on the Galactic radiation field. The resulting gamma-ray flux is no longer given by relation (60) but depends on the densities of CR electrons and positrons. These species will be generically designated here as electrons. The IC process is very important for DM species which preferentially annihilate into charged leptons, and most of the models designed to explain the PAMELA positron anomaly are excluded by the overproduction of IC photons to which they lead. The scattering of an incoming electron with energy E_e (and Lorentz factor $\gamma_e \equiv E_e/m_e$) on a radiation field of incoming photons with energies E_{in} generates the gamma-ray spectrum [110]

$$\begin{aligned} \mathcal{P}_i(E_\gamma, E_e, \mathbf{x}) = & \frac{3\sigma_{\text{T}}}{4\gamma_e^2} \int_{1/4\gamma_e^2}^1 \frac{dq}{q} \frac{dn_i}{dE_{\text{in}}} \{E_{\text{in}}(q), \mathbf{x}\} \\ & \times \left\{ 2q \ln q + q + 1 - 2q^2 + \frac{(1-q)\Gamma_e^2 q^2}{2(1+\Gamma_e q)} \right\} , \quad (65) \end{aligned}$$

where $\sigma_{\text{T}} = 0.665$ barn is the Thomson cross section. The parameter q is related to the energy E_{in} of the radiation field photon through

$$q = \frac{1}{\Gamma_e} \frac{E_\gamma}{(E_e - E_\gamma)} . \quad (66)$$

The dimensionless parameter $\Gamma_e \equiv 4E_{\text{in}}\gamma_e/m_e$ determines the regime of the IC scattering, *i.e.*, either ultra-relativistic ($\Gamma_e \gg 1$) or non-relativistic ($\Gamma_e \ll 1$)

in the Thomson limit. Incoming photons belong to the CMB, the IR radiation field and the light from stars. These three contributions are represented by the subscript i in relation (65). The flux at the Earth of IC photons is given by the convolution of the various contributions \mathcal{P}_i with the CR electron density $\psi_e \equiv dn_e/dE_e$ along the line of sight

$$\Phi_\gamma^{\text{IC}}(E_\gamma, \mathbf{u}) = \frac{1}{4\pi} \int_{\text{los}} ds \int_{m_e}^{m_\chi} dE_e \times \psi_e(E_e, \mathbf{x}) \times \sum_i \mathcal{P}_i(E_\gamma, E_e, \mathbf{x}) . \quad (67)$$

The CR electron density ψ_e is generated by the collisions of CR protons and helium nuclei on the ISM (background) and also by WIMP annihilations (DM signal). It needs to be calculated everywhere inside the Galactic magnetic halo.

In the case of the two-photon line, relation (60) leads to the estimate

$$\Phi_\gamma^{\text{DM}}(E_\gamma = m_\chi, \mathbf{u}) = 1.88 \times 10^{-13} \text{ photons cm}^{-2} \text{ s}^{-1} \text{ sr}^{-1} \times \frac{\langle \sigma_{\gamma\gamma} v \rangle_{29}}{m_{100}^2} \times J(\mathbf{u}) . \quad (68)$$

The annihilation cross section $\langle \sigma_{\gamma\gamma} v \rangle$ and the WIMP mass m_χ are respectively expressed in units of $10^{-29} \text{ cm}^3 \text{ s}^{-1}$ and 100 GeV. A Majorana type DM species has been assumed here with $\eta \equiv 1/2$. The los integral $J(\mathbf{u})$ has been redefined as

$$J(\mathbf{u}) = \{ \rho_\odot^2 r_\odot \}^{-1} \times \int_{\text{los}} \rho^2(\mathbf{x}) ds , \quad (69)$$

with a solar neighborhood DM density of $\rho_\odot = 0.3 \text{ GeV cm}^{-3}$. The galactocentric distance r_\odot of the solar system has been set equal to 8.5 kpc. The los integral J depends on the Galactic DM distribution. The various halo models of table 2 yield similar values all over the sky, except in the direction of the Galactic center where predictions can vary by several orders of magnitude, depending on the assumed profile. As shown in [111], where it has been averaged over a solid angle of 10^{-5} sr , J is respectively equal to 30 and 1.45×10^4 for the cored isothermal and NFW distributions. In the case of a Moore profile which has been adiabatically compressed by the collapse of the supermassive black hole lying at the center of the Milky Way, J may even reach the extreme value of 3×10^8 . The astrophysical uncertainties are enormous. The possibility of a strong signal has triggered a febrile activity around the Galactic center and motivated observations focusing in that direction. Let us concentrate, for instance, on the NFW profile of table 2. For small galactocentric distances, the DM distribution simplifies into

$$\rho(r) = \aleph \rho_\odot \left\{ \frac{r_\odot}{r} \right\} , \quad (70)$$

where the normalization constant $\aleph \simeq 2.03$. The los integral J is found equal to $\pi \aleph^2 / \alpha$ at an angular distance α from the Galactic center. Once averaged over a disk with angular radius θ , this leads to $\langle J \rangle = 2\pi \aleph^2 / \alpha$ and to a numerical value of $\sim 1500 \times (1^\circ / \theta)$.

6.2. Atmospheric Cherenkov telescopes – a new generation of instruments

High-energy photons can be detected by satellite borne instruments orbiting the Earth and free, therefore, from the screening of the atmosphere. Because of the reduced payload which can be carried up in orbit, the collecting area of gamma-ray telescopes like Fermi-LAT³ is quite reduced. Above a few tens of GeV, atmospheric Cherenkov telescopes (ACT) come into play and offer a nice alternative which complements space observations. The effective detecting area can be actually quite large insofar as any high-energy gamma-ray impinging upon the upper atmosphere generates a shower, and is degraded into many optical photons which ordinary telescopes spread on the ground can detect. The tracks left in the focal planes of these telescopes give the direction of the shower on the sky. Several instruments allow the stereoscopic reconstruction of the direction of the initial particle. The Cherenkov light illuminates on the ground a disk whose diameter is of order 250 m, hence a large effective area of $\sim 0.05 \text{ km}^2$ for each telescope, to be compared with the typical square meter collecting surface of a space instrument. The intensity of the image depends on the energy of the incident photon. The ACT technique is thus a powerful tool allowing the observation of the high-energy gamma-ray sky.

However, as for any other observation, a gamma-ray signal is only detectable as long as it emerges from the background. More specifically, the signal has to be larger than the statistical fluctuations, also called the noise, of the latter. For atmospheric Cherenkov telescopes, the dominant background arises from CR electrons that penetrate the atmosphere inside which they produce electromagnetic showers of the same type as those induced by high-energy photons. It is not possible to distinguish photons from electrons since both species lead to the same light pattern on the ground. Fermi-LAT measurements of the CR electron and positron flux can be fitted [59] by the power-law (39). Impinging CR hadrons also interact with the atmosphere. The showers which they generate tend to develop at a lesser altitude and are more widely spread on the ground than those of the electromagnetic type. Stereoscopy is a powerful tool to discriminate hadrons from electrons and gamma-rays since the pattern recognition of the light pool is then possible. Observations performed between 50 GeV and 2 TeV yield a hadron flux [112]

$$\Phi_{\text{had}}(E) = 1.8 \text{ GeV}^{-1} \text{ cm}^{-2} \text{ s}^{-1} \text{ sr}^{-1} (E/1 \text{ GeV})^{-2.75} . \quad (71)$$

A small fraction of the hadron-induced showers are mistaken for gamma-ray events though. This is the dominant source of background at high energy as hadrons have a harder spectrum than electrons. The HESS collaboration quotes a rejection factor of one misidentified event over a sample of 300 showers generated by CR protons. Satellite borne instruments do not suffer from the same problem. However, point sources can still be buried inside a Galactic gamma-ray diffuse emission produced, above 100 MeV, by the spallation of interstellar

3. See the web site <http://www-glast.stanford.edu/> and references therein.

gas by CR nuclei. The flux of this diffuse emission is given by the convolution along the los of the hydrogen density n_{H} with the gamma-ray emissivity I_{H} per hydrogen atom

$$\Phi_{\gamma}^{\text{sec}}(E_{\gamma}, \mathbf{u}) = \int_{\text{los}} n_{\text{H}}(\mathbf{x}) \times I_{\text{H}}(\mathbf{x}, E_{\gamma}) \times ds . \quad (72)$$

The Galactic diffuse emission is made of secondary photons resulting mostly from the interactions of high-energy CR protons and helium nuclei on the ISM. This process has already been discussed for antiprotons and positrons. It has been respectively described by the source terms $q_{\text{p}}^{\text{sec}}(\mathbf{x}, E_{\text{p}})$ in relation (12) of section 3.1 and $q_{e^{+}}^{\text{sec}}(\mathbf{x}, E_e)$ in relation (36) of section 4.2. The photon emissivity per hydrogen atom is defined as

$$I_{\text{H}}(\mathbf{x}, E_{\gamma}) = \frac{q_{\gamma}^{\text{sec}}(\mathbf{x}, E_{\gamma})}{4 \pi n_{\text{H}}(\mathbf{x})} , \quad (73)$$

and may be written as the convolution over proton energy of the CR proton flux with the differential photo-production cross section of proton-proton interactions

$$I_{\text{H}}(\mathbf{x}, E_{\gamma}) = \int \Phi_{\text{p}}(\mathbf{x}, E_{\text{p}}) \times dE_{\text{p}} \times \frac{d\sigma}{dE_{\gamma}}(E_{\text{p}} \rightarrow E_{\gamma}) . \quad (74)$$

The emissivity I_{H} is expressed in units of $\text{GeV}^{-1} \text{s}^{-1} \text{sr}^{-1}$ since it is essentially a production rate per unit of energy and solid angle. In the solar neighborhood, the effective gamma-ray emissivity of the ISM, whose atoms are illuminated by the local CR protons and helium nuclei, may be approximated, between 3 GeV and 1 TeV, by the power law [113]

$$I_{\text{H}}^{\text{eff}}(\odot, E_{\gamma}) = 3.55 \times 10^{-27} \text{ GeV}^{-1} \text{ s}^{-1} \text{ sr}^{-1} (E_{\gamma}/1 \text{ GeV})^{-2.76} . \quad (75)$$

This effective emissivity is scaled back to each hydrogen atom and can be readily used in expression (72) to infer the photon flux. The Galactic diffuse emission dominates over an extragalactic component which has been measured [114] with the EGRET instrument on board the CGRO satellite

$$\Phi_{\gamma}^{\text{eg}}(E_{\gamma}) = 7.32 \pm 0.34 \times 10^{-9} \text{ MeV}^{-1} \text{ cm}^{-2} \text{ s}^{-1} \text{ sr}^{-1} (E_{\gamma}/451 \text{ MeV})^{-2.10 \pm 0.03} . \quad (76)$$

An atmospheric Cherenkov telescope of the HESS caliber has an effective detecting area \mathcal{S} of order 0.1 km^2 with four mirrors spread on a $300 \text{ m} \times 300 \text{ m}$ square. One of the main targets of HESS is the Galactic center where the putative WIMPs might have collapsed, producing a hot spot in the gamma-ray sky. We will assume in what follows that the DM profile is given by the NFW distribution of table 2. The effective time \mathcal{T} during which the observation of the Galactic center is performed, disregarding the periods of daylight as well as the nights during which the Moon shines, will be taken to be a month. We infer an approximate acceptance of

$$\mathcal{S} \times \mathcal{T} \approx 0.01 \text{ km}^2 \text{ yr} . \quad (77)$$

Let us also assume that this HESS type telescope monitors a circular field of view with angular radius $\theta \sim 1^\circ$ surrounding the center of the Milky Way. For illustration purposes, the self-annihilation of WIMPs into photon pairs is the only process in which we will be interested here. It produces monochromatic gamma-rays with energy $E_\gamma = m_\chi$. The number of line photons collected during such a run is

$$N_\gamma^{\text{DM}} = 850 \text{ photons} \times \frac{\langle \sigma_{\gamma\gamma} v \rangle_{29}}{m_{100}^2} \times \left\{ \frac{\theta}{1^\circ} \right\} . \quad (78)$$

These monochromatic gamma-rays are detected within some energy bin whose width is set by the resolution of the telescope. We may safely take an energy resolution $\sigma(E)/E$ of order 10%, to be compared to the value of 15% in the case of HESS. The energy bin that contains the line has thus a width ΔE_γ of order $0.1 \times m_\chi$. The better the energy resolution, the narrower the line bin and the more visible the peak in the photon spectrum. As discussed above, all the bins are filled up predominantly by misidentified hadron and electron events. The monochromatic signal from annihilating DM species is detectable only if it exceeds the statistical fluctuations of that background. If electron induced showers are assumed to be the only source of background, although this may not be true at high energy where hadrons come also into play, the number of background events collected inside the line bin, during the run, amounts to

$$N_\gamma^{\text{BK}} = 4.3 \times 10^5 \text{ photons} \times (m_{100})^{-2.045} \times \left\{ \frac{\theta}{1^\circ} \right\}^2 . \quad (79)$$

The DM line signal N_γ^{DM} is deeply swamped into the background N_γ^{BK} and seems hopelessly out of reach. However, electronic and hadronic events are homogeneously spread on the sky since these cosmic radiations are isotropic at the Earth. Changing the direction toward which the telescope is pointing does not affect the number of background events. On the contrary, the line signal disappears as soon as the field of view no longer encompasses the Galactic center. By alternatively pointing the telescope on and off the source makes it possible to detect the line signal provided that it exceeds the statistical background fluctuations. A good estimate for these is given by the Poisson noise $(N_\gamma^{\text{BK}})^{1/2}$. Detection of a signal with a significance of n is therefore achieved whenever the signal to noise ratio is equal to

$$N_\gamma^{\text{DM}} / \sqrt{N_\gamma^{\text{BK}}} = n . \quad (80)$$

The HESS like telescope of this example would detect at the 3σ level a NFW distribution of DM species at the Galactic center should their mass and two-photon annihilation cross section fulfill the condition

$$\langle \sigma_{\gamma\gamma} v \rangle \geq 2.3 \times 10^{-29} \text{ cm}^3 \text{ s}^{-1} \times (m_{100})^{0.98} . \quad (81)$$

The HESS collaboration has observed the Galactic center with unprecedented accuracy [115, 116] above 160 GeV. A strong point-like source called HESS

J1745–290 is detected at the positions of the supermassive black hole Sagittarius A* and supernova remnant Sagittarius A East. Its spectral index is ~ 2.25 . An important gamma-ray diffuse emission is also seen in the same direction, with a similar spectral index. It is clearly associated with the band of molecular clouds lying in the central region and mapped from their CS line. These clouds have been recently penetrated by CR protons and nuclei accelerated by a nearby supernova event. The correlation between the intensity of the TeV diffuse emission and the gas column density of the clouds is striking and suggests a uniform density of cosmic rays. No line is observed though. Moreover, the gamma-ray spectrum is too hard to be compatible with a WIMP annihilation signal. As shown in [107], a Kaluza-Klein DM species could still yield the same flat energy distribution if the contributions from internal bremsstrahlung and τ lepton decays are included. The price to pay, however, is an unacceptably large mass m_χ of 10 TeV. A contribution from DM annihilation cannot be ruled out either, provided that it contributes less than 10% of the signal.

6.3. Current observations, constraints and prospects

The launch of the Fermi satellite in 2009 has considerably improved the picture in the field of indirect DM searches. The LAT instrument onboard the Fermi satellite has allowed for a tremendous recording of the gamma-ray sky with unprecedented statistics and resolution, overtopping the amount and quality of the data collected by previous space experiments, like EGRET or AGILE. Data taking is expected to last until 2014. The effective detection area reaches $\sim 10,000 \text{ cm}^2$ over an energy range spreading from $\sim 30 \text{ MeV}$ to $\sim 300 \text{ GeV}$, with an angular resolution $\sim 0.1^\circ$ in a field of view of $\sim 1/5$ of the sky. Such a low threshold together with the capability of observing the full sky in a short time make the Fermi-LAT instrument better than current ground-based gamma-ray telescopes for DM searches. The latter are actually complementary since they provide a better sensitivity for energies larger than 100-200 GeV, but only for rather localized sources (ground-based telescopes are optimized for a pointing mode). We still note that much larger Cherenkov telescope arrays may reach the required sensitivity in the future to start probing DM signals in several classes of targets efficiently [117]. Consequently, the following discussion will be strongly biased toward the Fermi-LAT data.

We will discuss the current results and prospects target by target, reviewing some predictions and constraints for DM signals from (i) the Galactic center, (ii) the diffuse Galactic and extragalactic emissions, and (iii) extragalactic sources (dwarf spheroidal galaxies, neighbor galaxies, and galaxy clusters). We emphasize that the observational constraints associated with these targets only concern the s-wave part of the annihilation cross section, while the p-wave part is also often relevant in setting the cosmological DM abundance. Hence, the canonical value of $\langle \sigma_{\text{ann}} v \rangle = 3 \times 10^{-26} \text{ cm}^3/\text{s}$ that will often appear in the following has to be taken with caution, keeping the previous remark in mind.

6.3.1. The Galactic center

The Milky Way is obviously the biggest nearby DM reservoir where to seek DM annihilation traces. Since DM is expected to concentrate at the centers of structures, the Galactic center (GC), which is located at ~ 8 kpc from the Sun, should be the most luminous known DM source for the Earthian observer. This region was actually observed with the EGRET telescope onboard the CGRO satellite, though with a poor angular resolution of $\sim 1^\circ$, which indeed led to the detection a gamma-ray signal in the 0.03-10 GeV energy range [118]. Interpretations in terms of DM annihilation were performed for supersymmetric candidates (*e.g.* [119]), but the main difficulty which arose (but was expected) was to distinguish between this putative exotic origin and an astrophysical origin of the signal. This points toward the challenging character of looking for DM annihilation traces toward the GC: this region is dominated by baryons, and high-energy astrophysical processes are known to take place (potential sites of CR acceleration, pion production through interactions of CRs with the ISM gas, inverse Compton from high-energy electrons, *etc.*). Anyway, the authors of Ref. [119] reached the conclusion that DM annihilation could provide a good fit to the EGRET data when taking neutralinos in the 50-100 GeV mass range (50 GeV being the lower limit they fixed to their scan over parameters), but only for central densities larger than usually expected. Adopting an NFW DM profile normalized to $\rho_\odot = 0.3$ GeV/cm³ at the Sun's position (taken at 8.5 kpc from the GC), they fell short by 1 order of magnitude, which they argue could be compensated by a more spiky profile resulting from baryon cooling effects known as adiabatic contraction [120, 121, 122]. We note that the current state-of-the-art numerical works in cosmological structure formation now seem to favor a picture where feedback effects dominate over cooling, making contraction scenarios much less motivated (*e.g.* [123]).

The GC was further observed, though at higher energies, with the HESS ground-based telescope, and a signal was reported in the 0.25-10 TeV energy range [115]. This signal is consistent with a point-like source coincident within 1' of Sgr A* (the data were taken with an angular resolution of $\sim 0.1^\circ$). The DM interpretation is made difficult because of the hard spectrum, well fitted with a power-law of spectral index ~ -2.2 up to 10 TeV, which implies very massive DM particles if one assumes their annihilation to be the main photon source. The exercise was still performed for supersymmetric as well as Kaluza-Klein candidates (*e.g.* [107] and [109], respectively), where multi-TeV mass particles were found able to saturate the signal, though with a loose fit and to the price of an arbitrarily large boost factor of ~ 1000 . Such an amplification is generally difficult to explain in terms of DM distribution, but non-perturbative effects were pointed out to significantly increase the annihilation cross section of such heavy particles [43], though by a factor limited to $\lesssim 100$ to simultaneously achieve the correct relic density [124]. Nevertheless, as for the EGRET signal, astrophysical scenarios were also shown to be plausible (*e.g.* [125, 126]), making the DM scenario less attractive. Despite the absence of a robust smoking gun for DM annihilation, the HESS data have still been shown very powerful to

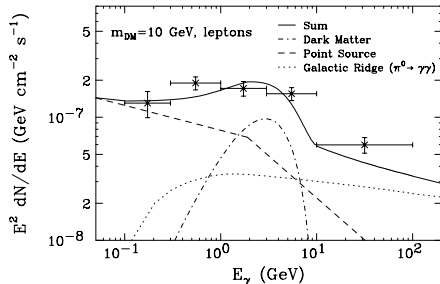


Figure 8: Gamma-ray excess found toward the GC in [128, 129], and tentative interpretation in terms of WIMPs annihilating into pairs of tau leptons. The plot is taken from Ref. [129]

constrain models proposed to fit the PAMELA data; examples can be found in [75, 127].

More recently, several studies were conducted relying on the publicly available Fermi data. The authors of Refs. [128, 129] have found evidences for an extended source centered around the GC, the intensity of which is seemingly hard to explain in terms of the point source located at the GC, probably also responsible for the TeV emission. These authors have attempted a DM interpretation of the signal, suggesting that the spatial and spectral fits to the data improved significantly by adding a $\sim 7 - 10$ GeV WIMP annihilating preferentially into taus, and distributed according to a rather spiky profile scaling like $\rho \propto r^{-1.3}$ (normalized to 0.4 GeV/cm^3 locally). They need an annihilation cross section of $\langle \sigma_{\text{ann}} v \rangle \sim 7 \times 10^{-27} \text{ cm}^3/\text{s}$, rather consistent with cosmological requirements. Moreover, they emphasized that the mass range is consistent with the recent hints coming from direct detection experiments — their result is shown in Fig. 8. Nevertheless, a criticism to this analysis can be found in [130], where no net excess is found with respect to canonical models of diffuse emission. More generally, we note that the GC is a region very complicated to model, though as fascinating as challenging, which makes DM searches very difficult toward this target unless very specific signatures are observed. Indeed, finding excesses with respect to *a fortiori* non-perfect descriptions of the region is not that a surprise. This statement is nicely reinforced by the recent finding, in the Fermi data, of large scale bubbles extending away from the GC [131], to which astrophysical explanations have been proposed [131, 132, 133] — while the believer’s eyes could see a DM signal, as apparent as in Fig. 7 of [134]. Hence, strong improvements in the understanding of CR acceleration and transport, in the modeling of the interstellar material, and in the census of the CR sources there, are clearly necessary to perform more reliable and detailed analyses of the GC and find DM signals in the near future — complementary with other targets and messengers. The encouraging point is that GC observations at gamma-ray frequencies still do not exclude a DM contribution. Regarding the experimental forecasts, a keypoint will be to improve the angular resolution and sensitivity in the 1-100 GeV energy range, which might be partly achieved with the new or coming generation of Cherenkov telescopes, like HESS-2 and CTA.

Finally, for completeness, we may also mention the possibility that DM annihilation could also contribute to the 511 keV emission extended around the

GC, which was measured to an unprecedented precision with the Integral satellite [135]. This would imply very light scalar DM candidates in the MeV mass range, which is formally not excluded [136]. Again, many classical alternatives exist in astrophysics, which makes it difficult to unambiguously discuss this intense emission in terms of DM. A specific review on this topic can be found in Ref. [137] for further details.

6.3.2. Diffuse Galactic and extra-galactic emissions

Fermi-LAT observations of the full gamma-ray sky have allowed to scrutinize the properties of the Galactic diffuse emission, as well as those of the isotropic extra-galactic component (see *e.g.* [138, 139]). DM annihilation in the Galactic halo is also expected to contribute to both these diffusion emissions, which makes the all-sky data suitable for searches for departure from conventional astrophysical predictions. This again necessitates reliable models of astrophysical foregrounds, and significant efforts are currently made to improve them (see *e.g.* [139, 113] for the Galactic component, and [140] for the extragalactic one).

To circumvent spurious effects coming from the potential use of an imperfect background model, a first strategy consists in looking for signatures which are very specific to DM: gamma-ray lines [103, 141, 142], or sharp spectral features stemming from internal bremsstrahlung diagrams [106, 109, 143]. The former signals are loop suppressed, while the latter come with significant amplitudes, inducing a sharp spectral bump close to the WIMP mass.

Gamma-ray line searches in the Fermi data have been performed by several groups, *e.g.* [144, 145]. No signal was found, and limits have been derived for annihilating as well as decaying DM. The results obtained in Ref. [145], valid in the 1-300 GeV energy range, are shown in Fig. 9. The authors assumed an NFW halo, with a local density of $\rho_{\odot} = 0.4 \text{ GeV/cm}^3$, and a scale radius of $r_s = 20 \text{ kpc}$ (variations of the halo shape appear as blue bands in the plots), and derived limits for the annihilation into a pair of photons, and for the decay into a photon and a neutrino. It is an easy exercise to recast their results for other final states (*e.g.* γX , where X is any massive particle). The obtained limits are not of concern for most of supersymmetric models leading to annihilating neutralino DM, while they become stringent for more effective models [146]. However, they strongly constrain the degree of R-parity breaking in scenarios of decaying gravitino DM, as well as on the stau NLSP lifetime, whenever relevant. We refer the reader to the original paper [145] for more details.

Further limits using three-body annihilation channels including virtual internal bremsstrahlung (VIB) photons⁴ were derived by the authors of Ref. [147]. They assumed an NFW halo profile with $\rho_{\odot} = 0.4 \text{ GeV/cm}^3$ and $r_s = 20 \text{ kpc}$, and parameterized the VIB contribution in terms of the mass splitting between the mediator and the DM particle $\mu \equiv (m_m/m_{\chi})^2$ (larger than 1 in the R-parity conserved supersymmetric context), the larger the values of μ the smaller the annihilation rates; though values close to 1 may correspond to co-annihilation regions. They selected a large region around the GC to maximize the signal-to-noise ratio, and performed a detailed analysis of the diffuse emission. While they found a $3.1\text{-}\sigma$ hint for a signal corresponding to a WIMP mass of ~ 150

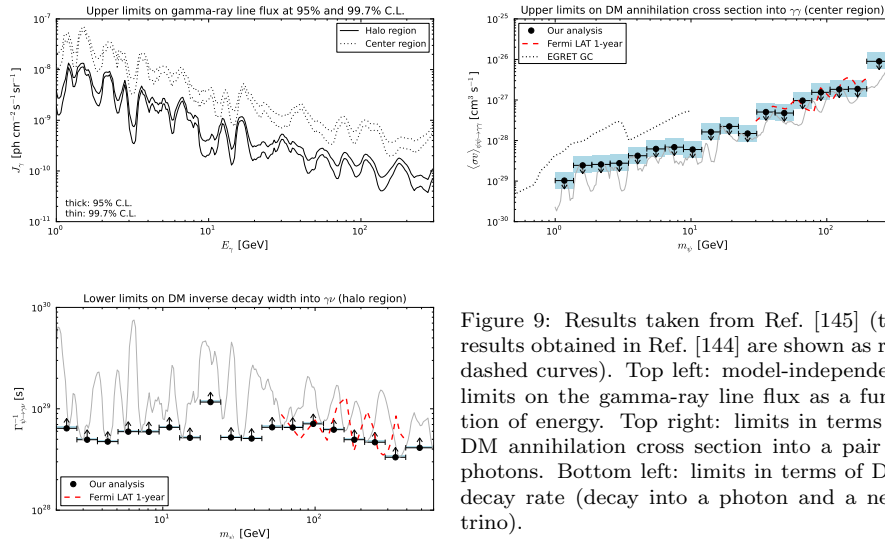


Figure 9: Results taken from Ref. [145] (the results obtained in Ref. [144] are shown as red dashed curves). Top left: model-independent limits on the gamma-ray line flux as a function of energy. Top right: limits in terms of DM annihilation cross section into a pair of photons. Bottom left: limits in terms of DM decay rate (decay into a photon and a neutrino).

GeV, they adopted a conservative approach in deriving limits on the 3-body annihilation cross section. Their results are shown in Fig. 10, where the blue horizontal lines are upper bounds corresponding to the requirement that the 3-body annihilation cross section (an s-wave), when taken alone, is such that the relic abundance $\Omega_\chi h^2 \geq 0.1$; indeed, 2-body contributions are expected, which should reduce the relic density significantly (VIB contributions, though s-waves, come with a α_{em}/π suppression factor). The green curves allow comparisons with the limits obtained from dwarf spheroidal galaxies in Ref. [148], and correspond to requiring $\langle\sigma_{\text{ann}}v\rangle/(5 \times 10^{-30} \text{cm}^3/\text{s}) \leq 8\pi (m_\chi/\text{GeV})^2/N_\gamma^{\text{tot}}$, where N_γ^{tot} is the total number of gamma-rays per annihilation (including the 2-body contribution). We note that the limits obtained for leptonic channels are generally better than those derived from dwarf galaxies.

Finally, the diffuse gamma-ray flux measured by Fermi [138, 149, 150, 151, 139] has also been used to put absolute upper limits on the continuum gamma-ray fluxes expected for most of DM candidates. We may illustrate the main results, though not exhaustively, by showing the constraints obtained in Ref. [152], where the authors used the estimate of the isotropic diffuse gamma-ray flux performed by the Fermi collaboration [150] to constrain DM contributions at the Galactic scale (one can also use the extragalactic contribution, though less powerful and more affected by theoretical uncertainties [152, 153, 154]). In addition to the DM induced prompt continuum gamma-ray emissions, the authors included the inverse Compton contributions for all leptonic annihilation channels.

4. As already mentioned in section 6.1, internal bremsstrahlung photons are made of *final state radiation* (FSR) and *virtual internal bremsstrahlung* (VIB) photons, the latter being associated with the radiation of a *t*-channel charged mediator (*e.g.* any sfermion in the super-symmetric context). These contributions can be separated in a gauge invariant way [143].

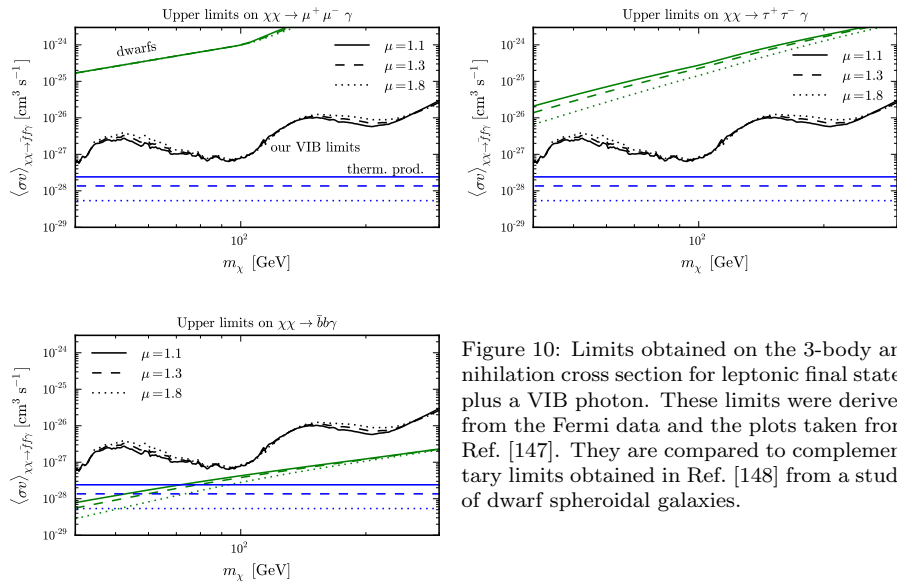


Figure 10: Limits obtained on the 3-body annihilation cross section for leptonic final states plus a VIB photon. These limits were derived from the Fermi data and the plots taken from Ref. [147]. They are compared to complementary limits obtained in Ref. [148] from a study of dwarf spheroidal galaxies.

Their results are reported in Fig. 11, where the $b\bar{b}$, $\tau^+\tau^-$, and $\mu^+\mu^-$ annihilation channels are considered as representative of most of DM models. The plots contain complementary limits from studies of dwarf galaxies and of the GC [155, 156, 157, 158], and also provide forecast limits for a 5-year Fermi-LAT sensitivity. We see that the Galactic diffuse emission leads to constraints at the limit of the interesting supersymmetric parameter space, assuming canonical cosmology and particle phenomenology, delineated as in Ref. [117]. On the other hand, as illustrated in the plots, such data make it possible to exclude more contrived configurations, for example those proposed to explain the so-called PAMELA excess [159, 160]. Many similar results have been reached independently, that we cannot, unfortunately, exhaustively cite here. Nevertheless, we emphasize that a reliable and global picture of the diffuse Galactic gamma-ray sky will only come out after important refinements in the astrophysical background modeling are achieved. These are now necessary for seeking DM annihilation traces into more detail.

6.3.3. Extragalactic sources

DM is also sought in extragalactic objects, like in nearby dwarf galaxies, galaxies, and clusters of galaxies.

The first class of objects, dwarf galaxies, is likely the most promising in terms of DM detection because these targets are strongly DM dominated, with no expected high-energy astrophysical phenomena (*i.e.* background free, though this has to be weighted by their positions in the sky where the Galactic foreground may be strong). Kinematic data are also available which allow to constrain the DM distributions in several systems, and it is shown that when using the current angular resolutions of gamma-ray telescopes at the ground or in space (say

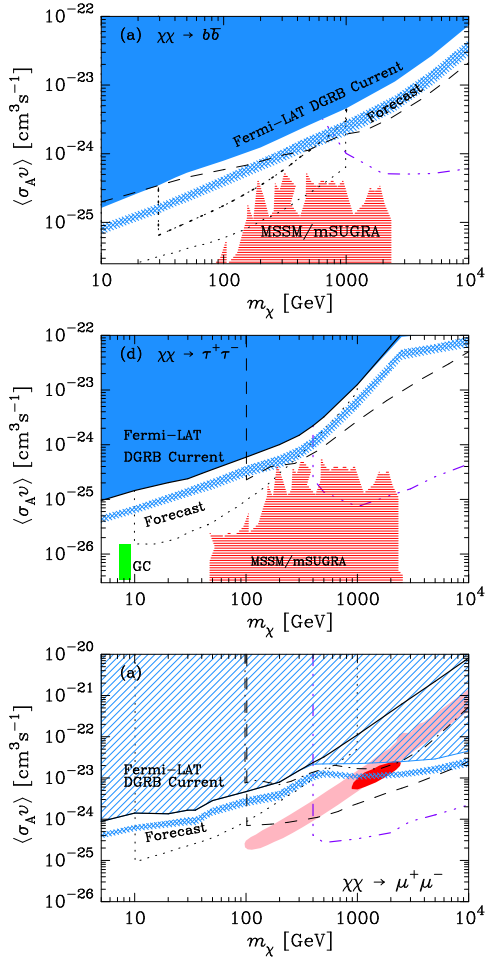


Figure 11: Plots taken from Ref. [152]. The dashed lines show the complementary limits derived from Fermi observations of the Draco dwarf galaxy in [155]; the thin dotted lines show those obtained by the stacking of dwarf galaxies in [156], except for the $\mu^+\mu^-$ case, where they correspond to the radio constraints found in [159]. The triple-dot-dashed lines are limits corresponding to the HESS observations of the GC [157, 158]. The small green rectangle shows the parameter space consistent with the controversial gamma-ray excess found toward the GC in [128, 129]. The solid line shows the Fermi limit without the inverse Compton contribution from leptonic annihilation channels. The red MSSM/MSUGRA regions were derived in [117]. The shade pink and red regions ($\mu^+\mu^-$ case) are those which are consistent with a DM interpretation of the positron fraction measured by PAMELA and of the electron+positron spectrum measured by Fermi [159, 160].

$\sim 5'$), the theoretical errors expected after the angular average of the squared DM density in each object, *e.g.* stemming from the large uncertainties in the inner slope, are actually rather small [161, 162]. Several observations of the so-called canonical dwarf galaxies (less than a ten of objects) were performed in the past by ground-based telescopes, but the limited observation times and high-energy threshold induced too weak sensitivities to get interesting limits (*e.g.* [163, 164, 165]). As for other targets, the Fermi advent has considerably improved the detection potential. So far, yet, no gamma-ray signal originating from a dwarf galaxy has ever been observed, leading several groups to compete to get the best limits (*e.g.* [155, 156, 148, 166]). In Fig. 12, we show the results obtained for individual dwarf galaxies in [155] (left panel), corresponding to 11 months of survey mode operation with Fermi, and those obtained by stacking all individual contributions in [148], corresponding to about 2 years of Fermi data. In the left panel, we see that Draco provides the best limit, though it lies

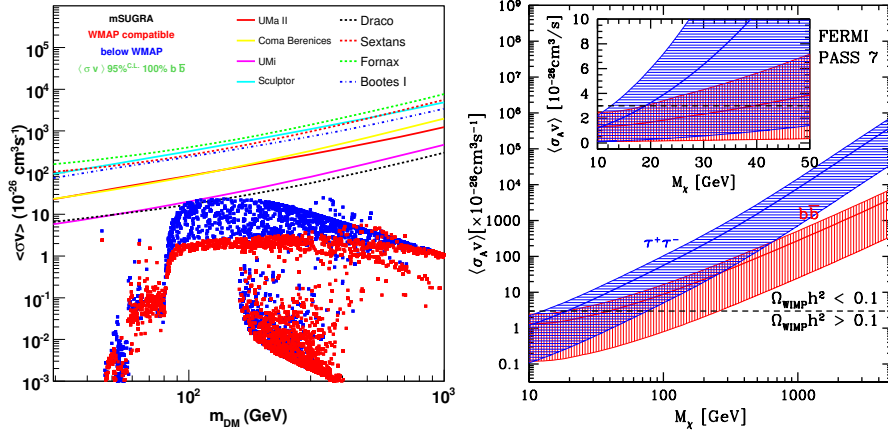


Figure 12: Left: indicative limits on the constrained MSSM parameter space from several dwarf galaxies, assuming a generic $b\bar{b}$ spectrum; taken from [155]. Right: limits after stacking individual limits, with a self-consistent treatment of statistical and systematic errors (the shaded areas show the systematic errors coming from uncertainties in the DM distribution inside the objects); taken from [148].

at about one order of magnitude away from the interesting parameter space. On the other hand, the stacking analysis is shown a very powerful alternative, which currently yields the best limits on the s-wave part of the WIMP annihilation cross section. We notice that despite the rather large systematic errors coming from uncertainties in the DM distribution inside the objects (encoded as the shaded areas in the plot), WIMP masses below ~ 50 GeV annihilating preferentially into tau leptons or b quarks at the canonical rate start to be in serious tension with the data. Beside exclusion prospects, this is also very encouraging in terms of detection prospects.

As regards expectations for the future, we refer the reader to Ref. [161], where the authors show that future ground-based observatories, like CTA, will allow for interesting complementary surveys with respect to Fermi, though further observations with Fermi are likely the best strategy for discovery purposes — 10 years of Fermi data would really drive us in the ballpark, though such a duration currently appears as unrealistic in terms of funding (the official end of Fermi operations is June 2012, though 2 supplementary years seem granted).

For completeness, it is important to mention that other extragalactic objects might also be interesting sources for DM searches. Neighbor galaxies, like M31 (Andromeda), are potentially good targets [167, 168, 102], but as for the Galaxy, it is rather difficult to predict the astrophysical background in these objects, where, at variance with dwarf galaxies, high-energy phenomena are expected. Several unsuccessful observations have been performed in the past, *e.g.* [169, 170, 171], but the constraints obtained on DM models were insignificant. Nevertheless, some giant galaxies, like M87 and NGC 1275 were recently observed at TeV gamma-ray energies, but with strong variabilities

(*e.g.* [172, 173, 174]). The latter objects usually belong to the broader class of radio emitters, which allow for rich multiwavelength analyses. Nevertheless, the observed variability makes it very difficult to try to interpret any signal in terms of DM annihilation or decay in these sources. The Fermi satellite has more recently allowed the first detections in gamma-ray frequencies of nearby galactic objects, M31 [175], the SMC [176] and LMC [177]. As already emphasized above, DM interpretations are difficult because of the presence of CR accelerators and gas in these objects, and these studies actually barely addressed the DM issue.

Finally, many efforts have been recently done to check whether galaxy clusters could offer additional targets for DM searches (*e.g.* [178, 179, 180, 181, 182, 183, 184]). Limits on DM candidates were again derived from the Fermi data [185, 186, 181], and we may also mention a recent claim for the detection of gamma-ray signals from a few clusters [187]. Nevertheless, we know that high-energy processes are at work in galaxy clusters, and it is still difficult to infer and predict the related astrophysical background [188, 179]. Moreover, we stress that galaxy clusters host giant elliptical galaxies, like the M87 and NGC 1275 galaxies discussed above. Since the latter have been demonstrated to be transient TeV emitters, the relevance of galaxy clusters for DM searches might fairly be questioned, though their observations remain solidly motivated from many other astrophysical arguments. Deeper investigations appear to be necessary, which could for instance rely on the state-of-the-art cosmological simulations including baryon dynamics and star formation.

7. Indirect dark matter searches with neutrinos

High-energy neutrinos are interesting messengers to seek for DM annihilation traces. They can be produced through the fragmentation or decay of unstable primary annihilation products, or directly in some more rare cases. Direct production is generically suppressed if DM is made of Majorana fermions because of helicity suppression. Nevertheless, it may naturally appear in other cases, like in extra-dimensional models. Beside being complementary to other astrophysical messengers as tracers of DM annihilation in the Galactic halo, neutrinos do provide an additional and very specific signature: they can also trace the gravitational capture of DM in celestial bodies, in particular in the Sun or the Earth. Detecting high-energy neutrinos from the Sun or the Earth would represent a very clean signature of DM capture and subsequent annihilation, hard to infer from other known phenomena. This idea was proposed in the mid 80's by several groups, notably by Press & Spergel [189] and Silk, Olive & Srednicki [190] for the Sun, and by Freese [191], Krauss, Srednicki & Wilczek [192], and Gaisser, Steigman & Tilav [193] for the Earth.

Active neutrinos are almost massless and thereby travel in the skies like photons: their sources can be traced back, which is of particular interest for DM searches. Neutrinos are less subject to absorption than photons but in the meantime more difficult to collect on Earth. The detection of astrophysical neutrinos is indeed very challenging because of their weak cross section with

ordinary matter, which entails gigantic detectors, and because of the copious diffuse atmospheric neutrino background coming from interactions of cosmic rays with the atmosphere. So far, the history of neutrino astronomy relies on confirmed observations of two objects only: the Sun, from which the electron-to-muon neutrino flavor oscillation was proven, and the supernova SN-1987A, the explosion of which allowed to derive a robust upper limit on the absolute neutrino mass scale. These sources were observed in the keV-MeV energy range. At higher energies, more global (and indirect) astrophysical pieces of information have been delivered from *e.g.* measurements of the atmospheric neutrino anisotropy in the TeV energy range, related to the anisotropy in the CR flux.

There are currently two main types of so-called neutrino telescopes in operation: MeV detectors historically optimized for solar/atmospheric electron/muon neutrinos — *e.g.* Super-Kamiokande⁵ (Super-K hereafter) — and GeV-PeV detectors mostly designed for muon neutrinos⁶ originating in high-energy astrophysical phenomena (supernova remnants, active galactic nuclei, DM annihilation, *etc.*) — *e.g.* AMANDA⁷-IceCube⁸ and ANTARES⁹-KM3¹⁰. These detectors are installed deep underground for protection against the CR background, and when dedicated to studies of astrophysical sources, the Earth itself is used to convert muon neutrinos into upward-going muons, the reconstructed directions of which allow a separation from the downward-going muons produced by interactions of cosmic rays in the atmosphere. Indeed, muons, when crossing such a detector, may produce Cherenkov light in the ice (AMANDA-IceCube are based at the South-Pole) or water (a tank of 50,000 tons of purified water for SuperK, the Mediterranean sea for ANTARES-KM3) that can be collected with arrays of photo-multipliers, allowing for direction reconstruction. The main background associated with this detection strategy comes from the atmospheric neutrinos generated by CR interactions in the atmosphere; although the amplitude of this background is large in the GeV-TeV range and makes neutrino astronomy challenging, predictions and measurements are available and under reasonable control (see *e.g.* [194, 195]). Very approximately, the atmospheric muon neutrino flux is of order $\phi_{\text{bg}}(E) \approx 6 \times 10^{-3} (E/100 \text{ GeV})^{-3.7} \text{ m}^{-2} \text{ s}^{-1} \text{ sr}^{-1}$. Assuming a full time exposure, an effective detection area of $\sim 10^{-2} \text{ m}^2$ (expected for a km-size neutrino telescope) and an optimistic flat angular resolution of 1° [196, 197], this corresponds to $\mathcal{O}(1 - 10)$ background event per year for a point-like source, among $\mathcal{O}(10^4)$ over half the sky.

In the following, we introduce the treatment of neutrino propagation (in vacuum or/and matter) necessary for proper predictions in the present context. Then, we shortly discuss DM searches with high-energy neutrinos from the Galactic halo before delving into more details the case of solar neutrinos. We

5. www-sk.icrr.u-tokyo.ac.jp/sk/index-e.html

6. Electron and tau neutrinos can also be reconstructed in some cases.

7. <http://amanda.uci.edu/>

8. <http://icecube.wisc.edu/>

9. <http://antares.in2p3.fr/>

10. <http://www.km3net.org/home.php>

illustrate each paragraph with a selection of recent results and sketch the main prospects.

7.1. Neutrino oscillations, interactions with matter, and muon flux at detectors

Before discussing the Galactic or solar origin of the DM-induced neutrinos, it is interesting to review how they propagate to the Earth, and how one can predict the flux converted into muons at detectors. A fundamental feature of neutrino phenomenology is flavor oscillation, which is a consequence of their non-zero masses; interaction and mass eigenstates are different [198]. This of course must be accounted for in predictions, since high-energy neutrino telescopes are mostly designed for muon neutrinos. All cases are relevant here: oscillation in vacuum (Galactic halo neutrinos), to which one may further have to combine oscillation in matter (neutrinos from the Sun or the Earth). In the latter case, additional effects implying neutral and charge currents (absorption and re-emission) must also be plugged in. In the following, we ignore the potential effect of putative sterile neutrinos. We refer the reader to Refs. [199, 200, 201] for extensive reviews.

The neutrino oscillation framework (in vacuum) is usually based on a few ingredients: the mixing matrix U (including unknown but possible CP-violating phases), from which one can express a flavor (mass) eigenstate as a linear combination of the mass (flavor) eigenstates, and a classical quantum evolution equation assuming plane waves:

$$|\nu_\alpha\rangle = U_{\alpha i}^* |\nu_i\rangle, \quad |\nu_i(t)\rangle = e^{-i E_i t} |\nu_i(0)\rangle, \quad (82)$$

where Greek indices refer to the flavor basis (e, μ, τ) while Latin indices refer to the mass basis (1,2,3). The oscillation probability between flavors α and β is then merely given by $\mathcal{P}_{\alpha\beta} = |\langle \nu_\beta | \nu_\alpha \rangle|^2$. Since masses are small, one can use the relativistic approximation such that $E_i \simeq p_i \simeq p \simeq E \simeq p + m_i^2/2E$, and the probability reads

$$\begin{aligned} \mathcal{P}_{\alpha\beta}(E, L = ct) = & \delta_{\alpha\beta} - 4 \sum_{j>i} \mathcal{R}e(U_{\alpha i}^* U_{\beta i} U_{\alpha j} U_{\beta j}^*) \sin^2 \left\{ \frac{\delta m_{ij}^2 L}{4 E_\nu} \right\} \\ & \pm 2 \sum_{j>i} \mathcal{I}m(U_{\alpha i}^* U_{\beta i} U_{\alpha j} U_{\beta j}^*) \sin \left\{ \frac{\delta m_{ij}^2 L}{2 E_\nu} \right\}. \end{aligned} \quad (83)$$

When distances get tremendous, *e.g.* when neutrinos originate in DM annihilation in the Galactic halo, the oscillation effects in vacuum average out and the probability is merely related to the raw mixing angles:

$$\langle \mathcal{P}_{\alpha\beta}(E) \rangle \xrightarrow{L \gg 1 \text{ AU}} \delta_{\alpha\beta} - 2 \sum_{j>i} \mathcal{R}e(U_{\alpha i}^* U_{\beta i} U_{\alpha j} U_{\beta j}^*). \quad (84)$$

Assuming no CP-violating phases, $\theta_{23} \simeq \pi/4$ and $\theta_{13} \simeq 0$, the neutrino flux at the Earth may be expressed as [202]

$$\begin{aligned} \phi_{\nu_e} & \approx \phi_{\nu_e}^0 - \frac{1}{4} \bar{\phi}_\nu \\ \phi_{\nu_\mu} & \approx \phi_{\nu_\tau} \approx \frac{1}{4} (\phi_{\nu_\mu}^0 + \phi_{\nu_\tau}^0) + \frac{1}{8} \bar{\phi}_\nu \\ \bar{\phi}_\nu & \equiv \sin^2 \theta_{12} (2 \phi_{\nu_e}^0 - \phi_{\nu_\mu}^0 - \phi_{\nu_\tau}^0), \end{aligned} \quad (85)$$

where any ϕ^0 denotes the flux without oscillation.

When neutrinos travel a significant distance inside a dense medium, the Mikheyev-Smirnov-Wolfenstein (MSW) effect [203, 204] must also be included — this is relevant to neutrinos crossing the Sun or the Earth. Then, the above formalism has to be enriched with a new interacting term in the Hamiltonian which modifies the dispersion relation [205, 206], and the flavor vector $\nu = (\nu_e, \nu_\mu, \nu_\tau)^t$ now evolves according to

$$\begin{aligned}\nu(t) &= e^{-iHt} \nu(0), \\ H &= \frac{1}{2E} U \text{diag}(0, \Delta m_{21}^2, \Delta m_{31}^2) U^\dagger + \text{diag}(\sqrt{2} G_F n_e, 0, 0),\end{aligned}\tag{86}$$

where H is the Hamiltonian expressed in the flavor basis, G_F is the Fermi constant and n_e is the electron density. The flavor asymmetry comes from that in coherent charged current interactions, electron neutrinos see the electrons present in the medium while the other neutrinos do not, leading to a flavor-dependent refraction index. One must also include other charged and neutral current interactions with nucleons (inelastic scattering), which get very important at high energy and mostly induce an energy redistribution toward lower energies because of successive absorption and re-emission processes (the conversion of tau neutrinos into tauons also induces extra flavor injection and a coupling in the evolution between neutrino and anti-neutrino species). This can be worked out with Monte Carlo methods [206]. An elegant and self-consistent alternative to such a two-fold treatment is that of the density matrix formalism [199, 207, 208], which combines oscillation and absorption, and provides identical results. In that case, the flavor density matrix ρ_ν obeys the following evolution equation:

$$\frac{d\rho_\nu}{dl} = -i[H, \rho_\nu] + \left. \frac{d\rho_\nu}{dl} \right|_{\text{NC}} + \left. \frac{d\rho_\nu}{dl} \right|_{\text{CC}} + \left. \frac{d\rho_\nu}{dl} \right|_{\text{in}},\tag{87}$$

where, in the right-hand side, the terms respectively describe the neutral current effects, the charged current effects, and the neutrino injection induced by DM annihilation. We emphasize that the injection term in a dense medium is different from what is obtained for annihilation in the Galactic halo, since some of the fragmentation or decay products of the primary particles, or even the primary particles themselves, can be absorbed before cascading. This is the case, for instance, for muons. Irrespective of the method, the full calculation has to be performed numerically. Furthermore, detailed models of the Sun or the Earth, when concerned, have to be used to get accurate predictions.

An important outcome is that for neutrinos from the Sun, absorption is responsible for an exponential energy cut-off above 100 GeV in the differential flux. For neutrinos injected at the center of the Earth, the cut-off is somewhat higher, around 10 TeV. Moreover, it turns out that oscillation in the Sun mixes tau and muon neutrinos; oscillation only affects electron neutrinos in vacuum on their way to the Earth. This is illustrated in Fig. 13, which was extracted from Ref. [206]. In the top left panel, one can see the injected neutrino spectra at the

Sun's core, where the annihilation of 250 GeV WIMPs into $\tau^+\tau^-$ was assumed. In the top right panel, propagation effects (oscillation and weak currents effects) are shown by evolving the injected spectra from the Sun's core to its surface; the mixing between tauon and muon neutrinos is made clear, as well as energy redistribution toward low energies, due to weak scatterings; the production of secondary muon and electron neutrinos is due to tauon decays, which are generated from tau neutrinos through charged current interactions. Oscillation in vacuum between the Sun and the Earth (the distance is fixed to 1 AU) further results in slightly mixing electron neutrinos with the other flavors, as sketched in the bottom left panel. The final neutrino spectra at the detector are shown in the bottom right panel, where the oscillation pattern appears as completely smeared out. This does not come from additional mixing in the Earth, but from a time average performed over a 1 year cycle, during which the variation in the distance between the Earth and the Sun is enough to erase the oscillating features. Therefore, the net propagation effects for neutrinos coming from the Sun mostly translate into an amplitude rescaling, as in the case of Galactic neutrinos, and a high-energy damping due to efficient absorption in the Sun above 100 GeV.

Once the neutrino flux at sea level is predicted, one still has to convert it in terms of muon flux at detectors (or other observables related to neutrinos, *e.g.* hadronic showers). Again, the full flavor evolution given *e.g.* in Eq. (87) must be adapted to the Earth medium to determine the neutrino flux at a certain distance from the detector. For a muon-optimized detector, the relevant distance is the mean free path of a muon in the surrounding material, typically 1 km for a TeV muon travelling in the ice. Another important point to take into account is the time and detector-location dependence of the neutrino arrival direction. Indeed, only upward-going muons can be used for astrophysical searches, and detection efficiency is angular dependent. Therefore, the effective detection area \mathcal{A}_{eff} is a quantity somewhat tricky to extract for neutrino telescopes. It basically depends on the neutrino flavor, energy and direction, and has to be determined for each source. Anyway, for a given astrophysical source located at point \mathbf{x}_* , the detector efficiency might be time-averaged and the differential detected event rate then merely reads

$$\frac{dN_\nu(\mathbf{x}_*)}{dt} = \int_{E_{\nu,\text{th}}} dE_\nu \frac{d\phi_\nu}{dE_\nu} \langle \mathcal{A}_{\text{eff}}(E_\nu, \mathbf{x}_*) \rangle. \quad (88)$$

The effective detection area is typically of order $\langle \mathcal{A}_{\text{eff}} \rangle \approx 10^{-3}$ to 10^{-2} m² $(E_\nu/300 \text{ GeV})^2$ for km-size instruments [196], where one power of energy comes from the neutrino conversion into muon and the other from the muon energy loss converted into Cherenkov photons. To illustrate how challenging detecting astrophysical neutrinos is, this has to be compared with the usual effective areas encountered in gamma-ray astronomy. For instance, the Fermi-LAT instrument¹¹ has an effective area of $\sim 0.5 - 1$ m² in the 0.1-100 GeV energy

11. <http://www-glast.stanford.edu/>

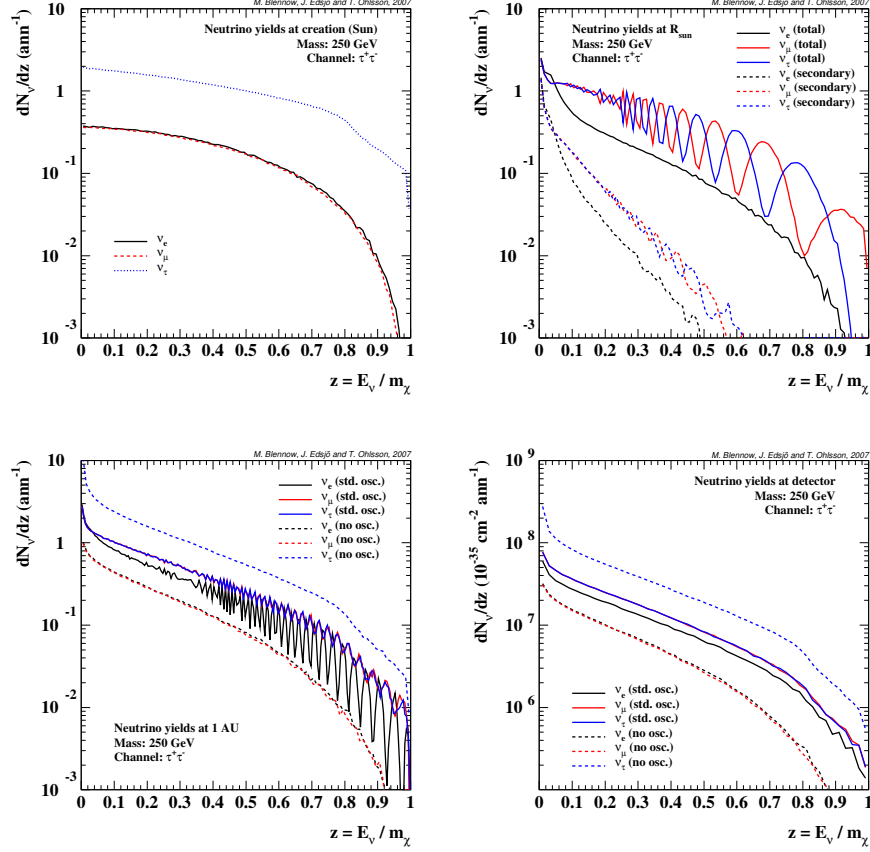


Figure 13: Evolution of the neutrino spectra between the Sun's core (top left), the Sun's surface (top right), the Earth's surface (bottom left), and the detector (bottom right). Legends are explicit, and more details are given in the text. These plots have been borrowed from Ref. [206].

range.

7.2. Neutrinos from DM annihilation in the Galactic halo

Since neutrinos are almost massless, they travel along geodesics like photons, and may therefore trace the (squared) DM distribution in the Galaxy or extra-galactic objects. Thus, as for indirect DM searches with gamma-rays, the Galactic center on the one hand, and neighbor dwarf galaxies on the other hand, are very good targets. In these specific cases, the neutrino flux prediction can be written the same way as for gamma-rays, except for the possibility of flavor oscillations (see Sect. 7.1). For an arbitrary flavor index α , it reads:

$$\frac{d\phi_\alpha(E)}{dE} = \sum_{\beta=e,\mu,\tau} \mathcal{P}_{\alpha\beta}(E) \frac{\eta}{4\pi} \frac{\langle \sigma_{\text{ann}} v \rangle_\beta}{m_\chi^2} \int_{\delta\Omega_{\text{obs}}} d\Omega \int_{\text{los}} dl \rho^2(l) , \quad (89)$$

where \mathcal{P} is the flavor oscillation probability, and $\rho(l)$ is the DM mass density along the line-of-sight l in the chosen direction. The integral is performed over a cone of angle $\delta\Omega_{\text{obs}}$ corresponding to the angular resolution of the telescope (assumed flat for simplicity here). This is therefore similar to the flux prediction made for gamma-rays except for the relevant angular size. Indeed, neutrino telescopes have generically angular resolutions worse than gamma-ray telescopes, ranging from a few degrees around a few GeV down to half a degree above a few TeV. Still, the predicted fluxes do not suffer from high-energy absorption like in the Sun, which is of interest for km-size neutrino telescopes, the effective detection areas of which typically increase like E^2 .

Nevertheless, the predictions obtained for the Galactic center are generically small compared to the current experimental sensitivities, typically of the order of 0.1-1 up-going muon at detectors per km^2 and per year, much smaller than the annihilation signal expected from the Sun as it will be shown below (see *e.g.* [209, 210]). Such predictions are usually based upon assuming a generic NFW DM profile, with an optimistic angular average of 1° around the Galactic center. The most optimistic estimate arises when requiring the potential complementary gamma-ray flux (model-dependent approach) to saturate the gamma-ray signal already measured at the Galactic center by different experiments, *e.g.* EGRET, HESS, Fermi. Proceeding so implicitly accounts for the still large uncertainties in our knowledge of the central DM distribution, which might be more cuspy than expected (*e.g.* because of the adiabatic compression triggered by baryon cooling), inducing fluxes significantly larger, around 100 up-going muons per km^2 and per year [209].

Conservative limits have been obtained for generic WIMPs fully annihilating into specific final states by the IceCube Collaboration [211]. They are reported in the $\langle\sigma_{\text{ann}}v\rangle$ - m_χ plane in Fig. 14 and shown to be rather far away from the relevant WIMP phase-space. This is essentially due to the poor exposure of IceCube to the Galactic center, since the experiment is located at the South Pole. Nevertheless, the analysis performed by the collaboration somehow compensates for this limitation by focusing on the high-latitude flux predictions, which are less subject to theoretical errors. Although this strongly damps the predictions, the DM density profile is in turn much less uncertain away than close to the Galactic center.

Finally, we note that other interesting and similar DM sources are the neighbor dwarf galaxies, which are DM dominated objects. Nevertheless, expectations are rather modest, and unless for TeV WIMP masses and decade timescale exposure, neutrino telescopes are poorly sensitive to such objects [213].

7.3. Neutrinos from DM annihilation in the Sun or the Earth

The interaction properties of DM with ordinary matter open the possibility of its gravitational capture and further accumulation in celestial bodies, in particular in the Earth and in the Sun which are the closest potential reservoirs. Indeed, DM particles can lose kinetic energy through elastic scattering with ordinary matter and may thus remain gravitationally bound to the encountered object — this happens when the final velocity is lower than the

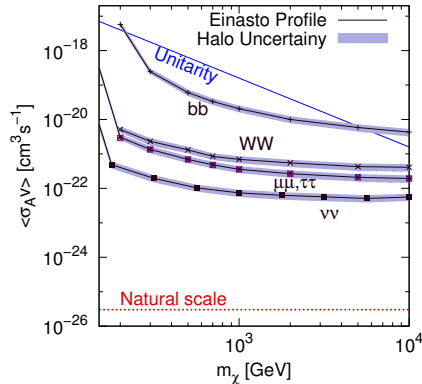


Figure 14: Limits on the WIMP annihilation cross section obtained from observations of the Galactic halo at intermediate latitudes performed with the IceCube neutrino telescope. The unitarity bound derived in Ref. [212] is also shown. See the text for more details. This plot has been taken from Ref. [211].

so-called escape velocity. If sufficiently accumulated at the center, annihilation turns on and injects high-energy standard particles in the dense medium, among which neutrinos are the only species that can escape. As we will review below, this implies that the annihilation rate is not fixed by the (squared) average local DM density around the body, but is instead intimately linked to the capture rate. Once produced in the object, neutrinos experience the oscillation and absorption pattern discussed in the previous section before reaching the detector. We will focus on the Sun in the following, as a template example. For even more insights, we refer the reader to the seminal works in Refs. [189, 190, 191, 192, 193, 214, 215], and also to subsequent developments found in *e.g.* Refs. [216, 217, 218, 219, 220, 221, 222, 208, 206, 223, 224, 225, 226]. Dedicated and sophisticated numerical codes can be found in Refs. [221, 206].

7.3.1. DM capture

A pedagogical introduction to DM capture can be found in [227]. In the Sun, the total number N of DM particles evolves with time and depends on capture, annihilation, and escape, respectively as follows:

$$\frac{dN}{dt} = C_c - C_a N^2 - C_e N, \quad (90)$$

although the latter can safely be neglected for particle masses above a few GeV [214, 215]. The capture rate Γ_c is readily identified to parameter C_c and depends on the elastic scattering cross section between DM and ordinary matter, while the annihilation rate reads

$$\Gamma_a(t) = \eta \int_{\text{Sun}} d^3\mathbf{x} \langle\sigma_{\text{ann}} v\rangle n^2(t, \mathbf{x}) = \frac{C_a}{2} N^2, \quad (91)$$

where n is the (time-dependent) number density of DM particles. We will further explain how to evaluate these parameters. Before, let's have a closer look to Eq. (90). Interestingly, we note that when dynamical equilibrium is reached, *i.e.* $dN_\chi/dt = 0$, the annihilation rate is then fully fixed by the capture

rate, with $\Gamma_a = C_c/2$. Nevertheless, this clearly depends on the annihilation parameter C_a and the capture rate, and the general solution to Eq. (90) is given by:

$$N(t) = \sqrt{\frac{C_c}{C_a}} \tanh \left\{ \frac{t}{\tau_c} \right\} \xrightarrow{t \gg \tau_c} \sqrt{\frac{C_c}{C_a}}, \quad (92)$$

$$\tau_c \equiv (C_c C_a)^{-1/2}.$$

For neutrino detection today, this equation has to be evaluated at a time corresponding to the age of the Sun, $t = t_\odot = 4.6$ Gyr. Dynamical equilibrium is reached when $t_\odot/\tau_c \gg 1$, which is usually the case for most DM candidates. Indeed, typical values are of order $\tau_{c,\odot} \approx 0.001 \tau_{c,\oplus} \approx 10^8$ yr — equilibrium is thereby barely reached in the Earth, while generically expected in the Sun. More precisely for the Sun, we have $t_\odot/\tau_{c,\odot} \approx \sqrt{(C_c/10^{25} \text{ s}^{-1})(\langle\sigma_{\text{ann}}v\rangle/10^{-30} \text{ cm}^3 \text{ s}^{-1})}$, which means that even with an annihilation cross section much lower today than the one relevant at thermal decoupling in the early universe (this is the case when annihilation is p-wave dominated), the annihilation rate in the Sun can still be maximal. Indeed, in terms of annihilation rate, Eq. (92) gives

$$\Gamma_a(t) = \frac{C_c}{2} \tanh^2 \left\{ \frac{t}{\tau_c} \right\} \xrightarrow{t \gg \tau_c} \frac{C_c}{2}, \quad (93)$$

which is independent of the annihilation cross section when equilibrium is reached. We therefore anticipate that the solar neutrino flux can provide very strong constraints to p-wave annihilation cross sections if the elastic scattering cross section is large enough, which is not the case with other indirect detection messengers. Given a point-like reservoir located at distance d from the Earth, the neutrino flux reads

$$\phi_\nu(E) = \frac{\epsilon_\nu(E) \Gamma_a}{4 \pi d^2} \frac{dN_\nu}{dE}, \quad (94)$$

where dN_ν/dE is the neutrino spectrum injected at the source and $\epsilon_\nu(E)$ accounts for the oscillation and absorption effects discussed in the previous section, which can significantly alter the original spectrum. The point-like approximation is usually very good for the Sun given the poor angular resolution achieved in neutrino astronomy, typically 1° or more for GeV-TeV neutrinos; this ceases to be the case for the Earth. In the following, we discuss the calculations of the annihilation parameter C_a and the capture rate C_c which both set the annihilation rate Γ_a .

To derive C_a , one has first to guess the spatial distribution of DM in the Sun. Spherical symmetry applies, and if dynamical relaxation is assumed, then the spatial distribution is fixed by the local gravitational potential Φ and the average kinetic energy (*i.e.* the average temperature \bar{T}) [214] according to

$$n(t, \mathbf{x}) = n(t, r) = n_0(t) e^{-m_\chi \Phi(r)/\bar{T}}, \quad (95)$$

$$\Phi(r) = \int_0^r dr' \frac{G_N M(r')}{r'^2}, \quad M(r) = 4 \pi \int_0^r dr' r'^2 \rho_{\text{sun}}(r'),$$

where n_0 is the average density at the core, G_N is Newton's constant, $M(r)$ is the solar mass within radius r , and ρ_{sun} is the solar mass density. Since $N = 4\pi \int_0^{R_{\text{sun}}} dr r^2 n(t, r)$, it comes

$$C_a = \frac{\int_0^{R_{\text{sun}}} dr r^2 \langle \sigma_{\text{ann}} v \rangle n^2(t, r)}{N^2} = \langle \sigma_{\text{ann}} v \rangle \frac{\int_0^{R_{\text{sun}}} dr r^2 e^{-2m_\chi \Phi(r)/T}}{\left[\int_0^{R_{\text{sun}}} dr r^2 e^{-m_\chi \Phi(r)/T} \right]^2}, \quad (96)$$

and we remark that we can express C_a in terms of effective volumes as

$$C_a = \langle \sigma_{\text{ann}} v \rangle \frac{V_2}{V_1^2}, \quad (97)$$

$$V_n \equiv \left[\frac{3 m_{\text{Pl}}^2 T_{\text{sun}}}{2 n m_\chi \rho_{\text{sun}}} \right]^{3/2} \simeq 6.6 \times 10^{28} \left[\frac{n m_\chi}{10 \text{ GeV}} \right]^{-3/2} \text{ cm}^3,$$

where the effective volume V_n has an explicit dependence in the solar core temperature T_{sun} and density ρ_{sun} [227]. For the Earth, this volume is $V_n \simeq 2.3 \times 10^{25} (n m_\chi / 10 \text{ GeV})^{-3/2} \text{ cm}^3$. Here, we have implicitly assumed that DM is concentrated at the Sun's core, and taken the corresponding constant values for the solar mass density and temperature. Instead, we may also evaluate these values at the mean orbital radius \bar{r} [225], so that we now have to solve the equation for C_a using $\rho_{\text{sun}}(r) = \rho_{\text{sun}}(\bar{r})$, and $T(r) = T(\bar{r})$. The mean orbital radius can be determined from the following implicit equation:

$$\bar{r} = \frac{\int_0^{R_{\text{sun}}} d^3 \mathbf{x} r n(t, r)}{\int_0^{R_{\text{sun}}} d^3 \mathbf{x} n(t, r)} = \frac{\int_0^{R_{\text{sun}}} dr r^3 e^{-m_\chi \Phi(r)/T(\bar{r})}}{\int_0^{R_{\text{sun}}} dr r^2 e^{-m_\chi \Phi(r)/T(\bar{r})}} = \sqrt{\frac{6 T(\bar{r})}{\pi^2 G_N \rho_{\text{sun}}(\bar{r}) m_\chi}}. \quad (98)$$

This equation can be solved numerically. Then, the solution for C_a is analytic and reads:

$$C_a = \left[\frac{\sqrt{2}}{\pi \bar{r}} \right]^3 \langle \sigma_{\text{ann}} v \rangle. \quad (99)$$

The authors of Ref. [225] have found that for masses larger than 1 GeV, a good numerical approximation to the previous result is given by

$$C_a \simeq 4.5 \times 10^{-30} \text{ cm}^{-3} \left[\frac{m_\chi - 0.6 \text{ GeV}}{10 \text{ GeV}} \right]^{3/2} \langle \sigma_{\text{ann}} v \rangle. \quad (100)$$

Here, the thermal average of the annihilation cross section $\langle \sigma_{\text{ann}} v \rangle$ should be performed according to a Maxwellian with the core temperature $T(\bar{r}) \approx 10^7 \text{ K} \approx 1 \text{ keV}$ as the characteristic temperature.

We now turn to the determination of the DM capture rate, which does depend on the scattering cross section and on the elemental distribution in the solar core [215]:

$$\Gamma_{c,\odot} = 4\pi \int_0^{R_{\text{sun}}} dr r^2 \left\{ \sum_i \frac{d\Gamma_{c,i}(r)}{dV} \right\}. \quad (101)$$

It involves the differential capture rate per shell volume unit induced by a solar element of label i :

$$\frac{d\Gamma_{c,i}(r)}{dV} = \frac{\rho_\chi \rho_i(r) \sigma_i}{2 m_\chi \mu_i^2} \int_0^{w_{\max}} dw \frac{f(w)}{w} \int_{Q_{\min}}^{Q_{\max}} dQ F_i^2(Q), \quad (102)$$

where ρ_χ is the local DM mass density, $\rho_i(r)$ the element mass density in the spherical shell at radius r , σ_i the WIMP-element scattering cross section, μ_i the WIMP-element reduced mass, $f(w)$ the normalized velocity distribution in the solar frame, w the velocity as unaffected by the solar gravitational potential, $F(Q)$ the nuclear form factor such that $F(0) = 1$, and Q the recoil energy¹². The dependence on the elastic cross section and on the local WIMP density makes clear the correlation arising between the neutrino signal expected from the Sun/Earth and the event rate predicted at direct detection experiments, especially when dynamical equilibrium is reached, in which case the annihilation rate is fully set by the capture rate. Additionally, we underline that given equivalent strengths for scalar (spin-independent) and axial-vector (spin-dependent) WIMP-nucleus interactions, capture in the Sun is usually dominated by the latter because of the prominence of light elements in the core (mostly hydrogen), while the former plays an important role for capture in the Earth.

In Eq. (102), the first integral is performed over the Galactic velocity w , which can easily be related to the velocity in the Sun v . Indeed, energy conservation tells us that before the elastic scattering off a nucleus, the global WIMP kinetic energy $\propto m_\chi w^2$ remains constant. Besides, when the WIMP falls in the Sun's gravitational potential, gravitational energy gets locally converted into kinetic energy. Therefore, the WIMP velocity in the Sun is given by $v^2 = w^2 + v_{\text{esc}}^2(r)$, where the escape velocity v_{esc} is defined as the velocity at which the kinetic energy equals the gravitational potential. The escape velocity at the Sun's surface is 617.8 km/s, to be compared to a value of 11.87 km/s for the Earth. A Maxwellian velocity distribution is usually assumed, which (in the Sun's frame) is given by

$$\frac{f(w)}{w} = \sqrt{\frac{3}{2\pi}} \frac{1}{\sigma_v v_\odot} \left[\exp \left\{ -\frac{3(w - v_\odot)^2}{2\sigma_v^2} \right\} - \exp \left\{ -\frac{3(w + v_\odot)^2}{2\sigma_v^2} \right\} \right], \quad (103)$$

where $v_\odot \simeq 220$ km/s is the velocity of the Sun in the Galactic frame, and $\sigma_v \simeq 270$ km/s is the velocity dispersion of DM species.

Kinematics must be inspected carefully, as detailed in [215, 228, 231] and very clearly summarized in [227]. A WIMP is captured as soon as its velocity is less than v_{esc} after scattering. Defining

$$\beta_\pm \equiv \frac{4 m_\chi m_i}{(m_\chi \pm m_i)^2}, \quad (104)$$

12. Form factors are different for scalar and spin-dependent interactions. Common references are [228, 229] for the former and [230] for the latter.

the fraction of WIMP energy lost in the collision, $f_Q = Q/E$, must lie in the range

$$\begin{aligned} 0 &\leq f_Q \leq \beta_+, \\ m_\chi w^2 &\leq 2Q \leq \beta_+ m_\chi (w^2 + v_{\text{esc}}^2), \end{aligned} \quad (105)$$

for the WIMP to be captured. At this stage, it is interesting to remark that for an isotropic scattering (disregarding the form factor suppression for a moment), the probability \mathcal{P} for a WIMP to scatter down to a velocity smaller than v_{esc} should be flat in the above range such that [227]

$$\mathcal{P}(w) = \frac{1}{(w^2 + v_{\text{esc}}^2)} \left\{ v_{\text{esc}}^2 - \frac{w}{\beta_-} \right\} \theta \left[v_{\text{esc}}^2 - \frac{w}{\beta_-} \right], \quad (106)$$

where θ is the Heaviside function. Incidentally, this equation shows that the probability of capture is maximized when β_- is maximized, *i.e.* when $m_\chi \approx m_i$. This actually corresponds to resonance effects, which depend on both the elemental distribution in the celestial reservoir and the escape velocity. This has been intensely discussed in Ref. [228] where these resonance effects were predicted to be important for capture in the Earth, due to the larger relative density of oxygen and metals.

Kinematics further helps define the ranges over which the integrals of Eq. (102) are performed:

$$\begin{aligned} w_{\text{max}}(r) &= \sqrt{\frac{4 m_\chi m_i}{(m_\chi - m_i)^2}} v_{\text{esc}}(r), \\ Q_{\text{min}} &= \frac{1}{2} m_\chi w^2, \\ Q_{\text{max}} &= \sqrt{\frac{4 m_\chi m_i}{(m_\chi + m_i)^2}} m_\chi v^2. \end{aligned} \quad (107)$$

From these integral boundaries, we understand why a departure from the Maxwellian law can have a significant impact on the predictions, as discussed into more details in *e.g.* Ref. [232].

7.3.2. Current limits on DM models and prospects

We start by emphasizing that in contrast with other indirect detection messengers, the solar neutrino signature is one of the best to discover DM annihilation because predictions do not suffer potentially big theoretical errors. Indeed, they mostly rely (i) on the knowledge of the local DM density and dynamics, which can be constrained reasonably well, (ii) on neutrino propagation in vacuum and matter, which is under control, and (iii) on the DM particle mass, and its annihilation and interaction properties. The latter point can be fixed for each DM model. The most important uncertainty affects the evaluation of the WIMP-atom elastic scattering cross section, because of uncertainties in the estimates of the spin contents of nucleons (spin-dependent interactions) and of

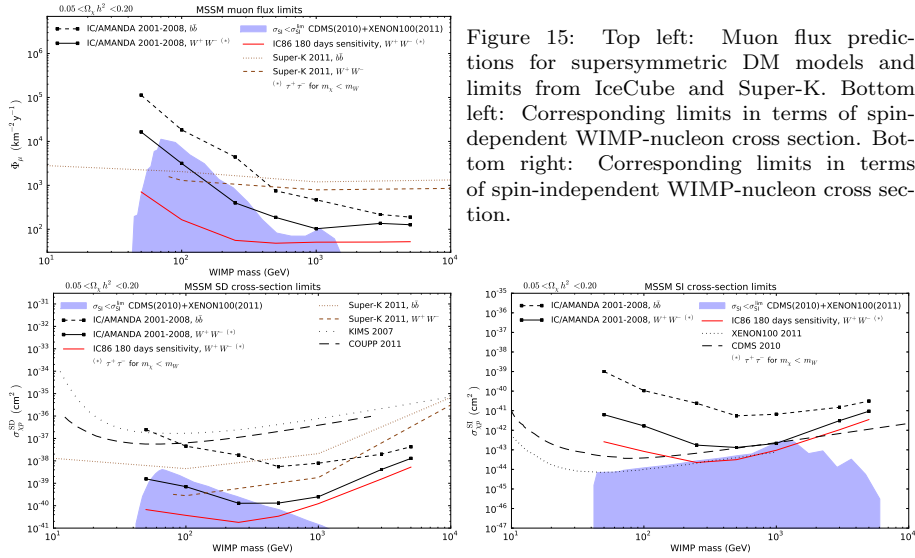


Figure 15: Top left: Muon flux predictions for supersymmetric DM models and limits from IceCube and Super-K. Bottom left: Corresponding limits in terms of spin-dependent WIMP-nucleon cross section. Bottom right: Corresponding limits in terms of spin-independent WIMP-nucleon cross section.

the nucleonic matrix elements (scalar interactions) — see *e.g.* [233]. Nevertheless, there are hopes to reduce these uncertainties in the near future thanks to improvements in hadronic physics or QCD, for which experimental data will come from existing colliders. Finally, as another big advantage over other astrophysical messengers, the main neutrino background is well measured and also under control.

Many predictions of the neutrino fluxes from the Sun and the Earth have been derived in the context of supersymmetric DM [227]. The reader can find extensive examples in *e.g.* [219, 220, 234, 235, 236]. Predictions in the frame of extra-dimensional theories are quantitatively similar (see *e.g.* [237, 238]). These predictions mostly concern the muon neutrino flux¹³, which can be reconstructed at detectors as upward-going muons after charged current conversion. The predicted fluxes, usually higher if induced by DM annihilation in the Sun than in the Earth’s interior, can reach 10^{11} - 10^{12} upgoing muon neutrinos per year and square kilometer above a detection threshold energy of $E_\nu^{\text{th}} \approx 10$ GeV, which translates into an upgoing muon flux of 10^2 - 10^3 $\text{km}^{-2}\text{yr}^{-1}$ at detectors. The full energy dependence has further to be taken into account properly to convolve these expectations with the detector efficiencies and to compare them with the background. For DM searches toward the Sun, we note that in addition to the atmospheric background, a contribution is also expected from interactions of cosmic rays in the Sun itself, although it has been shown negligible [239, 240].

Disregarding the details of predictions, we emphasize that such a muon flux level is within reach of some current experiments like Super-K [241] and Ice-

13. See Ref. [226] for prospects with tau neutrinos.

Cube [242], which have already derived interesting limits. These are shown in terms of muon flux in the top left panel of Fig. 15, taken from Ref. [242], on top of predictions associated with DM candidates arising in the minimal supersymmetric model (represented as the shaded area in the plot). Note that a broad range for the relic abundance was considered, down to a value as low as $\Omega_\chi h^2 = 0.05$. This implies that the reported shaded area contains models with optimistically large cross sections, most of which corresponding to the largest predicted muon fluxes. Some direct detection constraints have been included, coming from both a combined analysis of the CDMS and EDELWEISS data [243] and from XENON 100 [244]. Two types of limits appear in the panel, one assuming a soft neutrino spectrum arising in annihilation into b quarks, and another one assuming a harder neutrino spectrum originating in annihilation into W bosons; the latter case is obviously more constraining. The supersymmetric models in the shaded zone, in contrast, usually come with more complex spectra, in between these two cases. While the derived limits are shown to start tickling the upper part of the relevant parameter space, the sensitivity of the complete version of IceCube is drawn as the red solid curve for a duty cycle of 180 days. It clearly demonstrates the potential of neutrino telescopes to survey a large part of the supersymmetric parameter space.

As already emphasized above, the neutrino signal induced by DM annihilation in celestial bodies should exhibit a correlation with direct detection signals. For the Sun, the neutrino signal is mostly proportional to the spin-dependent elastic scattering cross section, while the scalar one may also, in some case, become important. Therefore, limits on the solar neutrino flux can easily be translated in terms of elastic scattering cross sections and compared with the sensitivities of direct detection experiments — this is obviously DM model dependent. The bottom panels of Fig. 15 nicely illustrate that, where the muon flux predictions of the top panel are replotted in terms of WIMP-nucleon spin-dependent scattering cross section (bottom left) and of scalar scattering cross section (bottom right). We clearly see that, for the former case, current neutrino telescopes are already very competitive with respect to existing direct detection experiments like KIM [245] or COUPP [246]. On the other hand, the scalar cross section is more poorly constrained.

The complementarity between direct DM detection and indirect detection is further illustrated in Fig. 16, taken from Ref. [225], where the authors used the Super-K data to extract limits on generic WIMP models. The used data set slightly differs from the previous example in that only fully contained events, *i.e.* upgoing muons stopping within the detector, were considered to reduce the background and enhance sensitivity [224]. The top (bottom) panels show the limits obtained on the spin-dependent (scalar) cross section, while the left (right) panels concern models for which the relic abundance is set by a fully s-wave (p-wave) annihilation cross section. Note that a dominating p-wave annihilation cross section makes indirect DM detection with other messengers irrelevant since annihilation in galactic halos is then velocity suppressed; neutrinos are therefore the only indirect detection possibility in this case. In the plots, the authors have assumed different pure annihilation final states, which are made explicit.

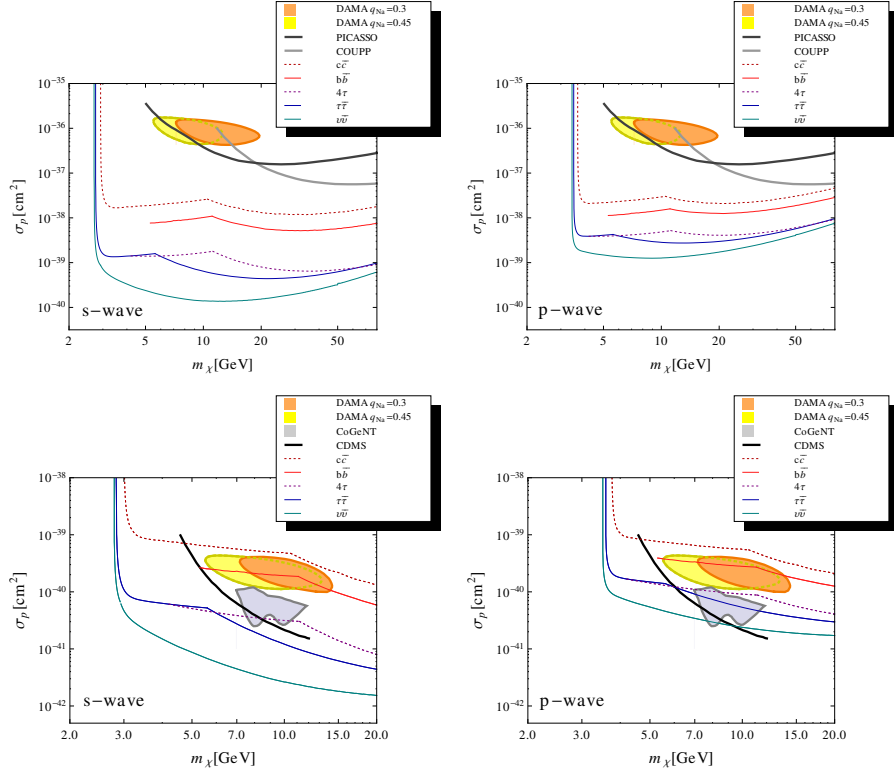


Figure 16: Limits on the spin-dependent (top) and spin-independent (bottom) WIMP-nucleon cross sections obtained from the Super-K data. The left (right) panels assume that the WIMP relic density is set by a pure s-wave (p-wave) annihilation cross section. Regions favored by some direct detection experiments appear as shaded areas. These plots have been taken from Ref. [225].

Finally, they have reported as shaded zones the regions corresponding to the excess events found in two direct detection experiments, DAMA [247] and CoGeNT [37], together with the limits obtained by the PICASSO [248], COUPP [246], and CDMS [243] collaborations.

Acknowledgements

We would like to thank C. Boehm and P. Brax, the editors of this special issue, for having invited us to express our point of view on the topic of WIMP indirect detection. PS expresses his gratitude to the Institut universitaire de France (IUF) for academically and financially supporting his research.

References

- [1] J. Silk, Dark Matter: the astrophysical case, this issue of Comptes Rendus de l'Académie des Sciences.
- [2] D. Hooper, T. Tait, Theories of particle dark matter, this issue of Comptes Rendus de l'Académie des Sciences.
- [3] E. Armengaud, Direct detection of WIMPs, this issue of Comptes Rendus de l'Académie des Sciences.
- [4] F. Casse, M. Lemoine, G. Pelletier, Transport of cosmic rays in chaotic magnetic fields, *Phys. Rev. D* 65 (2) (2002) 023002. [arXiv:astro-ph/0109223](#), [doi:10.1103/PhysRevD.65.023002](#).
- [5] D. Maurin, et al., Galactic Cosmic Ray Nuclei as a Tool for Astroparticle Physics, *Research Signposts, Recent Research Developments in Astronomy and Astrophysics* 2 (2004) 193. [arXiv:astro-ph/0212111](#).
- [6] R. D. Ekers, R. Sancisi, The radio continuum halo in NGC 4631, *Astron. Astroph.* 54 (1977) 973.
- [7] A. W. Strong, I. V. Moskalenko, Propagation of Cosmic-Ray Nucleons in the Galaxy, *Astrophys. J.* 509 (1998) 212–228. [arXiv:astro-ph/9807150](#), [doi:10.1086/306470](#).
- [8] C. Evoli, et al., Cosmic ray nuclei, antiprotons and gamma rays in the galaxy: a new diffusion model, *Journal of Cosmology and Astro-Particle Physics* 10 (2008) 18–+. [arXiv:0807.4730](#), [doi:10.1088/1475-7516/2008/10/018](#).
- [9] D. Maurin, et al., Cosmic Rays below Z=30 in a Diffusion Model: New Constraints on Propagation Parameters, *Astrophys. J.* 555 (2001) 585–596. [arXiv:astro-ph/0101231](#), [doi:10.1086/321496](#).
- [10] F. Donato, et al., Antiprotons in cosmic rays from neutralino annihilation, *Phys. Rev. D* 69 (6) (2004) 063501–+. [arXiv:astro-ph/0306207](#), [doi:10.1103/PhysRevD.69.063501](#).
- [11] A. Putze, L. Derome, D. Maurin, A Markov Chain Monte Carlo technique to sample transport and source parameters of Galactic cosmic rays. II. Results for the diffusion model combining B/C and radioactive nuclei, *Astron. Astroph.* 516 (2010) A66+. [arXiv:1001.0551](#), [doi:10.1051/0004-6361/201014010](#).
- [12] L. C. Tan, L. K. Ng, Parametrisation of hadron inclusive cross sections in p-p collisions extended to very low energies, *Journal of Physics G Nuclear Physics* 9 (1983) 1289–1308. [doi:10.1088/0305-4616/9/10/015](#).

- [13] T. Bringmann, P. Salati, Galactic antiproton spectrum at high energies: Background expectation versus exotic contributions, *Phys. Rev. D* 75 (8) (2007) 083006. [arXiv:astro-ph/0612514](#), [doi:10.1103/PhysRevD.75.083006](#).
- [14] L. C. Tan, L. K. Ng, Parameterization of σ invariant cross section in p-p collisions using a new scaling variable, *Phys. Rev. D* 26 (1982) 1179–1182. [doi:10.1103/PhysRevD.26.1179](#).
- [15] L. C. Tan, L. K. Ng, Calculation of the equilibrium antiproton spectrum, *Journal of Physics G Nuclear Physics* 9 (1983) 227–242. [doi:10.1088/0305-4616/9/2/015](#).
- [16] L. Bergström, J. Edsjö, P. Ullio, Cosmic Antiprotons as a Probe for Supersymmetric Dark Matter?, *Astrophys. J.* 526 (1999) 215–235. [arXiv:astro-ph/9902012](#), [doi:10.1086/307975](#).
- [17] E. W. Anderson, et al., Proton and Pion Spectra from Proton-Proton Interactions at 10, 20, and 30 BeV/c, *Physical Review Letters* 19 (1967) 198–201. [doi:10.1103/PhysRevLett.19.198](#).
- [18] R. Duperray, et al., Flux of light antimatter nuclei near Earth, induced by cosmic rays in the Galaxy and in the atmosphere, *Phys. Rev. D* 71 (8) (2005) 083013. [arXiv:astro-ph/0503544](#), [doi:10.1103/PhysRevD.71.083013](#).
- [19] F. Donato, N. Fornengo, D. Maurin, Antideuteron fluxes from dark matter annihilation in diffusion models, *Phys. Rev. D* 78 (4) (2008) 043506+. [arXiv:0803.2640](#), [doi:10.1103/PhysRevD.78.043506](#).
- [20] F. Donato, D. Maurin, P. Salati, A. Barrau, G. Boudoul, R. Taillet, Antiprotons from Spallations of Cosmic Rays on Interstellar Matter, *Astrophys. J.* 563 (2001) 172–184.
- [21] K. Agashe, G. Servant, Warped Unification, Proton Stability, and Dark Matter, *Physical Review Letters* 93 (23) (2004) 231805+. [arXiv:hep-ph/0403143](#), [doi:10.1103/PhysRevLett.93.231805](#).
- [22] K. Agashe, G. Servant, Baryon number in warped grand unified theories: model building and (dark matter related) phenomenology, *Journal of Cosmology and Astro-Particle Physics* 2 (2005) 2+. [arXiv:hep-ph/0411254](#), [doi:10.1088/1475-7516/2005/02/002](#).
- [23] A. Barrau, et al., Kaluza-Klein dark matter and galactic antiprotons, *Phys. Rev. D* 72 (6) (2005) 063507. [doi:10.1103/PhysRevD.72.063507](#).
- [24] O. Adriani, et al., PAMELA Results on the Cosmic-Ray Antiproton Flux from 60 MeV to 180 GeV in Kinetic Energy, *Physical Review Letters* 105 (12) (2010) 121101+. [arXiv:1007.0821](#), [doi:10.1103/PhysRevLett.105.121101](#).

- [25] J. F. Navarro, C. S. Frenk, S. D. M. White, A Universal Density Profile from Hierarchical Clustering, *Astrophys. J.*490 (1997) 493–+. [arXiv:astro-ph/9611107](#), [doi:10.1086/304888](#).
- [26] B. Moore, et al., Dark Matter Substructure within Galactic Halos, *Astrophys. J. Lett.*524 (1999) L19–L22. [arXiv:astro-ph/9907411](#), [doi:10.1086/312287](#).
- [27] J. F. Navarro, et al., The inner structure of Λ CDM haloes - III. Universality and asymptotic slopes, *MNRAS* 349 (2004) 1039–1051. [arXiv:astro-ph/0311231](#), [doi:10.1111/j.1365-2966.2004.07586.x](#).
- [28] J. Diemand, B. Moore, J. Stadel, Convergence and scatter of cluster density profiles, *MNRAS*353 (2004) 624–632. [arXiv:astro-ph/0402267](#), [doi:10.1111/j.1365-2966.2004.08094.x](#).
- [29] G. Gentile, et al., The cored distribution of dark matter in spiral galaxies, *MNRAS*351 (2004) 903–922. [arXiv:astro-ph/0403154](#), [doi:10.1111/j.1365-2966.2004.07836.x](#).
- [30] F. Donato, G. Gentile, P. Salucci, Cores of dark matter haloes correlate with stellar scalelengths, *MNRAS*353 (2004) L17–L22. [arXiv:astro-ph/0403206](#), [doi:10.1111/j.1365-2966.2004.08220.x](#).
- [31] R. Catena, P. Ullio, A novel determination of the local dark matter density, *JCAP*8 (2010) 4–+. [arXiv:0907.0018](#), [doi:10.1088/1475-7516/2010/08/004](#).
- [32] P. Salucci, et al., The dark matter density at the Sun’s location, *Astron. Astroph.*523 (2010) A83+. [arXiv:1003.3101](#), [doi:10.1051/0004-6361/201014385](#).
- [33] P. J. McMillan, Mass models of the Milky Way, *MNRAS*414 (2011) 2446–2457. [arXiv:1102.4340](#), [doi:10.1111/j.1365-2966.2011.18564.x](#).
- [34] J. Bovy, S. Tremaine, On the Local Dark Matter Density, *Astrophys. J.*756 (2012) 89. [arXiv:1205.4033](#), [doi:10.1088/0004-637X/756/1/89](#).
- [35] J. N. Bahcall, R. M. Soneira, The universe at faint magnitudes. I - Models for the galaxy and the predicted star counts, *Astrophys. J. Suppl. Series*44 (1980) 73–110. [doi:10.1086/190685](#).
- [36] Z. Ahmed, et al., Dark Matter Search Results from the CDMS II Experiment, *Science* 327 (2010) 1619–. [arXiv:0912.3592](#), [doi:10.1126/science.1186112](#).
- [37] C. E. Aalseth, et al., Results from a Search for Light-Mass Dark Matter with a p-Type Point Contact Germanium Detector, *Physical Review Letters* 106 (13) (2011) 131301–+. [arXiv:1002.4703](#), [doi:10.1103/PhysRevLett.106.131301](#).

- [38] J. Lavalle, 10 GeV dark matter candidates and cosmic-ray antiprotons, *Phys. Rev. D* 82 (8) (2010) 081302–+. [arXiv:1007.5253](#), [doi:10.1103/PhysRevD.82.081302](#).
- [39] D. G. Cerdeño, T. Delahaye, J. Lavalle, Cosmic-ray antiproton constraints on light singlino-like dark matter candidates, *Nuclear Physics B* 854 (2012) 738–779. [arXiv:1108.1128](#), [doi:10.1016/j.nuclphysb.2011.09.020](#).
- [40] P. Ullio, Indirect detection of neutralino dark matter candidates in anomaly-mediated supersymmetry breaking scenarios, *Journal of High Energy Physics* 6 (2001) 53. [arXiv:hep-ph/0105052](#), [doi:10.1088/1126-6708/2001/06/053](#).
- [41] S. Profumo, C. E. Yaguna, Statistical analysis of supersymmetric dark matter in the minimal supersymmetric standard model after WMAP, *Phys. Rev. D* 70 (9) (2004) 095004. [arXiv:hep-ph/0407036](#), [doi:10.1103/PhysRevD.70.095004](#).
- [42] J. Hisano, S. Matsumoto, M. M. Nojiri, Explosive Dark Matter Annihilation, *Physical Review Letters* 92 (3) (2004) 031303. [arXiv:hep-ph/0307216](#), [doi:10.1103/PhysRevLett.92.031303](#).
- [43] J. Hisano, et al., Nonperturbative effect on dark matter annihilation and gamma ray signature from the galactic center, *Phys. Rev. D* 71 (6) (2005) 063528–+. [arXiv:hep-ph/0412403](#), [doi:10.1103/PhysRevD.71.063528](#).
- [44] O. Adriani, et al., An anomalous positron abundance in cosmic rays with energies 1.5-100GeV, *Nature* 458 (2009) 607–609. [arXiv:0810.4995](#), [doi:10.1038/nature07942](#).
- [45] I. V. Moskalenko, A. W. Strong, Production and Propagation of Cosmic-Ray Positrons and Electrons, *Astrophys. J.* 493 (1998) 694–+. [arXiv:astro-ph/9710124](#), [doi:10.1086/305152](#).
- [46] E. A. Baltz, J. Edsjö, Positron propagation and fluxes from neutralino annihilation in the halo, *Phys. Rev. D* 59 (2) (1999) 023511. [arXiv:astro-ph/9808243](#), [doi:10.1103/PhysRevD.59.023511](#).
- [47] T. Delahaye, et al., Positrons from dark matter annihilation in the galactic halo: Theoretical uncertainties, *Phys. Rev. D* 77 (6) (2008) 063527–+. [arXiv:0712.2312](#), [doi:10.1103/PhysRevD.77.063527](#).
- [48] G. D. Badhwar, R. L. Golden, S. A. Stephens, Analytic representation of the proton-proton and proton-nucleus cross-sections and its application to the sea-level spectrum and charge ratio of muons, *Phys. Rev. D* 15 (1977) 820–831. [doi:10.1103/PhysRevD.15.820](#).
- [49] T. Kamae, et al., Parameterization of γ , e^\pm , and Neutrino Spectra Produced by p-p Interaction in Astronomical Environments, *Astrophys. J.* 647 (2006) 692–708. [arXiv:astro-ph/0605581](#), [doi:10.1086/505189](#).

- [50] O. Adriani, et al., PAMELA Measurements of Cosmic-Ray Proton and Helium Spectra, *Science* 332 (2011) 69–. [arXiv:1103.4055](#), [doi:10.1126/science.1199172](#).
- [51] T. Delahaye, et al., Systematic effects in the estimate of the local gamma-ray emissivity, *ArXiv e-prints*[arXiv:1109.0834](#).
- [52] AMS Collaboration, The Alpha Magnetic Spectrometer (AMS) on the International Space Station: Part I - results from the test flight on the space shuttle, *Phys. Rept.*366 (2002) 331–405. [doi:10.1016/S0370-1573\(02\)00013-3](#).
- [53] A. A. Abdo, et al., Measurement of the Cosmic Ray $e^+ + e^-$ Spectrum from 20GeV to 1TeV with the Fermi Large Area Telescope, *Physical Review Letters* 102 (18) (2009) 181101–+. [arXiv:0905.0025](#), [doi:10.1103/PhysRevLett.102.181101](#).
- [54] J. Lavalle, Impact of the spectral hardening of TeV cosmic rays on the prediction of the secondary positron flux, *MNRAS*414 (2011) 985–991. [arXiv:1011.3063](#), [doi:10.1111/j.1365-2966.2011.18294.x](#).
- [55] T. Delahaye, et al., Galactic secondary positron flux at the Earth, *Astron. Astroph.*501 (2009) 821–833. [arXiv:0809.5268](#), [doi:10.1051/0004-6361/200811130](#).
- [56] J. Chang, et al., An excess of cosmic ray electrons at energies of 300–800GeV, *Nature*456 (2008) 362–365. [doi:10.1038/nature07477](#).
- [57] F. Aharonian, et al., Energy Spectrum of Cosmic-Ray Electrons at TeV Energies, *Physical Review Letters* 101 (26) (2008) 261104–+. [arXiv:0811.3894](#), [doi:10.1103/PhysRevLett.101.261104](#).
- [58] F. Aharonian, et al., Probing the ATIC peak in the cosmic-ray electron spectrum with H.E.S.S., *Astron. Astroph.*508 (2009) 561–564. [arXiv:0905.0105](#), [doi:10.1051/0004-6361/200913323](#).
- [59] D. Grasso, et al., On possible interpretations of the high energy electron-positron spectrum measured by the Fermi Large Area Telescope, *Astroparticle Physics* 32 (2009) 140–151. [arXiv:0905.0636](#), [doi:10.1016/j.astropartphys.2009.07.003](#).
- [60] T. Delahaye, et al., Galactic electrons and positrons at the Earth: new estimate of the primary and secondary fluxes, *Astron. Astroph.*524 (2010) A51+. [arXiv:1002.1910](#), [doi:10.1051/0004-6361/201014225](#).
- [61] A. W. Strong, I. V. Moskalenko, O. Reimer, Diffuse Galactic Continuum Gamma Rays: A Model Compatible with EGRET Data and Cosmic-Ray Measurements, *Astrophys. J.*613 (2004) 962–976. [arXiv:astro-ph/0406254](#), [doi:10.1086/423193](#).

- [62] F. Donato, et al., Constraints on WIMP Dark Matter from the High Energy PAMELA \bar{p}/p Data, *Physical Review Letters* 102 (7) (2009) 071301–+. [arXiv:0810.5292](#), [doi:10.1103/PhysRevLett.102.071301](#).
- [63] E. Komatsu, et al., Seven-year Wilkinson Microwave Anisotropy Probe (WMAP) Observations: Cosmological Interpretation, *Astrophys. J. Suppl. Series* 192 (2011) 18. [arXiv:1001.4538](#), [doi:10.1088/0067-0049/192/2/18](#).
- [64] P. Salati, Quintessence and the relic density of neutralinos, *Physics Letters B* 571 (2003) 121–131. [arXiv:astro-ph/0207396](#), [doi:10.1016/j.physletb.2003.07.073](#).
- [65] S. Profumo, P. Ullio, SUSY dark matter and quintessence, *JCAP* 11 (2003) 6. [arXiv:hep-ph/0309220](#), [doi:10.1088/1475-7516/2003/11/006](#).
- [66] G. Kane, R. Lu, S. Watson, PAMELA satellite data as a signal of non-thermal wino LSP dark matter, *Physics Letters B* 681 (2009) 151–160. [arXiv:0906.4765](#), [doi:10.1016/j.physletb.2009.09.053](#).
- [67] M. Cirelli, R. Franceschini, A. Strumia, Minimal Dark Matter predictions for galactic positrons, anti-protons, photons, *Nuclear Physics B* 800 (2008) 204–220. [arXiv:0802.3378](#), [doi:10.1016/j.nuclphysb.2008.03.013](#).
- [68] N. Arkani-Hamed, et al., A theory of dark matter, *Phys. Rev. D* 79 (1) (2009) 015014–+. [arXiv:0810.0713](#), [doi:10.1103/PhysRevD.79.015014](#).
- [69] M. Pospelov, A. Ritz, Astrophysical signatures of secluded dark matter, *Physics Letters B* 671 (2009) 391–397. [arXiv:0810.1502](#), [doi:10.1016/j.physletb.2008.12.012](#).
- [70] M. Pospelov, A. Ritz, M. Voloshin, Secluded WIMP dark matter, *Physics Letters B* 662 (2008) 53–61. [arXiv:0711.4866](#), [doi:10.1016/j.physletb.2008.02.052](#).
- [71] M. Lattanzi, J. Silk, Can the WIMP annihilation boost factor be boosted by the Sommerfeld enhancement?, *Phys. Rev. D* 79 (8) (2009) 083523–+. [arXiv:0812.0360](#), [doi:10.1103/PhysRevD.79.083523](#).
- [72] M. Cirelli, et al., Model-independent implications of the e^+ , \bar{p} cosmic ray spectra on properties of Dark Matter, *Nuclear Physics B* 813 (2009) 1–21. [arXiv:0809.2409](#), [doi:10.1016/j.nuclphysb.2008.11.031](#).
- [73] O. Adriani, et al., New Measurement of the Antiproton-to-Proton Flux Ratio up to 100 GeV in the Cosmic Radiation, *Physical Review Letters* 102 (5) (2009) 051101. [arXiv:0810.4994](#), [doi:10.1103/PhysRevLett.102.051101](#).

- [74] E. Borriello, A. Cuoco, G. Miele, Secondary Radiation from the Pamela/ATIC Excess and Relevance for Fermi, *Astrophys. J. Lett.*699 (2009) L59–L63. [arXiv:0903.1852](#), [doi:10.1088/0004-637X/699/2/L59](#).
- [75] G. Bertone, et al., Gamma-ray and radio tests of the e^\pm excess from DM annihilations, *Journal of Cosmology and Astro-Particle Physics* 3 (2009) 9–+. [arXiv:0811.3744](#), [doi:10.1088/1475-7516/2009/03/009](#).
- [76] L. Bergström, et al., Gamma-ray and radio constraints of high positron rate dark matter models annihilating into new light particles, *Phys. Rev. D*79 (8) (2009) 081303–+(R). [arXiv:0812.3895](#), [doi:10.1103/PhysRevD.79.081303](#).
- [77] P. Meade, et al., Dark Matter interpretations of the e excesses after FERMI, *Nuclear Physics B* 831 (2010) 178–203. [arXiv:0905.0480](#), [doi:10.1016/j.nuclphysb.2010.01.012](#).
- [78] M. Cirelli, P. Panci, P. D. Serpico, Diffuse gamma ray constraints on annihilating or decaying Dark Matter after Fermi, *Nuclear Physics B* 840 (2010) 284–303. [arXiv:0912.0663](#), [doi:10.1016/j.nuclphysb.2010.07.010](#).
- [79] S. Galli, et al., Updated CMB constraints on dark matter annihilation cross sections, *Phys. Rev. D*84 (2) (2011) 027302. [arXiv:1106.1528](#), [doi:10.1103/PhysRevD.84.027302](#).
- [80] T. R. Slatyer, N. Padmanabhan, D. P. Finkbeiner, CMB constraints on WIMP annihilation: Energy absorption during the recombination epoch, *Phys. Rev. D*80 (4) (2009) 043526. [arXiv:0906.1197](#), [doi:10.1103/PhysRevD.80.043526](#).
- [81] J. Lavalle, et al., Clumpiness of dark matter and the positron annihilation signal, *Astron. Astroph.*462 (2007) 827–840. [arXiv:astro-ph/0603796](#), [doi:10.1051/0004-6361:20065312](#).
- [82] J. Lavalle, et al., Full calculation of clumpiness boost factors for antimatter cosmic rays in the light of Λ CDM N-body simulation results. Abandoning hope in clumpiness enhancement?, *Astron. Astroph.*479 (2008) 427–452. [arXiv:0709.3634](#), [doi:10.1051/0004-6361:20078723](#).
- [83] D. Cumberbatch, J. Silk, Local dark matter clumps and the positron excess, *MNRAS*374 (2007) 455–465. [arXiv:astro-ph/0602320](#), [doi:10.1111/j.1365-2966.2006.11123.x](#).
- [84] D. Hooper, A. Stebbins, K. M. Zurek, Excesses in cosmic ray positron and electron spectra from a nearby clump of neutralino dark matter, *Phys. Rev. D*79 (10) (2009) 103513. [arXiv:0812.3202](#), [doi:10.1103/PhysRevD.79.103513](#).

- [85] P. Brun, et al., Cosmic ray lepton puzzle in the light of cosmological N-body simulations, *Phys. Rev. D* 80 (3) (2009) 035023. [arXiv:0904.0812](#), [doi:10.1103/PhysRevD.80.035023](#).
- [86] J. Diemand, et al., Clumps and streams in the local dark matter distribution, *Nature* 454 (2008) 735–738. [arXiv:0805.1244](#), [doi:10.1038/nature07153](#).
- [87] A. Ibarra, D. Tran, Decaying dark matter and the PAMELA anomaly, *JCAP* 2 (2009) 21. [arXiv:0811.1555](#), [doi:10.1088/1475-7516/2009/02/021](#).
- [88] A. Ibarra, et al., Cosmic rays from leptophilic dark matter decay via kinetic mixing, *JCAP* 8 (2009) 17. [arXiv:0903.3625](#), [doi:10.1088/1475-7516/2009/08/017](#).
- [89] M. Garny, et al., Gamma-ray lines from radiative dark matter decay, *JCAP* 1 (2011) 32. [arXiv:1011.3786](#), [doi:10.1088/1475-7516/2011/01/032](#).
- [90] C. Chen, et al., Decaying Hidden Gauge Boson and the PAMELA and ATIC/PPB-BETS Anomalies, *Progress of Theoretical Physics* 122 (2009) 553–559. [arXiv:0811.3357](#).
- [91] S. Profumo, Dissecting cosmic-ray electron-positron data with Occam’s razor: the role of known pulsars, *Central European Journal of Physics* 10 (2012) 1–31. [arXiv:0812.4457](#), [doi:10.2478/s11534-011-0099-z](#).
- [92] P. Chardonnet, J. Orloff, P. Salati, Production of anti-matter in our galaxy, *Physics Letters B* 409 (1997) 313–320. [arXiv:astro-ph/9705110](#).
- [93] F. Donato, N. Fornengo, P. Salati, Antideuterons as a signature of supersymmetric dark matter, *Phys. Rev. D* 62 (4) (2000) 043003. [arXiv:hep-ph/9904481](#), [doi:10.1103/PhysRevD.62.043003](#).
- [94] M. Braun, V. Vechernin, Fragmentation deuterons from nucleon pairing, *Sov. J. Nucl. Phys.* 36:3 (1982) 357–362.
- [95] V. Choutko, F. Giovacchini, Cosmic Rays Antideuteron Sensitivity for AMS-02 Experiment, in: *International Cosmic Ray Conference*, Vol. 4 of *International Cosmic Ray Conference*, 2008, pp. 765–768.
- [96] C. J. Hailey, et al., Development of the gaseous antiparticle spectrometer for space-based antimatter detection, *Nuclear Instruments and Methods in Physics Research B* 214 (2004) 122–125. [arXiv:astro-ph/0306589](#), [doi:10.1016/j.nimb.2003.08.004](#).
- [97] C. J. Hailey, et al., Accelerator testing of the general antiparticle spectrometer; a novel approach to indirect dark matter detection, *JCAP* 1 (2006) 7. [arXiv:astro-ph/0509587](#), [doi:10.1088/1475-7516/2006/01/007](#).

- [98] J. E. Koglin, et al., Antideuterons as an indirect dark matter signature: design and preparation for a balloon-born GAPS experiment, *Journal of Physics Conference Series* 120 (4) (2008) 042011. doi:10.1088/1742-6596/120/4/042011.
- [99] T. Aramaki, et al., Antideuterons as an indirect dark matter signature: Si(Li) detector development and a GAPS balloon mission, *Advances in Space Research* 46 (2010) 1349–1353. doi:10.1016/j.asr.2010.06.036.
- [100] M. Kadastik, M. Raidal, A. Strumia, Enhanced anti-deuteron Dark Matter signal and the implications of PAMELA, *Physics Letters B* 683 (2010) 248–254. arXiv:0908.1578, doi:10.1016/j.physletb.2009.12.005.
- [101] Y. Cui, J. D. Mason, L. Randall, General analysis of antideuteron searches for dark matter, *Journal of High Energy Physics* 11 (2010) 17. arXiv:1006.0983, doi:10.1007/JHEP11(2010)017.
- [102] N. Fornengo, L. Pieri, S. Scopel, Neutralino annihilation into γ rays in the Milky Way and in external galaxies, *Phys. Rev. D* 70 (10) (2004) 103529–+. arXiv:hep-ph/0407342, doi:10.1103/PhysRevD.70.103529.
- [103] L. Bergström, H. Snellman, Observable monochromatic photons from cosmic photino annihilation, *Phys. Rev. D* 37 (1988) 3737–3741. doi:10.1103/PhysRevD.37.3737.
- [104] J. Hisano, S. Matsumoto, M. M. Nojiri, Unitarity and higher-order corrections in neutralino dark matter annihilation into two photons, *Phys. Rev. D* 67 (7) (2003) 075014. arXiv:hep-ph/0212022, doi:10.1103/PhysRevD.67.075014.
- [105] L. Bergström, Radiative processes in dark matter photino annihilation, *Physics Letters B* 225 (1989) 372–380. doi:10.1016/0370-2693(89)90585-6.
- [106] J. F. Beacom, N. F. Bell, G. Bertone, Gamma-Ray Constraint on Galactic Positron Production by MeV Dark Matter, *Physical Review Letters* 94 (17) (2005) 171301–+. arXiv:astro-ph/0409403, doi:10.1103/PhysRevLett.94.171301.
- [107] L. Bergström, et al., Gamma Rays from Kaluza-Klein Dark Matter, *Physical Review Letters* 94 (13) (2005) 131301. arXiv:astro-ph/0410359, doi:10.1103/PhysRevLett.94.131301.
- [108] A. Birkedal, et al., Robust Gamma Ray Signature of WIMP Dark Matter, *ArXiv High Energy Physics - Phenomenology e-prints* arXiv:hep-ph/0507194.
- [109] L. Bergström, et al., Gamma Rays from Heavy Neutralino Dark Matter, *Physical Review Letters* 95 (24) (2005) 241301–+. arXiv:hep-ph/0507229, doi:10.1103/PhysRevLett.95.241301.

- [110] G. R. Blumenthal, R. J. Gould, Bremsstrahlung, Synchrotron Radiation, and Compton Scattering of High-Energy Electrons Traversing Dilute Gases, *Reviews of Modern Physics* 42 (1970) 237–271.
- [111] L. Roszkowski, et al., On prospects for dark matter indirect detection in the Constrained MSSM, *Physics Letters B* 671 (2009) 10–14. [arXiv:0707.0622](#), [doi:10.1016/j.physletb.2008.11.061](#).
- [112] M. J. Ryan, J. F. Ormes, V. K. Balasubrahmanyam, Cosmic-Ray Proton and Helium Spectra above 50 GeV, *Physical Review Letters* 28 (1972) 985–988. [doi:10.1103/PhysRevLett.28.985](#).
- [113] T. Delahaye, et al., The GeV-TeV Galactic gamma-ray diffuse emission. I. Uncertainties in the predictions of the hadronic component, *Astron. Astroph.*531 (2011) A37. [arXiv:1102.0744](#), [doi:10.1051/0004-6361/201116647](#).
- [114] P. Sreekumar, et al., EGRET Observations of the Extragalactic Gamma-Ray Emission, *Astrophys. J.*494 (1998) 523. [arXiv:astro-ph/9709257](#), [doi:10.1086/305222](#).
- [115] F. Aharonian, et al., Very high energy gamma rays from the direction of Sagittarius A*, *Astron. Astroph.*425 (2004) L13–L17. [arXiv:astro-ph/0406658](#), [doi:10.1051/0004-6361:200400055](#).
- [116] F. Aharonian, et al., Discovery of very-high-energy γ -rays from the Galactic Centre ridge, *Nature*439 (2006) 695–698. [arXiv:astro-ph/0603021](#), [doi:10.1038/nature04467](#).
- [117] L. Bergström, T. Bringmann, J. Edsjö, Complementarity of direct dark matter detection and indirect detection through gamma rays, *Phys. Rev. D*83 (4) (2011) 045024. [arXiv:1011.4514](#), [doi:10.1103/PhysRevD.83.045024](#).
- [118] H. A. Mayer-Hasselwander, et al., High-energy gamma-ray emission from the Galactic Center, *Astron. Astroph.*335 (1998) 161–172.
- [119] A. Cesarini, et al., The Galactic center as a dark matter gamma-ray source, *Astroparticle Physics* 21 (2004) 267–285. [arXiv:astro-ph/0305075](#), [doi:10.1016/S0927-6505\(04\)00033-7](#).
- [120] G. R. Blumenthal, et al., Contraction of dark matter galactic halos due to baryonic infall, *Astrophys. J.*301 (1986) 27–34. [doi:10.1086/163867](#).
- [121] P. Gondolo, J. Silk, Dark Matter Annihilation at the Galactic Center, *Physical Review Letters* 83 (1999) 1719–1722. [arXiv:astro-ph/9906391](#), [doi:10.1103/PhysRevLett.83.1719](#).

- [122] O. Y. Gnedin, A. V. Kravtsov, A. A. Klypin, D. Nagai, Response of Dark Matter Halos to Condensation of Baryons: Cosmological Simulations and Improved Adiabatic Contraction Model, *Astrophys. J.*616 (2004) 16–26. [arXiv:astro-ph/0406247](#), [doi:10.1086/424914](#).
- [123] F. Governato, C. Brook, L. Mayer, A. Brooks, G. Rhee, J. Wadsley, P. Jonsson, B. Willman, G. Stinson, T. Quinn, P. Madau, Bulgeless dwarf galaxies and dark matter cores from supernova-driven outflows, *Nature*463 (2010) 203–206. [doi:10.1038/nature08640](#).
- [124] J. L. Feng, M. Kaplinghat, H.-B. Yu, Halo-Shape and Relic-Density Exclusions of Sommerfeld-Enhanced Dark Matter Explanations of Cosmic Ray Excesses, *Physical Review Letters* 104 (15) (2010) 151301. [arXiv:0911.0422](#), [doi:10.1103/PhysRevLett.104.151301](#).
- [125] F. Aharonian, A. Neronov, High-Energy Gamma Rays from the Massive Black Hole in the Galactic Center, *Astrophys. J.*619 (2005) 306–313. [arXiv:astro-ph/0408303](#), [doi:10.1086/426426](#).
- [126] M. Chernyakova, et al., The High-energy, Arcminute-scale Galactic Center Gamma-ray Source, *Astrophys. J.*726 (2011) 60. [arXiv:1009.2630](#), [doi:10.1088/0004-637X/726/2/60](#).
- [127] K. N. Abazajian, et al., Conservative constraints on dark matter from the Fermi-LAT isotropic diffuse gamma-ray background spectrum, *JCAP*11 (2010) 41. [arXiv:1002.3820](#), [doi:10.1088/1475-7516/2010/11/041](#).
- [128] D. Hooper, L. Goodenough, Dark matter annihilation in the Galactic Center as seen by the Fermi Gamma Ray Space Telescope, *Physics Letters B* 697 (2011) 412–428. [arXiv:1010.2752](#), [doi:10.1016/j.physletb.2011.02.029](#).
- [129] D. Hooper, T. Linden, Origin of the gamma rays from the Galactic Center, *Phys. Rev. D*84 (12) (2011) 123005. [arXiv:1110.0006](#), [doi:10.1103/PhysRevD.84.123005](#).
- [130] A. Boyarsky, D. Malyshev, O. Ruchayskiy, A comment on the emission from the Galactic Center as seen by the Fermi telescope, *Physics Letters B* 705 (2011) 165–169. [arXiv:1012.5839](#), [doi:10.1016/j.physletb.2011.10.014](#).
- [131] M. Su, T. R. Slatyer, D. P. Finkbeiner, Giant Gamma-ray Bubbles from Fermi-LAT: Active Galactic Nucleus Activity or Bipolar Galactic Wind?, *Astrophys. J.*724 (2010) 1044–1082. [arXiv:1005.5480](#), [doi:10.1088/0004-637X/724/2/1044](#).
- [132] R. M. Crocker, F. Aharonian, Fermi Bubbles: Giant, Multibillion-Year-Old Reservoirs of Galactic Center Cosmic Rays, *Physical Review Letters* 106 (10) (2011) 101102. [arXiv:1008.2658](#), [doi:10.1103/PhysRevLett.106.101102](#).

- [133] P. Mertsch, S. Sarkar, Fermi Gamma-Ray “Bubbles” from Stochastic Acceleration of Electrons, *Physical Review Letters* 107 (9) (2011) 091101. [arXiv:1104.3585](#), [doi:10.1103/PhysRevLett.107.091101](#).
- [134] L. Pieri, et al., Implications of high-resolution simulations on indirect dark matter searches, *Phys. Rev. D* 83 (2) (2011) 023518–+. [arXiv:0908.0195](#), [doi:10.1103/PhysRevD.83.023518](#).
- [135] J. Knödlseeder, et al., The all-sky distribution of 511 keV electron-positron annihilation emission, *Astron. Astroph.* 441 (2005) 513–532. [arXiv:astro-ph/0506026](#), [doi:10.1051/0004-6361:20042063](#).
- [136] C. Boehm, et al., MeV Dark Matter: Has It Been Detected?, *Physical Review Letters* 92 (10) (2004) 101301–+. [arXiv:astro-ph/0309686](#), [doi:10.1103/PhysRevLett.92.101301](#).
- [137] N. Prantzos, et al., The 511 keV emission from positron annihilation in the Galaxy, *Reviews of Modern Physics* 83 (2011) 1001–1056. [arXiv:1009.4620](#), [doi:10.1103/RevModPhys.83.1001](#).
- [138] A. A. Abdo, et al., Fermi Large Area Telescope Measurements of the Diffuse Gamma-Ray Emission at Intermediate Galactic Latitudes, *Physical Review Letters* 103 (25) (2009) 251101–+. [doi:10.1103/PhysRevLett.103.251101](#).
- [139] M. Ackermann, et al., Fermi-LAT Observations of the Diffuse γ -Ray Emission: Implications for Cosmic Rays and the Interstellar Medium, *Astrophys. J.* 750 (2012) 3. [arXiv:1202.4039](#), [doi:10.1088/0004-637X/750/1/3](#).
- [140] K. N. Abazajian, S. Blanchet, J. P. Harding, Contribution of blazars to the extragalactic diffuse gamma-ray background and their future spatial resolution, *Phys. Rev. D* 84 (10) (2011) 103007. [arXiv:1012.1247](#), [doi:10.1103/PhysRevD.84.103007](#).
- [141] A. Bouquet, P. Salati, J. Silk, gamma-ray lines as a probe for a cold-dark-matter halo, *Phys. Rev. D* 40 (1989) 3168–3186. [doi:10.1103/PhysRevD.40.3168](#).
- [142] L. Bergström, J. Kaplan, Gamma ray lines from TeV dark matter, *Astroparticle Physics* 2 (1994) 261–268. [arXiv:hep-ph/9403239](#), [doi:10.1016/0927-6505\(94\)90005-1](#).
- [143] T. Bringmann, L. Bergström, J. Edsjö, New gamma-ray contributions to supersymmetric dark matter annihilation, *Journal of High Energy Physics* 1 (2008) 49–+. [arXiv:0710.3169](#), [doi:10.1088/1126-6708/2008/01/049](#).

- [144] A. A. Abdo, et al., Fermi Large Area Telescope Search for Photon Lines from 30 to 200 GeV and Dark Matter Implications, *Physical Review Letters* 104 (9) (2010) 091302. [arXiv:1001.4836](#), [doi:10.1103/PhysRevLett.104.091302](#).
- [145] G. Vertongen, C. Weniger, Hunting dark matter gamma-ray lines with the Fermi LAT, *JCAP*5 (2011) 27. [arXiv:1101.2610](#), [doi:10.1088/1475-7516/2011/05/027](#).
- [146] J. Goodman, et al., Gamma ray line constraints on effective theories of dark matter, *Nuclear Physics B* 844 (2011) 55–68. [arXiv:1009.0008](#), [doi:10.1016/j.nuclphysb.2010.10.022](#).
- [147] T. Bringmann, et al., Fermi LAT search for internal bremsstrahlung signatures from dark matter annihilation, *JCAP*7 (2012) 54. [arXiv:1203.1312](#), [doi:10.1088/1475-7516/2012/07/054](#).
- [148] A. Geringer-Sameth, S. M. Koushiappas, Exclusion of Canonical Weakly Interacting Massive Particles by Joint Analysis of Milky Way Dwarf Galaxies with Data from the Fermi Gamma-Ray Space Telescope, *Physical Review Letters* 107 (24) (2011) 241303. [arXiv:1108.2914](#), [doi:10.1103/PhysRevLett.107.241303](#).
- [149] A. A. Abdo, et al., Fermi LAT Observation of Diffuse Gamma Rays Produced Through Interactions Between Local Interstellar Matter and High-energy Cosmic Rays, *Astrophys. J.*703 (2009) 1249–1256. [arXiv:0908.1171](#), [doi:10.1088/0004-637X/703/2/1249](#).
- [150] A. A. Abdo, et al., Spectrum of the Isotropic Diffuse Gamma-Ray Emission Derived from First-Year Fermi Large Area Telescope Data, *Physical Review Letters* 104 (10) (2010) 101101. [arXiv:1002.3603](#), [doi:10.1103/PhysRevLett.104.101101](#).
- [151] A. A. Abdo, et al., Constraints on cosmological dark matter annihilation from the Fermi-LAT isotropic diffuse gamma-ray measurement, *JCAP*4 (2010) 14. [arXiv:1002.4415](#), [doi:10.1088/1475-7516/2010/04/014](#).
- [152] K. N. Abazajian, S. Blanchet, J. P. Harding, Current and future constraints on dark matter from prompt and inverse-Compton photon emission in the isotropic diffuse gamma-ray background, *Phys. Rev. D*85 (4) (2012) 043509. [arXiv:1011.5090](#), [doi:10.1103/PhysRevD.85.043509](#).
- [153] C. Arina, M. H. G. Tytgat, Constraints on light WIMP candidates from the isotropic diffuse gamma-ray emission, *JCAP*1 (2011) 11–+. [arXiv:1007.2765](#), [doi:10.1088/1475-7516/2011/01/011](#).
- [154] P. D. Serpico, et al., Extragalactic gamma-ray signal from dark matter annihilation: a power spectrum based computation, *MNRAS*421 (2012) L87–L91. [arXiv:1109.0095](#), [doi:10.1111/j.1745-3933.2011.01212.x](#).

- [155] A. A. Abdo, et al., Observations of Milky Way Dwarf Spheroidal Galaxies with the Fermi-Large Area Telescope Detector and Constraints on Dark Matter Models, *Astrophys. J.*712 (2010) 147–158. [arXiv:1001.4531](#), [doi:10.1088/0004-637X/712/1/147](#).
- [156] M. Ackermann, et al., Constraining Dark Matter Models from a Combined Analysis of Milky Way Satellites with the Fermi Large Area Telescope, *Physical Review Letters* 107 (24) (2011) 241302. [arXiv:1108.3546](#), [doi:10.1103/PhysRevLett.107.241302](#).
- [157] A. Abramowski, et al., Search for a Dark Matter Annihilation Signal from the Galactic Center Halo with H.E.S.S., *Physical Review Letters* 106 (16) (2011) 161301. [arXiv:1103.3266](#), [doi:10.1103/PhysRevLett.106.161301](#).
- [158] K. N. Abazajian, J. P. Harding, Constraints on WIMP and Sommerfeld-enhanced dark matter annihilation from HESS observations of the galactic center, *JCAP*1 (2012) 41. [arXiv:1110.6151](#), [doi:10.1088/1475-7516/2012/01/041](#).
- [159] P. Meade, M. Papucci, T. Volansky, Dark matter sees the light, *Journal of High Energy Physics* 12 (2009) 52. [arXiv:0901.2925](#), [doi:10.1088/1126-6708/2009/12/052](#).
- [160] M. Papucci, A. Strumia, Robust implications on dark matter from the first FERMI sky γ map, *JCAP*3 (2010) 14. [arXiv:0912.0742](#), [doi:10.1088/1475-7516/2010/03/014](#).
- [161] A. Charbonnier, et al., Dark matter profiles and annihilation in dwarf spheroidal galaxies: perspectives for present and future γ -ray observatories - I. The classical dwarf spheroidal galaxies, *MNRAS*418 (2011) 1526–1556. [arXiv:1104.0412](#), [doi:10.1111/j.1365-2966.2011.19387.x](#).
- [162] M. G. Walker, et al., Dark Matter in the Classical Dwarf Spheroidal Galaxies: A Robust Constraint on the Astrophysical Factor for γ -Ray Flux Calculations, *Astrophys. J. Lett.*733 (2011) L46. [arXiv:1104.0411](#), [doi:10.1088/2041-8205/733/2/L46](#).
- [163] J. Albert, et al., Upper Limit for γ -Ray Emission above 140 GeV from the Dwarf Spheroidal Galaxy Draco, *Astrophys. J.*679 (2008) 428–431. [arXiv:0711.2574](#), [doi:10.1086/529135](#).
- [164] V. A. Acciari, et al., VERITAS Search for VHE Gamma-ray Emission from Dwarf Spheroidal Galaxies, *Astrophys. J.*720 (2010) 1174–1180. [arXiv:1006.5955](#), [doi:10.1088/0004-637X/720/2/1174](#).
- [165] A. Abramowski, et al., H.E.S.S. constraints on dark matter annihilations towards the sculptor and carina dwarf galaxies, *Astroparticle Physics* 34 (2011) 608–616. [arXiv:1012.5602](#), [doi:10.1016/j.astropartphys.2010.12.006](#).

- [166] I. Cholis, P. Salucci, Extracting limits on Dark Matter annihilation from dwarf Spheroidal galaxies at gamma-rays, ArXiv e-prints arXiv:1203.2954.
- [167] E. A. Baltz, et al., Detection of neutralino annihilation photons from external galaxies, Phys. Rev. D 61 (2) (1999) 023514–+. arXiv:astro-ph/9909112, doi:10.1103/PhysRevD.61.023514.
- [168] A. Falvard, et al., Supersymmetric dark matter in M31: can one see neutralino annihilation with CELESTE?, Astroparticle Physics 20 (2004) 467–484. arXiv:astro-ph/0210184, doi:10.1016/S0927-6505(03)00215-9.
- [169] F. A. Aharonian, et al., Search for TeV gamma ray emission from the Andromeda galaxy, Astron. Astroph. 400 (2003) 153–159. arXiv:astro-ph/0302347, doi:10.1051/0004-6361:20021895.
- [170] J. Lavalle, et al., Indirect search for dark matter in M 31 with the CELESTE experiment, Astron. Astroph. 450 (2006) 1–8. arXiv:astro-ph/0601298, doi:10.1051/0004-6361:20054340.
- [171] M. Wood, et al., A Search for Dark Matter Annihilation with the Whipple 10 m Telescope, Astrophys. J. 678 (2008) 594–605. arXiv:0801.1708, doi:10.1086/529421.
- [172] F. Aharonian, et al., Fast Variability of Tera-Electron Volt γ Rays from the Radio Galaxy M87, Science 314 (2006) 1424–1427. arXiv:astro-ph/0612016, doi:10.1126/science.1134408.
- [173] E. Aliu, et al., VERITAS Observations of Day-scale Flaring of M 87 in 2010 April, Astrophys. J. 746 (2012) 141. arXiv:1112.4518, doi:10.1088/0004-637X/746/2/141.
- [174] J. Aleksić, et al., Detection of very-high energy γ -ray emission from $\text{jASTROBJ}_{\text{jNGC 1275}}$ / $\text{ASTROBJ}_{\text{i}}$ by the MAGIC telescopes, Astron. Astroph. 539 (2012) L2. arXiv:1112.3917, doi:10.1051/0004-6361/201118668.
- [175] A. A. Abdo, et al., Fermi Large Area Telescope observations of Local Group galaxies: detection of M 31 and search for M 33, Astron. Astroph. 523 (2010) L2. arXiv:1012.1952, doi:10.1051/0004-6361/201015759.
- [176] A. A. Abdo, et al., Detection of the Small Magellanic Cloud in gamma-rays with Fermi/LAT, Astron. Astroph. 523 (2010) A46. doi:10.1051/0004-6361/201014855.
- [177] A. A. Abdo, et al., Observations of the Large Magellanic Cloud with Fermi, Astron. Astroph. 512 (2010) A7. doi:10.1051/0004-6361/200913474.

- [178] S. Colafrancesco, S. Profumo, P. Ullio, Multi-frequency analysis of neutralino dark matter annihilations in the Coma cluster, *Astron. Astroph.*455 (2006) 21–43. [arXiv:astro-ph/0507575](#), [doi:10.1051/0004-6361:20053887](#).
- [179] A. Pinzke, C. Pfrommer, L. Bergström, Prospects of detecting gamma-ray emission from galaxy clusters: Cosmic rays and dark matter annihilations, *Phys. Rev. D*84 (12) (2011) 123509. [arXiv:1105.3240](#), [doi:10.1103/PhysRevD.84.123509](#).
- [180] M. A. Sánchez-Conde, et al., Dark matter searches with Cherenkov telescopes: nearby dwarf galaxies or local galaxy clusters?, *JCAP*12 (2011) 11. [arXiv:1104.3530](#), [doi:10.1088/1475-7516/2011/12/011](#).
- [181] X. Huang, G. Vertongen, C. Weniger, Probing dark matter decay and annihilation with Fermi LAT observations of nearby galaxy clusters, *JCAP*1 (2012) 42. [arXiv:1110.1529](#), [doi:10.1088/1475-7516/2012/01/042](#).
- [182] C. Combet, D. Maurin, E. Nezri, E. Pointecouteau, J. A. Hinton, R. White, Decaying dark matter: Stacking analysis of galaxy clusters to improve on current limits, *Phys. Rev. D*85 (6) (2012) 063517. [arXiv:1203.1164](#), [doi:10.1103/PhysRevD.85.063517](#).
- [183] E. Nezri, R. White, C. Combet, J. A. Hinton, D. Maurin, E. Pointecouteau, gamma-rays from annihilating dark matter in galaxy clusters: stacking vs single source analysis, *ArXiv e-prints*[arXiv:1203.1165](#).
- [184] D. Maurin, C. Combet, E. Nezri, E. Pointecouteau, Disentangling cosmic-ray and dark matter induced gamma-rays in galaxy clusters?, *ArXiv e-prints*[arXiv:1203.1166](#).
- [185] M. Ackermann, et al., Constraints on dark matter annihilation in clusters of galaxies with the Fermi large area telescope, *JCAP*5 (2010) 25. [arXiv:1002.2239](#), [doi:10.1088/1475-7516/2010/05/025](#).
- [186] S. Zimmer, J. Conrad, for the Fermi-LAT Collaboration, A. Pinzke, A Combined Analysis of Clusters of Galaxies - Gamma Ray Emission from Cosmic Rays and Dark Matter, *ArXiv e-prints*[arXiv:1110.6863](#).
- [187] J. Han, et al., Evidence for extended gamma-ray emission from galaxy clusters, *ArXiv e-prints*[arXiv:1201.1003](#).
- [188] A. Pinzke, C. Pfrommer, Simulating the γ -ray emission from galaxy clusters: a universal cosmic ray spectrum and spatial distribution, *MNRAS*409 (2010) 449–480. [arXiv:1001.5023](#), [doi:10.1111/j.1365-2966.2010.17328.x](#).
- [189] W. H. Press, D. N. Spergel, Capture by the sun of a galactic population of weakly interacting, massive particles, *Astrophys. J.*296 (1985) 679–684. [doi:10.1086/163485](#).

- [190] J. Silk, K. Olive, M. Srednicki, The photino, the sun, and high-energy neutrinos, *Physical Review Letters* 55 (1985) 257–259. doi:10.1103/PhysRevLett.55.257.
- [191] K. Freese, Can scalar neutrinos or massive Dirac neutrinos be the missing mass?, *Physics Letters B* 167 (1986) 295–300. doi:10.1016/0370-2693(86)90349-7.
- [192] L. M. Krauss, M. Srednicki, F. Wilczek, Solar System constraints and signatures for dark-matter candidates, *Phys. Rev. D* 33 (1986) 2079–2083. doi:10.1103/PhysRevD.33.2079.
- [193] T. K. Gaisser, G. Steigman, S. Tilav, Limits on cold-dark-matter candidates from deep underground detectors, *Phys. Rev. D* 34 (1986) 2206–2222. doi:10.1103/PhysRevD.34.2206.
- [194] G. D. Barr, T. K. Gaisser, P. Lipari, S. Robbins, T. Stanev, Three-dimensional calculation of atmospheric neutrinos, *Phys. Rev. D* 70 (2) (2004) 023006. arXiv:astro-ph/0403630, doi:10.1103/PhysRevD.70.023006.
- [195] M. Honda, T. Kajita, K. Kasahara, S. Midorikawa, Improvement of low energy atmospheric neutrino flux calculation using the JAM nuclear interaction model, *Phys. Rev. D* 83 (12) (2011) 123001. arXiv:1102.2688, doi:10.1103/PhysRevD.83.123001.
- [196] J. Carr, et al., the KM3NeT Consortium, Detector design studies for a cubic kilometre Deep Sea neutrino telescope KM3NeT, *Journal of Physics Conference Series* 136 (4) (2008) 042063. arXiv:0711.2145, doi:10.1088/1742-6596/136/4/042063.
- [197] F. Halzen, S. R. Klein, Invited Review Article: IceCube: An instrument for neutrino astronomy, *Review of Scientific Instruments* 81 (8) (2010) 081101. arXiv:1007.1247, doi:10.1063/1.3480478.
- [198] B. Pontecorvo, Neutrino Experiments and the Problem of Conservation of Leptonic Charge, *Soviet Journal of Experimental and Theoretical Physics* 26 (1968) 984.
- [199] A. Strumia, F. Vissani, Neutrino masses and mixings and..., *ArXiv High Energy Physics - Phenomenology e-prints* arXiv:hep-ph/0606054.
- [200] M. C. Gonzalez-Garcia, M. Maltoni, Phenomenology with massive neutrinos, *Phys. Rept.* 460 (2008) 1–129. arXiv:0704.1800, doi:10.1016/j.physrep.2007.12.004.
- [201] J. K. Becker, High-energy neutrinos in the context of multimessenger astrophysics, *Phys. Rept.* 458 (2008) 173–246. arXiv:0710.1557, doi:10.1016/j.physrep.2007.10.006.

- [202] G. Barenboim, C. Quigg, Neutrino observatories can characterize cosmic sources and neutrino properties, *Phys. Rev. D* 67 (7) (2003) 073024. [arXiv:hep-ph/0301220](#), [doi:10.1103/PhysRevD.67.073024](#).
- [203] L. Wolfenstein, Neutrino oscillations in matter, *Phys. Rev. D* 17 (1978) 2369–2374. [doi:10.1103/PhysRevD.17.2369](#).
- [204] S. P. Mikheev, A. I. Smirnov, Resonant amplification of neutrino oscillations in matter and solar-neutrino spectroscopy, *Nuovo Cimento C Geophysics Space Physics C* 9 (1986) 17–26. [doi:10.1007/BF02508049](#).
- [205] T. Ohlsson, H. Snellman, Neutrino oscillations with three flavors in matter: Applications to neutrinos traversing the Earth, *Physics Letters B* 474 (2000) 153–162. [arXiv:hep-ph/9912295](#), [doi:10.1016/S0370-2693\(00\)00008-3](#).
- [206] M. Blennow, J. Edsjö, T. Ohlsson, Neutrinos from WIMP annihilations obtained using a full three-flavor Monte Carlo approach, *JCAP* 1 (2008) 21. [arXiv:0709.3898](#), [doi:10.1088/1475-7516/2008/01/021](#).
- [207] M. Cirelli, et al., Spectra of neutrinos from dark matter annihilations, *Nuclear Physics B* 727 (2005) 99–138. [arXiv:hep-ph/0506298](#), [doi:10.1016/j.nuclphysb.2005.08.017](#).
- [208] V. Barger, et al., High energy neutrinos from neutralino annihilations in the Sun, *Phys. Rev. D* 76 (9) (2007) 095008. [arXiv:0708.1325](#), [doi:10.1103/PhysRevD.76.095008](#).
- [209] G. Bertone, et al., Neutrinos from dark matter annihilations at the galactic center, *Phys. Rev. D* 70 (6) (2004) 063503. [arXiv:astro-ph/0403322](#), [doi:10.1103/PhysRevD.70.063503](#).
- [210] A. E. Erkoca, et al., Muon fluxes and showers from dark matter annihilation in the Galactic center, *Phys. Rev. D* 81 (9) (2010) 096007. [arXiv:1002.2220](#), [doi:10.1103/PhysRevD.81.096007](#).
- [211] R. Abbasi, et al., Search for dark matter from the Galactic halo with the IceCube Neutrino Telescope, *Phys. Rev. D* 84 (2) (2011) 022004. [arXiv:1101.3349](#), [doi:10.1103/PhysRevD.84.022004](#).
- [212] K. Griest, M. Kamionkowski, Unitarity limits on the mass and radius of dark-matter particles, *Physical Review Letters* 64 (1990) 615–618. [doi:10.1103/PhysRevLett.64.615](#).
- [213] P. Sandick, et al., Sensitivity of the IceCube neutrino detector to dark matter annihilating in dwarf galaxies, *Phys. Rev. D* 81 (8) (2010) 083506. [arXiv:0912.0513](#), [doi:10.1103/PhysRevD.81.083506](#).
- [214] K. Griest, D. Seckel, Cosmic asymmetry, neutrinos and the sun, *Nuclear Physics B* 283 (1987) 681–705. [doi:10.1016/0550-3213\(87\)90293-8](#).

- [215] A. Gould, Weakly interacting massive particle distribution in and evaporation from the sun, *Astrophys. J.*321 (1987) 560–570. doi:10.1086/165652.
- [216] J. Edsjö, P. Gondolo, WIMP mass determination with neutrino telescopes, *Physics Letters B* 357 (1995) 595–601. arXiv:hep-ph/9504283, doi:10.1016/0370-2693(95)00930-J.
- [217] A. Bottino, et al., Signals of neutralino dark matter from Earth and Sun, *Astroparticle Physics* 3 (1995) 65–75. arXiv:hep-ph/9408391, doi:10.1016/0927-6505(94)00028-2.
- [218] V. Berezhinsky, et al., Searching for relic neutralinos using neutrino telescopes, *Astroparticle Physics* 5 (1996) 333–352. arXiv:hep-ph/9603342, doi:10.1016/0927-6505(96)00035-7.
- [219] J. Edsjö, Aspects of Neutrino Detection of Neutralino Dark Matter, Ph.D. thesis, , Uppsala Univ. (preprint hep-ph/9704384), (1997) (Oct. 1997). arXiv:hep-ph/9704384.
- [220] L. Bergström, J. Edsjö, P. Gondolo, Indirect detection of dark matter in km-size neutrino telescopes, *Phys. Rev. D*58 (10) (1998) 103519. arXiv:hep-ph/9806293, doi:10.1103/PhysRevD.58.103519.
- [221] P. Gondolo, et al., DarkSUSY: computing supersymmetric dark matter properties numerically, *JCAP*7 (2004) 8–+. arXiv:astro-ph/0406204, doi:10.1088/1475-7516/2004/07/008.
- [222] F. Halzen, D. Hooper, Prospects for detecting dark matter with neutrino telescopes in light of recent results from direct detection experiments, *Phys. Rev. D*73 (12) (2006) 123507. arXiv:hep-ph/0510048, doi:10.1103/PhysRevD.73.123507.
- [223] V. Niro, et al., Investigating light neutralinos at neutrino telescopes, *Phys. Rev. D*80 (9) (2009) 095019. arXiv:0909.2348, doi:10.1103/PhysRevD.80.095019.
- [224] J. L. Feng, et al., Testing the Dark Matter interpretation of the DAMA/LIBRA result with Super-Kamiokande, *JCAP*1 (2009) 32. arXiv:0808.4151, doi:10.1088/1475-7516/2009/01/032.
- [225] R. Kappl, M. W. Winkler, New limits on dark matter from Super-Kamiokande, *Nuclear Physics B* 850 (2011) 505–521. arXiv:1104.0679, doi:10.1016/j.nuclphysb.2011.05.006.
- [226] N. Fornengo, V. Niro, Downward-going tau neutrinos as a new prospect of detecting dark matter, *Journal of High Energy Physics* 11 (2011) 133. arXiv:1108.2630, doi:10.1007/JHEP11(2011)133.

- [227] G. Jungman, M. Kamionkowski, K. Griest, Supersymmetric dark matter, *Phys. Rept.*267 (1996) 195–373. [arXiv:hep-ph/9506380](#), [doi:10.1016/0370-1573\(95\)00058-5](#).
- [228] A. Gould, Resonant enhancements in weakly interacting massive particle capture by the earth, *Astrophys. J.*321 (1987) 571–585. [doi:10.1086/165653](#).
- [229] J. D. Lewin, P. F. Smith, Review of mathematics, numerical factors, and corrections for dark matter experiments based on elastic nuclear recoil, *Astroparticle Physics* 6 (1996) 87–112. [doi:10.1016/S0927-6505\(96\)00047-3](#).
- [230] M. T. Ressell, D. J. Dean, Spin-dependent neutralino-nucleus scattering for $A \sim 127$ nuclei, *Phys. Rev. C*56 (1997) 535–546. [arXiv:hep-ph/9702290](#), [doi:10.1103/PhysRevC.56.535](#).
- [231] A. Gould, Direct and indirect capture of weakly interacting massive particles by the earth, *Astrophys. J.*328 (1988) 919–939. [doi:10.1086/166347](#).
- [232] F. Ling, Is the dark disc contribution to dark matter signals important?, *Phys. Rev. D*82 (2) (2010) 023534–+. [arXiv:0911.2321](#), [doi:10.1103/PhysRevD.82.023534](#).
- [233] J. Ellis, K. A. Olive, C. Savage, Hadronic uncertainties in the elastic scattering of supersymmetric dark matter, *Phys. Rev. D*77 (6) (2008) 065026–+. [arXiv:0801.3656](#), [doi:10.1103/PhysRevD.77.065026](#).
- [234] J. L. Feng, K. T. Matchev, F. Wilczek, Prospects for indirect detection of neutralino dark matter, *Phys. Rev. D*63 (4) (2001) 045024. [arXiv:astro-ph/0008115](#), [doi:10.1103/PhysRevD.63.045024](#).
- [235] V. Bertin, E. Nezri, J. Orloff, Neutrino indirect detection of neutralino dark matter in the CMSSM, *European Physical Journal C* 26 (2002) 111–124. [arXiv:hep-ph/0204135](#), [doi:10.1140/epjc/s2002-01043-0](#).
- [236] R. Trotta, R. Ruiz de Austri, C. Pérez de los Heros, Prospects for dark matter detection with IceCube in the context of the CMSSM, *JCAP*8 (2009) 34. [arXiv:0906.0366](#), [doi:10.1088/1475-7516/2009/08/034](#).
- [237] D. Hooper, G. D. Kribs, Probing Kaluza-Klein dark matter with neutrino telescopes, *Phys. Rev. D*67 (5) (2003) 055003. [arXiv:hep-ph/0208261](#), [doi:10.1103/PhysRevD.67.055003](#).
- [238] M. Blennow, H. Melbésus, T. Ohlsson, Neutrinos from Kaluza-Klein dark matter in the Sun, *JCAP*1 (2010) 18. [arXiv:0910.1588](#), [doi:10.1088/1475-7516/2010/01/018](#).
- [239] D. Seckel, T. Stanev, T. K. Gaisser, Signatures of cosmic-ray interactions on the solar surface, *Astrophys. J.*382 (1991) 652–666. [doi:10.1086/170753](#).

- [240] G. Ingelman, M. Thunman, High energy neutrino production by cosmic ray interactions in the Sun, *Phys. Rev. D* 54 (1996) 4385–4392. [arXiv:hep-ph/9604288](#), [doi:10.1103/PhysRevD.54.4385](#).
- [241] T. Tanaka, et al., An Indirect Search for Weakly Interacting Massive Particles in the Sun Using 3109.6 Days of Upward-going Muons in Super-Kamiokande, *Astrophys. J.* 742 (2011) 78. [arXiv:1108.3384](#), [doi:10.1088/0004-637X/742/2/78](#).
- [242] R. Abbasi, et al., Multiyear search for dark matter annihilations in the Sun with the AMANDA-II and IceCube detectors, *Phys. Rev. D* 85 (4) (2012) 042002. [arXiv:1112.1840](#), [doi:10.1103/PhysRevD.85.042002](#).
- [243] Z. Ahmed, et al., Combined limits on WIMPs from the CDMS and EDELWEISS experiments, *Phys. Rev. D* 84 (1) (2011) 011102. [arXiv:1105.3377](#), [doi:10.1103/PhysRevD.84.011102](#).
- [244] E. Aprile, et al., Dark Matter Results from 100 Live Days of XENON100 Data, *Physical Review Letters* 107 (13) (2011) 131302. [arXiv:1104.2549](#), [doi:10.1103/PhysRevLett.107.131302](#).
- [245] H. S. Lee, et al., Limits on Interactions between Weakly Interacting Massive Particles and Nucleons Obtained with CsI(Tl) Crystal Detectors, *Physical Review Letters* 99 (9) (2007) 091301. [arXiv:0704.0423](#), [doi:10.1103/PhysRevLett.99.091301](#).
- [246] E. Behnke, others., Improved Limits on Spin-Dependent WIMP-Proton Interactions from a Two Liter CF₃I Bubble Chamber, *Physical Review Letters* 106 (2) (2011) 021303. [arXiv:1008.3518](#), [doi:10.1103/PhysRevLett.106.021303](#).
- [247] R. Bernabei, et al., First results from DAMA/LIBRA and the combined results with DAMA/NaI, *European Physical Journal C* (2008) 167–+[arXiv:0804.2741](#), [doi:10.1140/epjc/s10052-008-0662-y](#).
- [248] S. Archambault, et al., Dark matter spin-dependent limits for WIMP interactions on ¹⁹F by PICASSO, *Physics Letters B* 682 (2009) 185–192. [arXiv:0907.0307](#), [doi:10.1016/j.physletb.2009.11.019](#).